USE OF REMOTELY SENSED IMAGERY TO MAP SUDDEN OAK DEATH (*PHYTOPHTHORA RAMORUM*) IN THE SANTA CRUZ MOUNTAINS

by

Trinka Gillis

A Thesis Presented to the
FACULTY OF THE USC GRADUATE SCHOOL
UNIVERSITY OF SOUTHERN CALIFORNIA
In Partial Fulfillment of the
Requirements for the Degree
MASTER OF SCIENCE
(GEOGRAPHIC INFORMATION SCIENCE AND TECHNOLOGY)

May 2014

DEDICATION

I dedicate this work to Dr. Wayne Caplinger, whose enthusiasm for life was only equaled by its unexpected brevity, and to all whose lives are cut short before their time.

ACKNOWLEDGEMENTS

I would like to thank my advisor, Dr. John Wilson, for his valuable feedback and faith in my work, and committee members Dr. Su Jin Lee and Dr. Tarek Rashed, whose advice and suggestions were indispensable in carrying out this project. I would also like to thank my professors in the GIST program, whose lessons made this thesis possible. Last but not least, I would like to acknowledge the support of my husband, who gave up a year of weekends so that I could pursue this dream.

TABLE OF CONTENTS

LIST OF TABLES

LIST OF FIGURES

LIST OF ABBREVIATIONS

ADAR	Airborne Data Registration
ADS	USDA Forest Health Monitoring Program Aerial Detection Survey
AOI	Area of Interest
BLM	Bureau of Land Management
CalFire	California Department of Forestry and Fire Protection
CALVEG	Classification and Assessment with Landsat of Visible Ecological Groupings
CDR	Climate Data Record
COMTF	California Oak Mortality Task Force
FRAP	Fire and Resource Assessment Program
GAP	California Gap Analysis Project
HLH	Healthy Tree Land Cover
MODIS	Moderate Resolution Imaging Spectroradiometer
NAIP	National Agricultural Imagery Program
NASA	National Aeronautics and Space Administration
NBR	Normalized Burn Ratio
NDII	Normalized Difference Infrared Index
NDMI	Normalized Difference Moisture Index
NDVI	Normalized Difference Vegetation Index
NLCD	National Land Cover Database
NPS	National Park Service
PR	*Phytophthora ramorum*
RGI	Red Green Index
RMSE	Geometric Root Mean Square Error
SD	Serious Tree Death

SLC	Scan Line Corrector
SOD	Sudden Oak Death
SWIR/NIR	Short Wave Infrared/Near Infrared
TC Bright	Tasseled Cap Brightness
TC Green	Tasseled Cap Greenness
TC Wet	Tasseled Cap Wetness
TM	Thematic Mapper
USDA	US Department of Agriculture
USGS	US Geological Survey

ABSTRACT

This project sought a method to map Sudden Oak Death distribution in the Santa Cruz Mountains of California, a coastal mountain range and one of the locations where this disease was first observed. The project researched a method to identify forest affected by SOD using 30 m multi-spectral Landsat satellite imagery to classify tree mortality at the canopy-level throughout the study area, and applied that method to a time series of data to show pattern of spread. A successful methodology would be of interest to scientists trying to identify areas which escaped disease contagion, environmentalists attempting to quantify damage, and land managers evaluating the health of their forests. The more we can learn about the disease, the more chance we have to prevent further spread and damage to existing wild lands.

The primary data source for this research was springtime Landsat Climate Data Record surface reflectance data. Non-forest areas were masked out using data produced by the National Land Cover Database and supplemental land cover classification from the Landsat 2011 Climate Data Record image. Areas with other known causes of tree death, as identified by Fire and Resource Assessment Program fire perimeter polygons, and US Department of Agriculture Forest Health Monitoring Program Aerial Detection Survey polygons, were also masked out. Within the remaining forested study area, manually-created points were classified based on the land cover contained by the corresponding Landsat 2011 pixel. These were used to extract value ranges from the Landsat bands and calculated vegetation indices. The range and index which best differentiated healthy from dead trees, SWIR/NIR, was applied to each Landsat scene in the time series to map tree mortality. Results Validation Points, classified using Google Earth high-resolution aerial imagery, were created to evaluate the accuracy of the mapping methodology for the 2011 data.

Results indicated three areas which had largely escaped Sudden Oak Death infestation and one area with high tree mortality that was not previously identified as Sudden Oak Death. However, the methodology identified widespread tree death throughout the study area, including in 1994, when little tree death should have been found. This indicated that healthy tree canopy was able to produce a spectral signature matching that of pixels containing some dead trees. In addition, the number of pixels classified as containing tree death varied widely from year to year, suggesting that seasonal variation plays a much larger role in the spectral signature than anticipated. Finally, an analysis of the Results Validation Points showed a high rate of false positives, with only 24 percent mapping accuracy for tree death. This demonstrated conclusively that the methodology and mapping results were unreliable.

The project demonstrates that Landsat data did not work for this study due to spectral confusion and seasonal variation. Results might have been improved if a custom index was devised to remove some of the false positives, if the definition of serious tree death was limited to pixels containing a greater percentage of dead tree canopy, and/or if seasonal differences in rainfall and temperature had been considered when choosing Landsat scenes to represent each year.

CHAPTER ONE: INTRODUCTION

In the 1990s, oak trees suddenly began dying in the San Francisco Bay area of California. Twenty years later, much is understood about the disease and cause, but no effective means of control exists. This project sought to increase knowledge of Sudden Oak Death (SOD) by finding a method to map tree morality over the 20-year period that the disease has been active in California. Methods for mapping the disease and its pattern of spread could be adapted to other areas to evaluate forest health, quantify the scale of the disease, and evaluate success at disease management. The more we learn about the disease, the more tools we have to prevent further spread and damage to existing wild lands.

1.1 Sudden Oak Death

The first observed occurrences of SOD were in 1994, in Mill Valley and Santa Cruz, California (Garbelotto, Svihra and Rizzo 2001, Mascheretti et al. 2008). In 2000 the aerially-dispersed oomycete, water mold, *Phytophthora ramorum* (PR) was identified as the causal agent (Rizzo, Garbelotto and Hansen 2005). PR is believed to have been introduced to California via infected rhododendron (*Rhododendron spp*.) and viburnum (*Viburnum spp*.) ornamental plants. The fungus was transmitted via wind and rain to nearby wild lands, where it became established in additional susceptible hosts.

On the central California coast, SOD primarily kills California black oak (*Quercus kelloggii*), coast live oak (*Quercus agrifolia*) and tanoak (*Lithocarpus densiflorus*) (Barrett et al. 2006), but is transmitted by many other trees and shrubs, as well as by human activity. New SOD outbreaks like those shown in Figure 1 are discovered each year. In the US, nurseries are closely monitored for infected plants, and stream baiting techniques are used to determine where PR

might spread next. No cure exists for SOD, but preventive applications of anti-fungal agent have successfully been applied to individual uninfected susceptible trees after nearby infected trees were removed. The wide variety of carrier vegetation, low natural resistance to the disease, and the natural means of contagion make it a difficult infection to fight.

Figure 1 Sudden Oak Death at Mescal Ridge, Carmel, Big Sur, Monterey County 2012
Photograph by Tom Coleman, US Forest Service

The total acreage affected by SOD in California has not been estimated. As of 2013, SOD affects areas from southern Oregon to the San Luis Obispo area of California. Figure 2 shows vulnerable habitat in northern California, and Meentemeyer et al. (2004) calculated that 10,305 km^2 (2.5 percent of California's land area) are at high or very high risk for SOD infection. Additional at-risk environments include the Sierra Nevada and the Appalachian mountain ranges in the US, as well as parts of Europe and Asia. As of October 2013, efforts to contain PR

infection in the UK are responsible for the felling of over 16,000 ha (39,536 acres) of Japanese larch (Forestry Commission UK 2014), an economically important timber tree. The large-scale loss of California oak trees, which play a vital role in the coastal forest ecosystem, will have serious consequences for wildlife and the landscape. Today's forests will be unrecognizable to future generations. More knowledge about the infection, including locations and patterns of spread, may aid in attempts to minimize contagion.

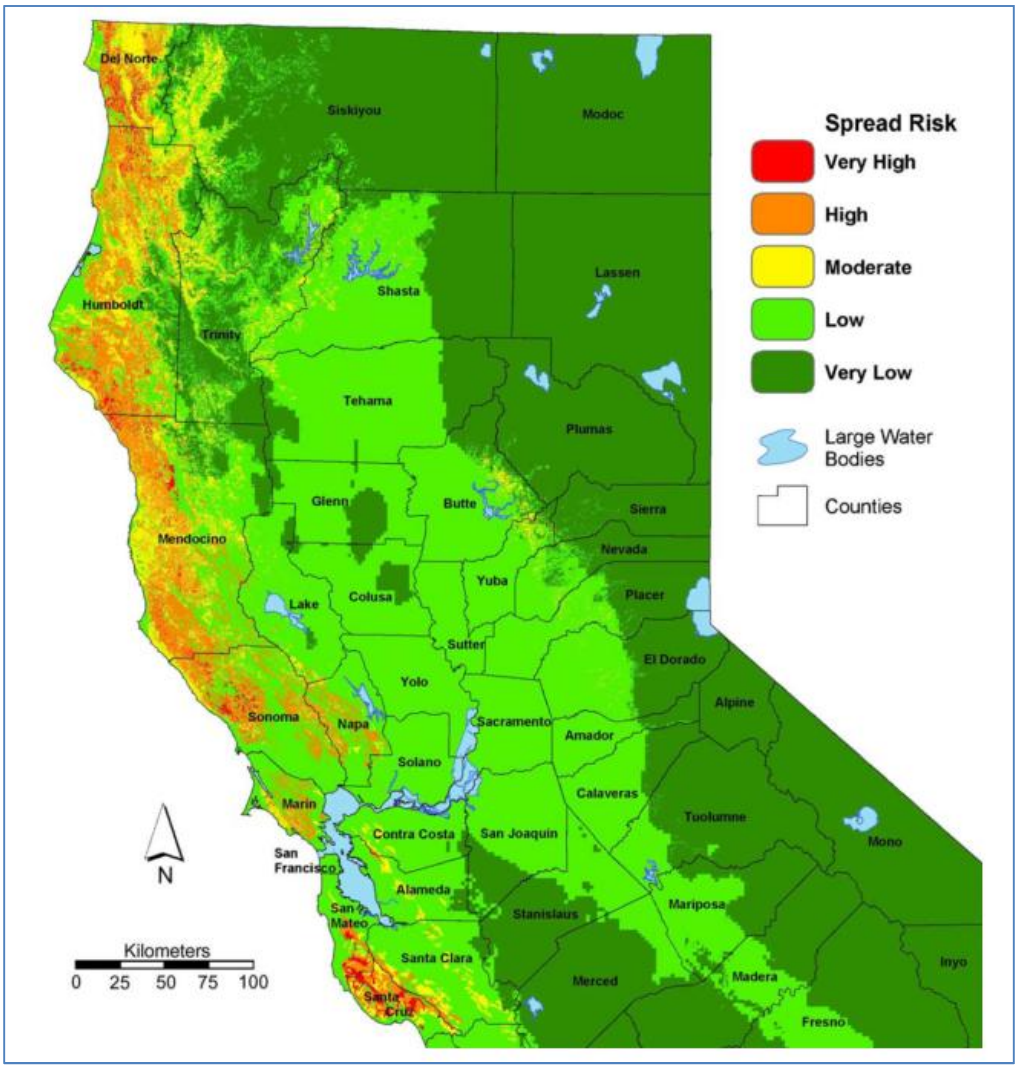

Figure 2 Predicted spread risk for *P. ramorum* in northern California
Source: Meentemeyer et al. (2004)

1.2 Role of Remote Sensing in SOD Studies

Remote sensing has been used to increase SOD knowledge through modeling risk, identifying infected trees, and mapping current disease locations. Modeling risk areas is valuable to manage and prevent the spread of the disease, but mapping infected locations is necessary to evaluate success at disease management.

The California central coast is widely accepted as the proper host environment for SOD, but models based on remotely-sensed data have identified other susceptible regions. These studies used variables such as vegetation, slope, aspect, precipitation, temperature and humidity to map areas with a hospitable environment and vegetation likely to be infected. These risk models covered large areas, from parts of California to the entire world. One worldwide study (Kluza et al. 2007) predicted wide distribution of SOD from San Diego to Vancouver Island, throughout the Sierra Nevada mountains, and in the southeastern US, with additional risk areas in South America, southern Africa, southern Europe, the UK, and Asia, especially South Korea and Japan. Risk maps are valuable to identify areas where land managers need to watch out for SOD, but they highlight the fact that the disease has the potential to infect very large areas which are not easily monitored from the ground.

Remotely-sensed imagery has been used to identify SOD infections in small areas using canopy-level tree health as an indicator of disease presence. In the Big Sur area of central California, south of this project's study area, Meentemeyer et al. (2008) manually digitized dead trees from 0.33 m resolution aerial imagery to calculate 20 percent mortality in infected areas. A similar study (Liu, Kelly and Gong 2006) used 1 m Airborne Data Registration (ADAR) images to classify land cover and map SOD in China Camp State Park, north of this project's study area.

Both of these studies used high-resolution aerial imagery, the data storage needs and cost of which often prevent application over a large area.

The only program which attempts to map SOD infection on a large scale is the United States Department of Agriculture (USDA) Forest Health Monitoring Program Aerial Detection Survey (ADS) (Heath et al. 2012) which uses aerial monitoring to map forest health hazards over large areas. The USDA studies produce generalized maps of threats, focus on different hazards and regions from year to year, and rely heavily on observation of changes from a moving aircraft.

SOD has the potential to quickly infect large areas. The scale of the infestation and inaccessible and remote locations prevent individual tree observation, so remote sensing is a promising tool for disease monitoring. Many land management agencies have limited budgets, so an effective monitoring method needs to use low-cost data in order to be applicable by others. Moderate resolution data, such as Landsat, offers the opportunity to monitor large areas repetitively with minimal data cost and minimal data storage requirements.

1.3 Research Questions

The biology of SOD has been extensively studied, and maps have been created showing individual confirmed infections, but no methods exist to map SOD on a large scale. The goals of this project were to find the best index to map SOD in the selected study area using Landsat data, and apply that method to a series of annual images to analyze the rate and pattern of spread from 1994 to the present. A simple method to map SOD locations over a large area will give us an estimate of the scope of the disease, and may attract more attention to the disease and funding for research. The same method, applied to multiple years of imagery, would produce a view of the

disease over time, including the rate and pattern of spread. This could identify previously unnoticed contaminated areas, identify areas which escaped damage, and lead to a better overall understanding of the disease.

This is a pilot project which analyzed the accuracy of different vegetation indices at differentiating tree mortality from healthy forest in the Santa Cruz Mountains on the central California coast. The hope was that a successful method could be adapted and applied in other areas where SOD threatens, to form a picture of the scope of SOD infestation throughout the state. SOD spreads quickly, and many of its prime habitats are difficult to access. Remote sensing provides the only practical monitoring approach in these areas. Landsat moderate-resolution (30 m) satellite data, available from the US Geological Survey (USGS) is high-quality, free and readily available for most of the world, which makes it the ideal tool for organizations with limited budgets which cannot purchase higher resolution data. Landsat data is re-collected every 16 days so the likelihood of finding suitable cloud-free data is high, and the pixel size strikes a balance which requires some adjustments for mixed pixels, but minimizes storage space and processing time.

Canopy-level tree health provides a glimpse of changes that are occurring at multiple levels of the forest. A disease like SOD affects old and young trees, and when the tallest and most well-established trees die, the devastation in the understory has already taken place. Mapping SOD using canopy-level tree health as an indicator of disease extent has been performed with high resolution imagery on a local scale, but high-resolution imagery prevents large-scale analysis because of data costs and storage needs. This study attempted to map disease extent using moderate-resolution data over a large area. Although all tree mortality in the study area is not due to SOD, this study masked out areas where other circumstances were known to

have affected large numbers of trees. This study used canopy-level tree mortality as a proxy to indicate areas where SOD has had the strongest impact on the environment.

The goals of this project were to find a method to identify SOD-affected forest in the study area using Landsat data, and use a time series data set to identify the rate and pattern of spread. Questions that needed to be addressed include:

1. Can canopy-level tree death indicating SOD infestation be accurately identified and mapped using Landsat remotely-sensed imagery?
2. Are vegetation indices alone sufficient to differentiate tree health and tree mortality from other types of land cover?
3. Will existing supplemental land cover data sets improve or simplify the classification process?

The resulting methodology to evaluate SOD contagion in California would be of interest to scientists, environmentalists and land managers who might adapt this methodology to map SOD damage in other areas.

1.4 Thesis Outline

The next chapter provides background on SOD, a synopsis of studies analyzing tree health after insect infestation, and a summary of the ways that remote sensing data has been used to further our knowledge of SOD. An understanding of the origin, spread and control of SOD is necessary to understand the need for additional information about the disease. Satellite data alone has never been used to map SOD, but the tree health studies demonstrate successful techniques that were used to map changes in tree health, which could be adapted to this study of SOD. In addition,

chapter two includes a discussion of the ways that remote sensing techniques or data have been used to study SOD, and how this project will add to our knowledge.

Chapter 3 describes the data sources and methodology used in this study, which relied on aerial imagery to classify land cover points, land classification raster and several vector layers to refine the study area, in addition to Landsat scenes, which were the primary data source. This chapter describes how the study area was built, as well as how the most effective index was chosen to differentiate healthy trees from tree death. This chapter also describes the method used to evaluate the accuracy of the final classification results.

Chapter 4 presents maps of the results, including an analysis of new areas of tree mortality, and a comparison to other SOD map data. This chapter concludes with an analysis and discussion of the accuracy of the mapping results.

Chapter 5 discusses the implications of the project results, offers suggestions for further work, and reflects on success at responding to the project's research questions.

CHAPTER TWO: RELATED WORK

When SOD was first discovered, scientists focused on identifying the origin and spread methods of the disease in an effort to learn how to control it. Twenty years after the first reported sighting, mapping the current extent of this still uncontrolled pathogen is our next feasible step in understanding the disease. The hope is that effective techniques which used satellite imagery to map declining tree health in other forest landscapes can be adapted to fill this gap in our knowledge of SOD.

2.1 Biology of SOD

SOD spreads naturally and rapidly, and there is no effective means of control. Understanding the biology of SOD helps explain the long-term effect on our forests, and why controlling it is so difficult.

SOD earned its name because infected trees can change appearance from healthy to dead in as little as three months, but SOD is not the only result of PR infection. PR may infect susceptible plants in three possible ways (Hansen, Parke and Sutton 2005, Rizzo, Garbelotto and Hansen 2005). Sudden Oak Death, shown in Figure 3, the most serious infection, causes bleeding ulcers on the trunk and limbs which weaken the tree and lead to death (Parke et al. 2007, Collins et al. 2009). In California, only three types of trees develop SOD: California black oak (*Quercus kelloggii*), coast live oak (*Quercus agrifolia*) and tanoak (*Lithocarpus densiflorus*). Trees infected with SOD do not produce spores or spread the disease (Mascheretti et al. 2008). PR spores are produced by vegetation infected with the non-lethal Ramorum Blight, evidenced by leaf discoloration (Mascheretti et al. 2008), as shown in Figure 4. California bay laurel (*Umbellularia californica*) is the primary sporulator for PR in California (Davidson et al. 2005),

but as of 2012 more than 40 species, listed in Appendix A, are known to host the disease. Tanoak trees (*Lithocarpus densiflorus*) are unusual because they have been observed with both types of infection: they develop SOD in California and Ramorum Blight in Oregon (Grünwald et al. 2012).

PR spores are spread naturally and by human action. Wet, warm spring seasons provide optimal conditions for PR spore creation (Davidson et al. 2005), and the spores are dispersed by rain splash and wind-driven rain. Infected soil transported via nursery plants (Cushman and Meentemeyer 2008) and via tires and shoes of recreational forest users (Davidson et al. 2005) cause long-distance dispersal of PR. Although stream monitoring has detected PR up to 20 km downstream of a known infection site (Davidson et al. 2005, Sutton et al. 2009), research does not indicate that infection patterns follow streams.

Figure 3 Coast live oak showing the bleeding ulcers typical of Sudden Oak Death
Photo: Steve Tjosvold, UC Cooperative Extension

Figure 4 California bay laurel (*Umbellularia californica*) infected with Ramorum blight
Photo: John Bienapfl, University of California Davis

Attempted methods for controlling PR include burning of host trees, chemical sprays, antimicrobial applications, and creation of a disease-break area that contains no possible hosts (Filipe et al. 2012, McGinnis 2008). There is no effective means to cure an infected tree, and preventive methods need to be applied to individual trees in order to be most effective. Fire as disease suppression is only effective if all PR-infected California bay laurel trees are completely destroyed (Beh et al. 2012). No current control methods can avert large-scale infection.

Ramage, O'Hara and Forrestel (2011) believe that PR will remain permanently in California forests because numerous species host the disease without succumbing to it. Tanoak (*Lithocarpus densiflorus*), whose acorns are an important animal food source, may become extinct because it has no genetic resistance and it can both transmit the disease and die from it (Ramage, O'Hara and Forrestel 2011, Maloney et al. 2005, Ramage and O'Hara 2010).

PR poses a danger to the long-term existence of all SOD-susceptible trees. We cannot predict what California forests will look like 50 years from now: although the first SOD-infected trees died more than a decade ago, new vegetation has been slow to take over. Mapping disease locations could expose a disease-resistant strain of trees, or demonstrate environmental variables which impede SOD spread, and might lead scientists to discover new means of control.

2.2 Remote Sensing of Tree Health

Remote sensing data describes data collected at a long distance from the object or location being viewed. For the purposes of this study, remote sensing data refers to aerial- or satellite–collected data, including images. Collecting data from a distance makes it possible to quickly collect information which encompasses a large land area while sacrificing some detail.

Remotely sensed images can be collected aerially or via satellite. High resolution aerial photography provides fine detail for land change analysis, but it is expensive to collect, each image covers a relatively small area, and it is difficult to obtain historical data meeting specifications. Satellites' high altitude means the imagery is generally of lower resolution than aerial photography, but their orbit around the Earth allows consistent repeated collection over multiple years, so it is a good choice for historical land change analysis.

Satellite data sources can be compared based on spatial, spectral or temporal resolution. Spatial resolution describes the land area covered by a single pixel. The smaller the land area covered by each pixel, the finer the spatial resolution. Spectral resolution expresses the number of bands collected for each scene. Collecting more bands requires more instruments and data storage on the satellite. Temporal resolution describes the time lapse between repeated collections in the same area, and is a function of the land area covered by each image. No

existing satellites have high resolution in all three areas, so choosing a satellite data source requires compromise.

The Landsat satellite missions, a joint program between the USGS and National Aeronautics and Space Administration (NASA) have collected data covering all non-polar regions of the world since 1972. This project primarily uses Landsat 5 TM data, which has a 30 m spatial resolution, 16-day repeat cycle, and seven bands of data. Landsat Climate Data Record (CDR) reflectance images, corrected to remove atmospheric distortion, were used to facilitate comparison between data sets collected under different weather conditions and at different times of day. Each Landsat scene covers approximately 100 square miles and the data is available for free download from the USGS. The frequent collection over the same areas makes it likely that a researcher can obtain cloud-free images of a study area, and the low cost of data makes it inexpensive for agencies to adapt this methodology to their needs.

Multi-spectral image analysis applies algorithms which highlight information contained in separate spectral bands. Vegetation analysis relies primarily on the green, red, near infrared and shortwave infrared bands to classify vegetation and measure vegetation health. Landsat's seven bands are: (1) blue; (2) green; (3) red; (4) near infrared; (5) shortwave infrared; (6) thermal; and (7) a second shortwave infrared band. The most common indices used to categorize vegetation are shown in Table 1.

There are no recent studies of SOD contagion using satellite imagery, but a Mahon et al. (2002) study attempted to map potential SOD infection on the California central coast in 2000. By comparing image changes from 1996 to 2000 using the Tasseled Cap transformation applied to Landsat imagery, with supplements of aerial imagery, field study, and other remotely sensed and land classification data, they were able to identify large potential SOD concentrations in

Table 1 Multi-spectral indices used to detect vegetation health

Index	**Landsat Formula**	**Notes**
Short Wave Infrared/Near Infrared (SWIR/NIR)	Band5 / Band4	Detects moisture content, an indication of health, water stress or drought
Normalized Burn Ratio (NBR)	(Band4-Band7) / Band4 + Band7)	Identifies burned areas and quantifies severity. Occasionally used to assess vegetation health.
Normalized Difference Moisture Index (NDMI) (also known as Normalized Difference Infrared Index (NDII)	(Band4-Band5) / Band4+Band5)	Detects water content, a measure of vegetation health.
Normalized Difference Vegetation Index (NDVI)	(Band4-Band3) / Band4+Band3)	Detects green plant canopies indicating vegetation health and density. Used to quantify photosynthetic capacity.
Red Green Index (RGI)	Band3 / Band2	As tree health declines, the red value increases, causing this index to increase. Useful for detecting dead or dying trees.
Tasseled Cap brightness (TC Bright) (also known as Kauth-Thomas transformation)	0.2043*Band1 + 0.4158*Band2 + 0.5524*Band3 + 0.5741*Band4 + 0.3124*Band5 + 0.2303*Band7	Measures image brightness. Used to differentiate dark and light soils.
Tasseled cap greenness (TC Green) (also known as Kauth-Thomas transformation)	-0.1603*Band1 – 0.2819*Band2 – 0.4934*Band3 + 0.7940*Band4 – 0.0002*Band5 – 0.1446*Band7	Detects greenness, a measure of vegetation density and photosynthetically-active vegetation.
Tasseled cap wetness (TC Wet) (also known as Kauth-Thomas transformation)	0.0315*Band1 + 0.2021*Band2 + 0.3102*Band3 + 0.1594*Band4 – 0.6806*Band5 – 0.6109*Band7	Detects wetness, indicating surface moisture, vegetation density and dried vegetation.

three coastal counties and small concentrations in three other counties, confirmed with aerial data. At the time of publication, field verification was incomplete but preliminary results indicated that the change detected was potential SOD. The researchers admitted that pixel-level analysis likely overestimated mortality, but an aggregation would result in missed positives. They concluded that change detection methods were able to successfully identify subtle changes in canopy cover.

Many studies similar to this project have used Landsat scenes to assess insect infestation. Studies of beetle-caused mortality used a variety of vegetation indices, including Tasseled Cap, NDMI, SWIR/NIR and NBR to identify areas of infestation and evaluate severity. Their methods give us clues to effective ways to map SOD.

One project in the Santa Fe National Forest (Vogelmann, Tolk and Zhu 2009), for example, evaluated conifer tree health over an 18-year period using eight Landsat scenes, and found an original way to validate results using the ADS data. Using the SWIR/NIR index, more sensitive to conifer health than NDVI, researchers evaluated increases and decreases in the SWIR/NIR index indicating forest health changes. When researchers compared their results to the ADS insect defoliation maps, they found annual variability in the quality of the ADS data. However, by combining multiple years of ADS data, disregarding areas which had only been identified as damaged in a single year, areas which their study identified as experiencing consistently decreasing tree health correlated with areas reported as damaged by the USDA over multiple years. Their study concluded that this Landsat time series effectively captured decline in forest health and that Landsat data is particularly well-suited to studies over large areas.

Another study in Colorado compared the accuracy of different vegetation indices and band combinations applied to single- and multiple-date Landsat data to map bark-beetle caused

tree mortality (Meddens et al. 2013). Seven vegetation indices were calculated: RGI, NDVI, NDMI, SWIR/NIR and the three Tasseled cap indices (see Table 1 for additional details). Land cover classifications created from a 30 cm aerial image were aggregated to the Landsat pixel size to classify the portions of each land cover within an equivalent Landsat pixel. This study obtained 91 percent overall accuracy using single-date image classification with the Tasseled Cap indices to map red-stage (dying) trees, and 89 percent accuracy with multi-date image analysis and the SWIR/NIR index. Although the single-date method was more accurate with high mortality, the researchers concluded that both methods resulted in high classification accuracy using Landsat data.

Several other studies used a variety of indices with Landsat data to evaluate insect impact on forest health. In an unusual choice, the NBR, primarily used by fire sciences, was used to evaluate beetle infestation impact on ground fuels which might affect the severity of forest fires (Meigs, Kennedy and Cohen 2011) in Oregon. They found a correlation between the presence of coarse woody detritus and Landsat spectral change, consistent with Landsat's sensitivity to vegetation cover. This study successfully used NBR to map both short- and long-term spectral change, and concluded that methods which only focus on short-term changes miss many of the signs of insect infestation.

Similarly, a Canadian forest study (Goodwin et al. 2008) successfully used the NDMI with multiple years of imagery to identify forest stands declining due to beetle infestation, with 71 to 86 percent accuracy. These researchers believed that analyzing imagery from more than two years might be more accurate. These researchers found significant variation in NDMI values for healthy forest, approximately 50 percent variation around the mean. As the infestation worsened, the mean and the extremes decreased and mapping accuracy increased. The

researchers concluded that NDMI showed greater changes in beetle-infested areas than in the healthy forest, but spectral confusion was a problem in areas with low levels of infestation.

These studies indicate that Landsat imagery can successfully detect changes in tree health. Spectral confusion is a concern, and accuracy increases as tree mortality increases, but both single- and multi-date imagery produce successful results under a variety of circumstances. These beetle-damage studies are different from SOD studies in several important ways. The trees in these examples were all conifers, but the three species killed by SOD are broadleaf, so the same vegetation indices may not be the most effective. Another important difference is the way the foliage changes. Beetle-induced death takes several years, and dying trees can be recognized by red foliage indicating tree stress. Trees infected with SOD display bleeding lesions for several years, but at the final stage the foliage changes from green to yellow to brown within a few weeks (Alexander and Swain 2010), which may be difficult to capture on imagery.

Like these studies, the SOD study will be evaluating health of sub-pixel-sized features. Several studies above observed that results were more accurate in areas with greater mortality, so this study differentiates between pixels containing lower and higher levels of mortality. This project also minimizes the mixed-pixel dilemma by masking out non-forested areas, decreasing the incidence of pixels containing non-forest land cover types with conflicting spectral responses. Several of these researchers were measuring tree health change over time, including both decline and improvement. Trees infected with SOD have no chance of recovery, so this study evaluates index values in a binary approach: pixels containing only healthy trees or containing some dead trees. The index values chosen will determine how sensitive the formula is at detecting areas with small occurrences of tree death relative to overall canopy.

These studies indicate that there are multiple effective methods and indices to effectively measure tree health using Landsat imagery and additional data. Whether a study used a single year or multiple years of remotely sensed imagery, they were all able to successfully identify decreasing tree health. This study will draw on several techniques used in the studies above, particularly an evaluation of the accuracy of different vegetation indices, and a comparison of results to ADS data.

Remotely sensed data has been used to study SOD by providing inputs for disease risk models, aerial imagery has been used to identify infected trees in localized areas, and aerial monitoring has been used to identify generalized disease locations.

Remotely sensed data, such as temperature, slope, aspect, weather or vegetation is often an input in the creation of risk maps. Risk maps can be useful for land managers to learn which areas to monitor for signs of the disease, but inexact models can cause certain areas to be unmonitored, or give a false sense of security to residents, who fail to take simple precautions to prevent introduction of the disease. Many different remotely sensed variables can be weighted, resulting in dramatically different models. Unfortunately, the accuracy of risk models can usually only be determined many years after their creation.

A 2007 SOD risk model used remotely sensed data, including topographic, climatic data, and raster data to create a worldwide view of disease potential. Kluza et al. (2007) predicted wide distribution of SOD on the west coast of North America, from San Diego to Vancouver Island and throughout the Sierra Nevada mountains, as shown in Figure 5. In addition, this model showed large risk in the southeastern US, with additional risk areas in South America, southern Africa, southern Europe, the UK, and Asia, including South Korea and Japan. This model puts

risk in many areas where PR infection has not yet been detected, but the accuracy of this model cannot be evaluated at this time.

Two early SOD risk models for California used land cover data created from remotely sensed raster data, which may have caused inaccuracies in their final result. A 2004 model

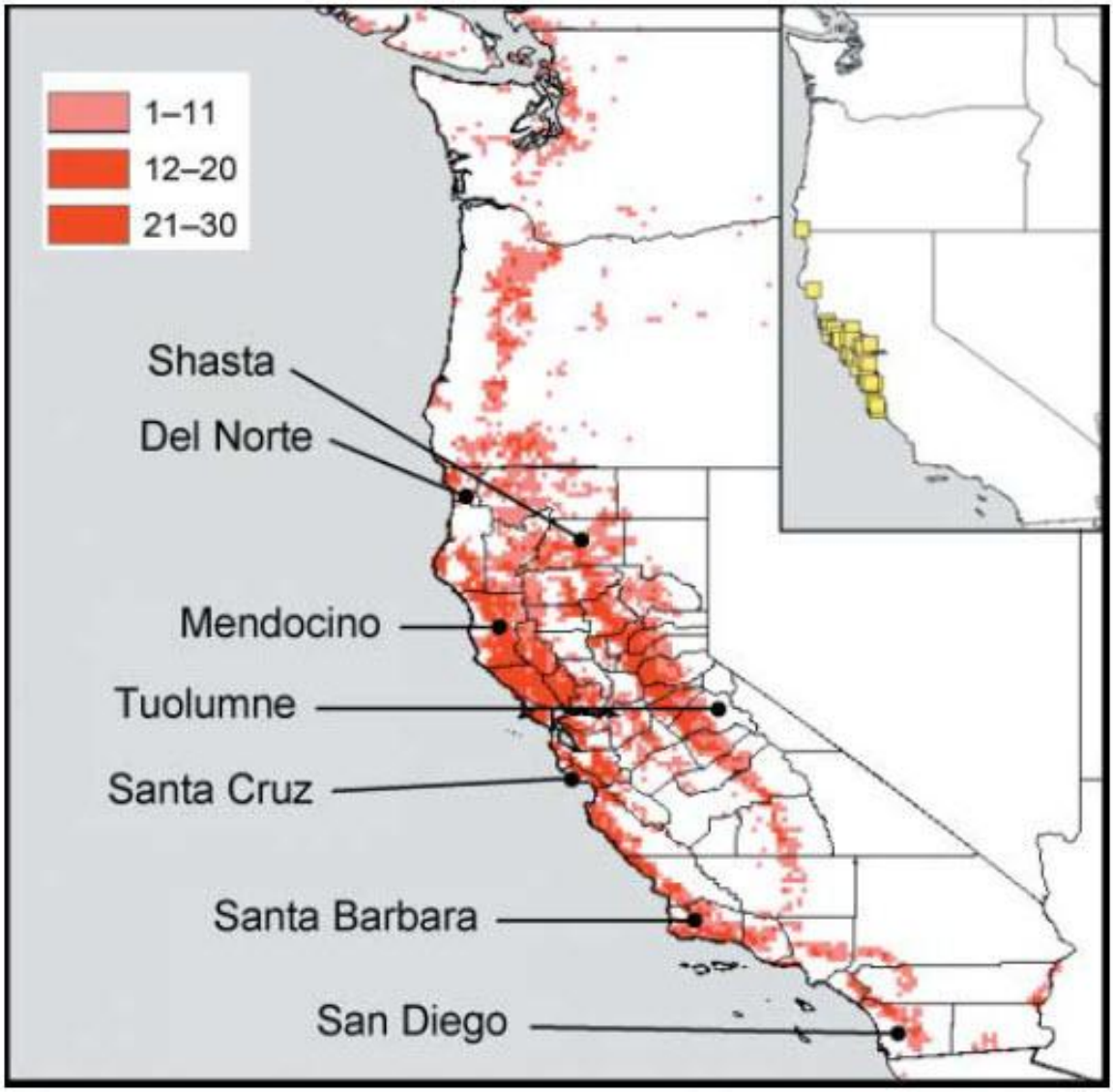

Figure 5 Risk for SOD distribution on the west coast. The value indicates the number of models used to predicted risk in that area. The inset shows confirmed infections as of 2007. Source: Kluza et al. (2007)

(Meentemeyer et al. 2004), which used Classification and Assessment with Landsat of Visible Ecological Groupings (CALVEG) and California Gap Analysis Project (GAP) data, was found to have underestimated the risk for many areas due to inexact vegetation mapping used as an input to the model. A 2005 study (Guo, Kelly and Graham 2005) also used the GAP dataset as one of their inputs, so may have similar problems.

High-resolution remotely sensed imagery can be useful for detailed land cover analysis. It can minimize mixed pixels and increase detail, but its cost can prevent use by organizations with small budgets, and the relatively small area covered by a single image makes it difficult to use for analyzing disease extant over a large scale. Two SOD studies were conducted using high-resolution aerial imagery to determine the severity of the SOD outbreak in localized areas. In the Big Sur area, Meentemeyer et al. (2008) manually digitized dead trees from 0.33 m resolution aerial imagery and calculated 20 percent mortality in infected areas. After field study, the researchers determined that counting dead trees at the canopy level underestimated overall mortality due to dead trees below the canopy and trees that had fallen over. In China Camp State Park in Marin County, Liu, Kelly and Gong (2006) used 1 m resolution Airborne Data Registration (ADAR) images to build a land cover classification model which would accurately identify dead trees due to SOD, but they discovered that bare areas and dead trees displayed similar spectral signatures, and that newly-leafed oaks have a low NIR value which can make them appear dead. Although high-resolution imagery minimizes the problem of mixed pixels, the researchers chose to smooth the results to minimize noise in the output. The moderate-resolution Landsat data used in this study have larger scene areas than aerial images, to better facilitate landscape analysis over an extended area, and a low cost for its use by cash-strapped organizations, but requires adjustment for mixed pixels with sub-pixel-sized features.

Remote sensing aerial monitoring is used to map current disease locations through the ADS. These surveys are collected by technicians in a moving aircraft who visually identify areas of decreasing forest health and mark them on a hand-held device. The quality of the results varies from year to year due to different operators collecting the data, and not all areas are updated annually. In addition, the data is only collected for regions where forest health changes are anticipated, so these surveys are unlikely to detect SOD outbreaks in new areas. However, these are a useful input to a study like this for results comparison.

2.3 Mapping of SOD

Very few maps exist online which show the extent of SOD. Those that do exist are small-scale and quickly outdated. One notable dynamic map which must be mentioned is the SODMAP by OakMapper, a sample of which is shown in Figure 6 (Kelly and Tuxen 2001, Kelly and Tuxen 2003, Kelly, Tuxen and Kearns 2004). This Google-Earth-based map displays locations of confirmed SOD infections maintained by the California Oak Mortality Task Force (COMTF). Data is updated annually and covers all of California. Unfortunately, the scale of the SOD epidemic is many times greater than the SODMAP shows. Since SODMAP relies on human observation and laboratory analysis, the majority of infections it shows are near roads or other easily-accessible areas. The results of a successful project like this could be used to build an online map showing the spread of SOD disease extent in the study area over the past 20 years, and the methodology could be adapted to create a map of SOD infection for the entire state. Although the locations would not be confirmed SOD infections, they would more realistically depict the extent of the epidemic.

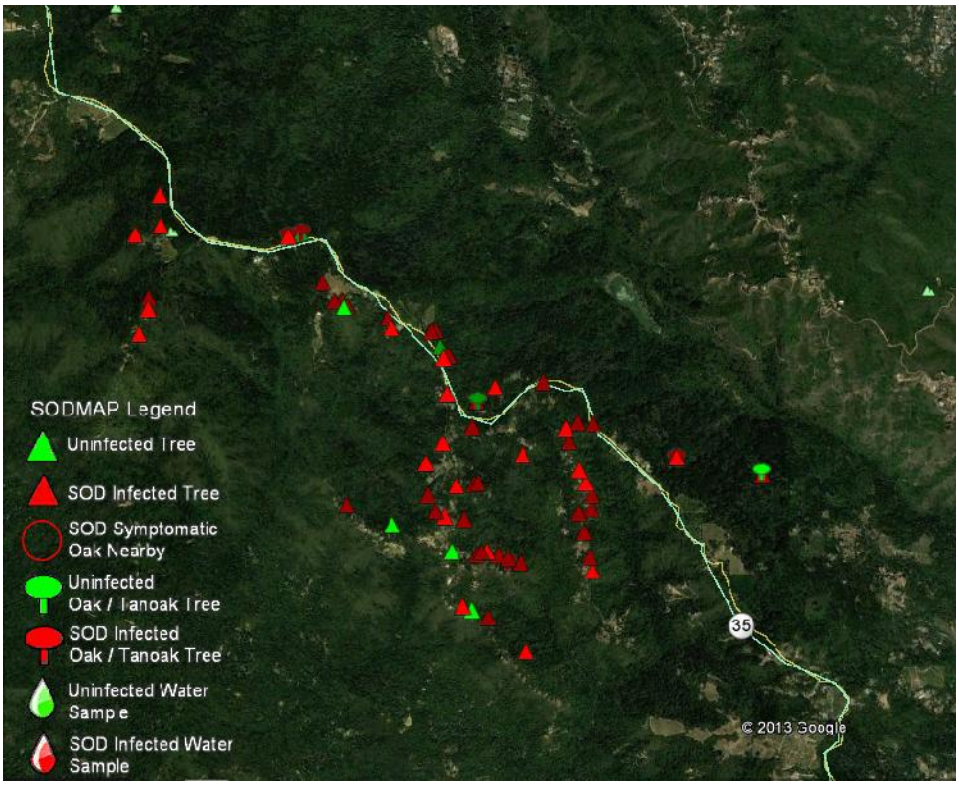

Figure 6 A sample image from SODMAP by Oakmapper, displaying PR-infected trees in the Santa Cruz Mountains
Source: Kelly and Tuxen (2003)

Remote sensing data and techniques have been used to build models of SOD disease risk, identify individual dead trees and conduct aerial surveys, but satellite data has not been used to map disease extent recently or identify progress over an extended period of time. This presents a unique opportunity to expand our knowledge of SOD using techniques like those described above. This study endeavored to find a methodology effective at identifying dead trees at the canopy level using remotely sensed data. A successful methodology, adapted to other areas, will make it possible to evaluate forest health on a large scale, quantify damage, discover SOD in areas where it was not previously noticed, identify risk areas that remain untouched, and lead to new discoveries.

CHAPTER THREE: DATA AND METHODOLOGY

This project's primary goal was to identify an index and range that successfully differentiated Landsat pixels containing healthy trees at the canopy level from those containing tree death, as a proxy for mapping trees killed by SOD, and to use that to map SOD spread since its discovery. This chapter describes the study area, the data and the methodology used for this research. Satellite scenes are the primary data source, supplemented by aerial images and additional raster and vector data which define the study area. The data section of this chapter discusses each of these sources in detail, as well as the limitations of the data, an understanding of which is necessary to avoid drawing unreasonable inferences from the results. The methodology followed is then described in detail, including data preparation, refining the study area, and choosing the most effective index for mapping SOD. A thorough understanding of the data and methodology will assist other researchers in interpreting these results, understanding their limitations, and adapting this process to map SOD in other regions.

3.1 Description of Study Area

This project's study area is the Santa Cruz Mountains in Central California (37° 08' N, 122° 8' W), a coastal mountain range on the San Francisco Peninsula, shown in Figure 7, with the dense urban areas of San Francisco and San Jose to the north, east and south. The climate is Mediterranean, with dry summers and wet winters, but fog often occurs on the west side of the range in summer. Elevation ranges from sea level to 3,786 feet (1,154 m), with many moderately steep valleys. Hilltops often are covered with grass and drought-resistant bushes, while valleys and lower elevations include conifers and broadleaf forests. Half of the area is state and county parkland and open space preserves, which enjoy heavy recreational use. The remainder is

privately owned, with scattered residences and isolated agricultural areas. The area of interest is 1,834 km^2, of which approximately 706 km^2 is forested. Many areas are steep and densely vegetated, with few roads or trails.

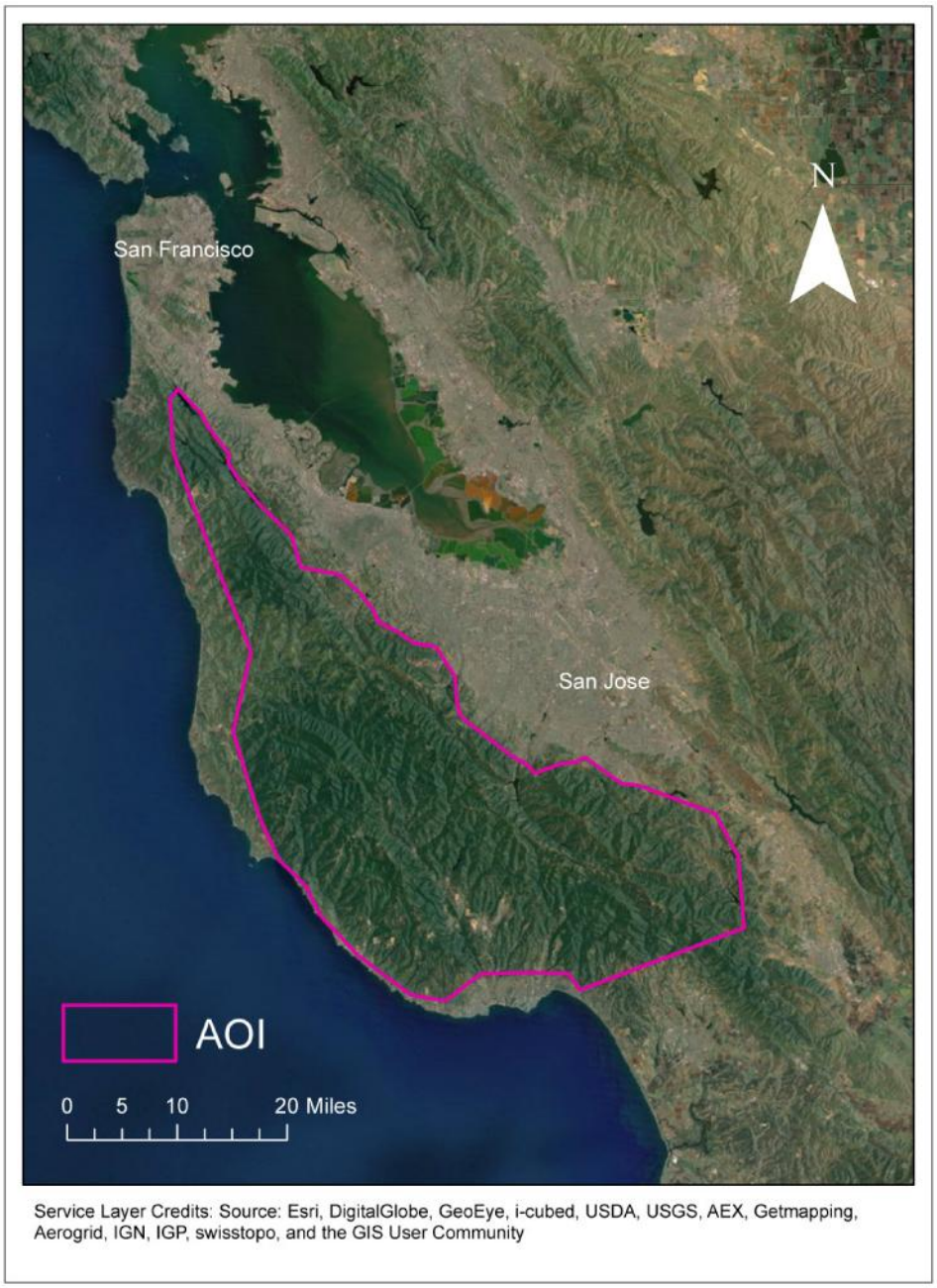

Figure 7 The area of interest in the Santa Cruz Mountains of central California

3.2 Data

This study utilizes raster and vector data, as shown in Table 2, to map the locations and spread of SOD from 1994 to 2011. The primary data source is Landsat CDR, supplemented by other sources which help refine the study area. NLCD raster data classifies land cover into forested and non-forested areas. FRAP polygons identify locations of recent wildfires, and ADS polygons map locations of tree damage due to multiple causes. These three data sets were used to create the study area, limiting it to forested areas without other known causes of change. In addition, for the purposes of sampling Landsat raster values, Land Cover Points and Results Validation Points were created and categorized based on May 2011 Google Earth Historical Imagery. All data was referenced to the North American Datum 1983 HARN California Teale Albers projected coordinate system (m), except for data displayed in Google Earth, which used the World Geographic System 1984. This section describes each data set used in this project and errors that the data may contain.

Table 2 Data used for this analysis

Description	Type	Data sets used	Creator
Landsat CDR Reflectance images	Raster	1992-2011	USGS
National Land Cover Database (NLCD) polygons	Raster	1992, 2011	USGS
Fire and Resource Assessment (FRAP) polygons	Vector	1985-2012	CalFire
Aerial Detection Survey (ADS) polygons	Vector	2005-2013	USDA
Google Earth Historical Imagery	Raster	May 1, 2011	Google
Land Cover Points	Vector	May 1, 2011	Trinka Gillis
Results Validation Points	Vector	May 1, 2011	Trinka Gillis

3.2.1 Landsat Satellite Data

Landsat CDR images were the primary data source for this project. Landsat 5 Thematic Mapper (TM) satellite images collect seven bands of data, detailed in Table 3, covering non-polar Earth with repeat collection every 16 days (DOI-USGS 1989-2011). Bands 1-5 and 7 were used for this study. CDR images are created from Landsat Level 1 images, which are systematically

Table 3 Landsat 5 TM bands

Band	Wavelength (μm)	Resolution (m)	Common Uses
Band 1 - Blue	0.45-0.52	30	Measures visible blue light. Useful for mapping sediment, coastal habitats, water depth, and distinguishing soil/rock/vegetation.
Band 2 – Green	0.52-0.60	30	Measures visible green light. Useful for identifying vegetation and measuring plant health
Band 3 – Red	0.63-0.69	30	Measures visible red light. Vegetation absorbs red light, so it produces low values in this band. Useful to distinguish vegetation, soil, and vegetation health.
Band 4 – Near Infrared	0.77-0.90	30	Water absorbs most light in this wavelength, producing low values, while soil and vegetation produce high values. Useful for distinguishing water, vegetation varieties, soil/crop/water contrasts
Band 5 - Short-wave Infrared	1.55-1.75	30	Sensitive to moisture. Useful to measure soil and vegetation moisture content, clouds and snow.
Band 6 – Thermal Infrared	10.40-12.50	120	Measures surface temperature. Useful for geology, measures plant heat stress, locates clouds.
Band 7 – Short-wave Infrared	2.09-2.35	30	Similar to band 5, measures moisture. Distinguishes water/soil/rock.

Source: Quinn (2001), DOI-USGS (1989-2011), Geospatial Innovation Facility UC Berkeley and Center for Biodiversity and Conservation (2003)

corrected for geometric and radiometric accuracy using ground control points, with a DEM used for topographic accuracy (DOI-USGS 2014). CDR images are further corrected to surface reflectance values using Moderate Resolution Imaging Spectroradiometer (MODIS) formulas to remove atmospheric distortion caused by water vapor, ozone, geopotential height, aerosol optical thickness and elevation (DOI-USGS 2013). The CDR images used in this project are all classified as LIT, indicating standard terrain correction. Reflectance images facilitate comparison between data sets collected at different times of day and under different weather conditions. This study used WRS2 path 44 row 34 images, which contain the entire study area, and favored April and May images to avoid spectral confusion caused by early-senescing California buckeye and newly-leafed oaks, both of which can be spectrally confused with dead trees. Images from 1992-2011 were used, as shown in Table 4. The number of ground control points used for the geometric correction, and the resulting Root Mean Square Error (RMSE) are also summarized in Table 4. All images had maximum 10 percent cloud cover.

Unfortunately, 2011 was the last year that acceptable springtime Landsat 5 images are available for this area. If this methodology were to be applied to later data, Landsat 7 and Landsat 8 scenes would need to be used. Landsat 7 data is available from 1999 to the present in CDR format, but scenes collected after May 2003 have a striping issue due to a failed Scan Line Corrector (SLC). Landsat 8 was launched in 2013, but is not yet available in CDR format. This project therefore relied exclusively on Landsat 5 data.

The 2011 Landsat image was used as the basis for all this project's calculations. To facilitate comparison and analysis, eight indices were calculated using ArcMap Raster Calculator. Values for five of the indices – NDVI, SWIR/NIR, NDMI, RGI and NBR – were

Table 4 Landsat 5 TM scenes used in project (path 44 row 34)

Imagery Date	Ground Control Points	Geometric RMSE (m)
April 6, 1992	143	4.387
June 12, 1993	218	3.525
March 11, 1994	153	4.583
March 30, 1995	154	3.798
May 3, 1996	183	3.687
April 4, 1997	194	3.446
June 26, 1998	221	3.151
June 29, 1999	242	2.793
April 28, 2000	184	3.575
May 1, 2001	203	3.501
June 5, 2002	223	3.235
April 5, 2003	N/A	N/A
April 23, 2004	197	3.511
April 10, 2005	169	3.919
June 16, 2006	216	3.443
April 16, 2007	190	3.776
June 5, 2008	215	3.193
May 7, 2009	182	3.825
April 24, 2010	155	3.766
April 27, 2011	151	3.766

multiplied by 1,000 to preserve data precision. Values for Tasseled Cap indices were calculated and used in their original form.

The 2011 Landsat image was used as the basis for all this project's calculations. To facilitate comparison and analysis, eight indices were calculated using ArcMap Raster Calculator. Values for five of the indices – NDVI, SWIR/NIR, NDMI, RGI and NBR – were multiplied by 1,000 to preserve data precision. Values for Tasseled Cap indices were calculated and used in their original form.

Although Landsat CDR images are geometrically and radiometrically corrected, pixels from different years do not align and pixel values vary for the same location over different years. Measures of geometric distortion for each image are indicated by the RMSE values in Table 4. Pixels could have been aligned, and values could have been normalized for this project, but to do

so would introduce additional error. To facilitate location comparison of pixels, all were converted to centroid points and were evaluated using proximity functions. Other common errors with Landsat data include missing pixels and saturated bands.

3.2.2 National Land Cover Database Classified Raster Data

This project used 1992 and 2011 National Land Cover Database (NLCD) classified raster data to construct a study area. The NLCD is produced by the USGS to characterize land cover and monitor changes throughout the US, and is now updated every five years. Using Landsat data as its primary source, the NLCD categorizes land cover into 16 classes listed in Table 5, using a decision tree model with training points, and an algorithm which merges cover types to preserve land cover logic.

Table 5 NLCD land cover classes

Land Cover Classification
Open Water
Perennial Ice/Snow
Developed, Open Space
Developed, Low Intensity
Developed, Medium Intensity
Developed, High Intensity
Barren Land (Rock/Sand/Clay)
Deciduous Forest
Evergreen Forest
Mixed Forest
Shrub/Scrub
Grassland/Herbaceous
Pasture/Hay
Cultivated Crops
Woody Wetlands
Emergent Herbaceous Wetlands

Note: Four additional classes were used in Alaska only
Source: Jin et al. (2013)

There are several sources of inaccuracy in the NLCD. Although the classification is conducted at the pixel level, classification of mixed pixels is a problem, and smoothing the result to create more consistent land cover decreases accuracy. Errors can be observed by laying the NLCD data over a high resolution aerial photo. The creators have allowed for ambiguity, however, in the category descriptions. For example, forest categories are described as containing a minimum of 20 percent total vegetation of trees greater than 5 m tall, with more than 75 percent of species matching the category description. This allows up to 80 percent of land cover to be small trees and up to 25 percent to be types not described by the category. Because of the generalized categorization and observed inaccuracies, this data set was not sufficient to define the study area without supplemental resources.

3.2.3 Fire and Resource Assessment Program Vector Data

This project also used the Fire and Resource Assessment Program (FRAP) polygons to identify areas burned in wildfires and prescribed fires in 1985 or later, and remove them from the study area. This step was included to prevent the changed spectral response of dead trees in burned areas from incorrectly being mapped as SOD. The California Department of Forestry and Fire Protection (CalFire) maintains a comprehensive FRAP database, last updated in 2012, which includes fire data gathered by CalFire, the USDA Forest Service Region 5, the Bureau of Land Management (BLM), the National Park Service (NPS), certain counties, and other agencies.

Although the FRAP database attempts to track all wildfires and prescribed fires 10 acres or larger on all public and private lands in California, inaccuracies occur due to the differing standards of the reporting agencies. The year that an agency began collecting data, the minimum

size of fire that they report, the data creation method and accuracy of the polygons vary. Observed errors include perimeters which truncate at administrative boundaries and duplicate fires reported by multiple agencies.

3.2.4 USDA Aerial Detection Survey Vector Data

The ADS polygons indicating tree damage due to causes other than SOD were used to refine the study area. ADS polygons are created by the USDA through summer aerial surveys which detect and map tree mortality and damage. Surveyors in an aircraft flying 1,000 feet above ground level mark areas of tree damage and cause on a hand-held device. The resulting polygons are used to report on status of known threats, and to estimate acreage and number of trees affected (USDA-FS Forest Health Monitoring Program 1978-2013, Heath et al. 2012, USDA-FS Pacific Southwest Region 2014). The USFS decides annually which regions or diseases to focus on, but SOD is often a main concern. ADS data is available for 1978-2013, but collection was erratic and polygons were highly generalized prior to 2005, so this project only uses data from 2005 onwards.

The ADS polygons and attributes associated with them are fuzzy, subject to the experience, training and subjective opinion of the surveyor, as well as the sun angle and viewing window. Polygons from different years often overlap. Researchers mapping tree health in New Mexico (Vogelmann, Tolk and Zhu 2009) found that areas mapped as damaged by the ADS for multiple years correlated to damage severity, but areas mapped by the ADS as damaged in only a single year were unreliable, possibly due to the use of inexperienced mapping technicians.

3.2.5 Google Earth Historical Aerial Imagery

This project also used a Google Historical Imagery dataset from May 1, 2011, with sub-meter natural color imagery, to verify the land cover type and tree health in spring 2011. Google maintains a database of historical imagery within Google Earth, displayed with a terrain model. The type of imagery, the quality, and the area covered varies. Images with no source identified in Google Earth are Google copyright and are often high quality. Images cannot be exported, but ArcMap shape files can be converted to the WGS84 projection and displayed within Google Earth. The capture date of this Google high-quality aerial imagery is ideal for visualizing the canopy land cover at the time of the April 27, 2011 Landsat scene used as the base data set for this project.

Misalignments of up to 2 m have been observed when comparing Google imagery from different dates, but these displacements are not large enough to affect classification for this project.

Although National Agricultural Imagery Program (NAIP) aerial images created by the USDA Farm Service Agency could have been used, preliminary work revealed that those images were often overexposed or captured with a low sun angle, both of which caused color distortion that caused healthy trees to appear dead.

3.2.6 Land Cover Points

To identify spectral ranges for each land cover type in the study area, Land Cover Points were created, randomly and manually, at least 45 m apart. The points were projected to WGS84 to display in Google Earth with May 2011 imagery. The Google Earth imagery was used to categorize each point into one of the classes shown in Table 6, with the location of the 2011

Landsat pixel relative to the point taken into consideration when assigning a classification. Locations with mixed pixels other than those examples mentioned below were discarded. The distinction between minor and serious tree death (SD) was necessary to obtain values which clearly distinguished healthy areas from dead trees in later processing. Although no pixels contained more than 40 percent dead trees, pixels which contained less than 10 percent dead trees produced a spectral signature similar enough to healthy forest that including them in a single land cover type with a larger canopy area of dead trees blurred the distinction between the classes. This project's goal was to identify and map only the serious tree death.

Although care was taken to consistently and correctly classify the land cover types, the classification process was, inevitably, subject to some operator error.

3.2.7 Results Validation Points

To evaluate the efficacy of the Landsat image classification, 300 results validation points were randomly generated throughout the refined study area. These points were displayed over the May

Table 6 Land Cover Points classification categories

Code	Description	Points
10	Agricultural land	4
20	Barren land	31
30	Herbaceous	44
40	Healthy forest	68*
51	Minor death (forest with <10% dead trees as percentage of pixel area)	26
52	Serious death (forest with >10% dead trees as percentage of pixel area)	33
60	Shrubbery	66
70	Buildings (mixed pixels included)	24
80	Road (mixed pixels included)	20
90	Water	16
Total		301

* A random subset of 33 points was used to compare to an equal number of points classified as serious tree death.

2011 Google Earth image, as described above, and assigned a land cover code shown in Table 7, taking into account the relative location of the 2011 Landsat pixel. Approximately 10 percent of the randomly generated points were classified as SD and 68 percent were classified as healthy tree land cover (HLH).

Although care was taken to correctly classify the land cover types, the classification process was subject to operator judgment on the approximate location of the pixel and the percent of pixel covered by dead trees.

Table 7 Results Validation Points within study area

Class	**Code**	**Number of Points**
Healthy trees	0	204
Minor death (< 10% of pixel area)	1	37
Serious death (>10% of pixel area)	2	31
Mixed land cover classes	9	28
Total		**300**

3.3 Methodology

In addition to data sourcing and preparation, work on this project consisted of refining the study area to remove non-forested areas from consideration, identifying the index most effective at distinguishing dead tree areas from healthy forest, validating results, and extrapolating the chosen index and range to the entire study area. An outline of the workflow that was deployed is shown in Figure 8. To refine the study area, a mask was created from three types of data – recently burnt areas, areas identified as having tree diseases other than SOD, land cover identified as non-forest – and supplemented by raster data identifying non-forest land cover. An analysis of Landsat band ratios was used to determine the most effective index for identifying

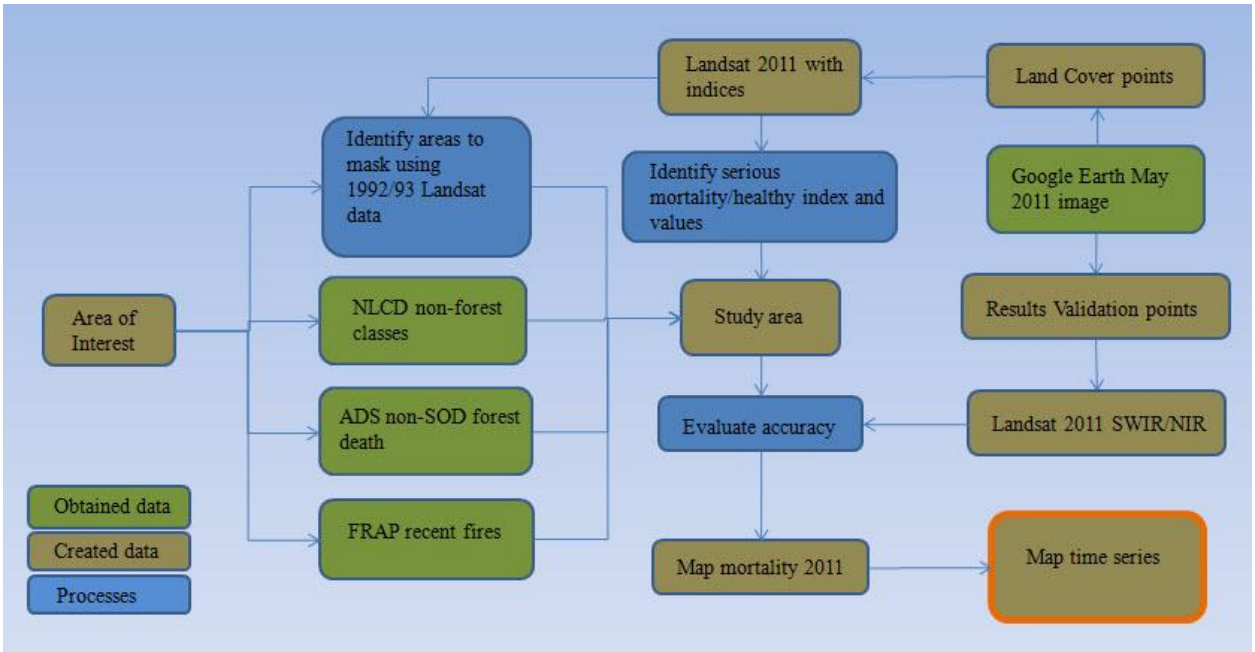

Figure 8 The methodology for data extraction and analysis that was created and used for this project

dead trees, and this result was applied to multiple years of imagery to map the spread of SOD over time.

3.3.1 Refining the Study Area

This project's Area of Interest was the Santa Cruz Mountains. Preliminary results demonstrated that shrub land cover shared spectral ranges with areas of dead trees. To minimize false identification of dead trees, this project needed to develop an accurate land cover mask that would limit the study area to only forested land.

The basis for the mask was the 1992 and 2011 NLCD classified raster data, from which the non-forest categories were converted to polygons. The combination of early and late NLCD data sets was used to more effectively mask out land use changes that occurred during the period of the study. These layers failed to remove all non-forested areas from the study area.

Large-area land cover classifications, such as NLCD, seek to classify all land cover in the US into a small number of classes, and seek to minimize noise. Because of this, small areas of one type of land cover, pixels on the edge of other land covers, and mixed pixels are often merged with other classes, all of which created problems for this study. Observations of the NLCD data overlaid over an aerial image, a sample of which is shown in Figure 9, reveals that many non-forested areas were incorrectly classified as forest. Edges of land cover types are generalized and often contain vegetation which could cause inaccurate results. As a result, a mask created from NLCD non-forest categories does not remove all non-forested areas from the study area. This project used the NLCD as the primary land cover classification, but it needed to be supplemented by other data to remove shrub from the study area and increase confidence in the final results. This was accomplished using Landsat raster data.

To remove as much shrubbery from the study area as possible, it was necessary to identify the index applied to Landsat data which best differentiated healthy trees and shrubs in this environment. Using the Land Cover Points described above, the Extract Values to Points and Zonal Statistics as Table tools were used to extract raster values for each index based on the Landsat 2011 scene. The mean and standard deviation values of each land cover class produced significant overlap. Instead, the histograms representing healthy trees and shrub land cover types were visually compared, as in Figures 10 and 11, to determine which ranges captured the most values. Histograms for NBR, SWIR/NIR and TC Wet, displayed in Figures 10-15, showed the best separation between the two classes. An analysis of possible differentiation ranges, shown in Table 8, showed that NBR with values greater than 640 was the most effective range to separate healthy forest from shrub. When applied to the Land Cover Points set, this value removed 92 percent of the shrub points and only 4 percent of the healthy tree points.

Figure 9 The NLCD classification did not adequately remove non-forested areas from the study area. Areas outlined in white were identified as non-forest classes using the NLCD 1992 and 2011 layers. This sample shows many non-forested areas were not correctly classified.

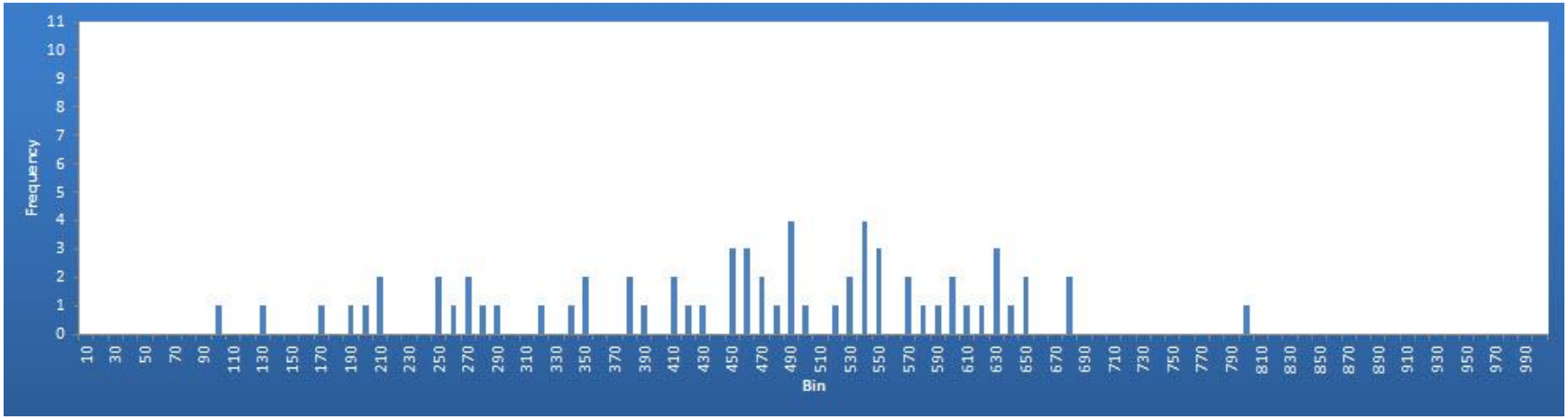

Figure 10 The NBR Land Cover Points histogram for shrubs

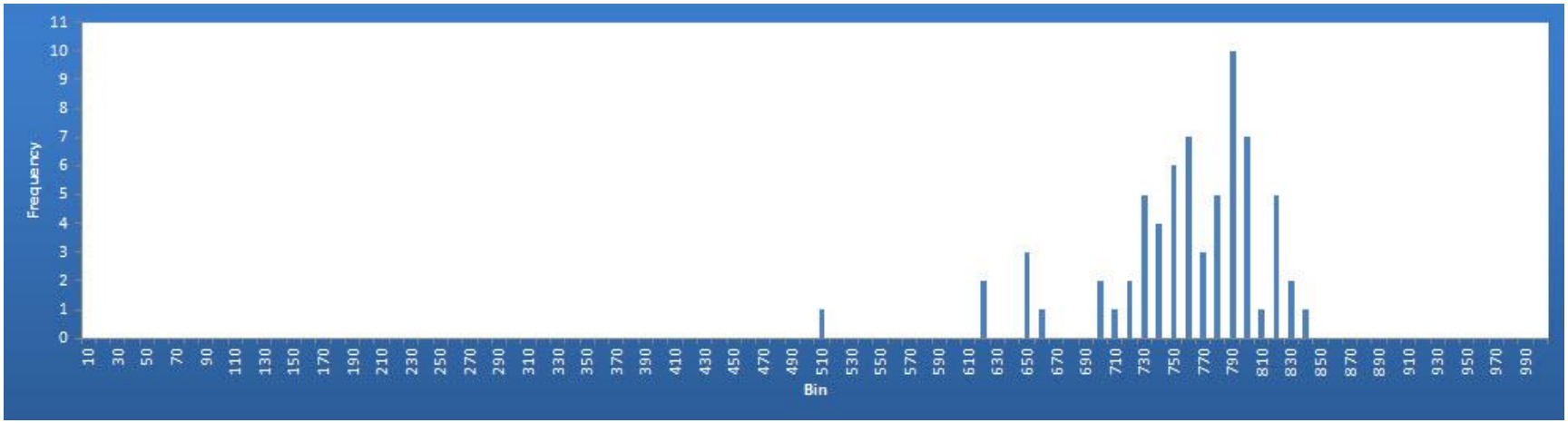

Figure 11 The NBR Land Cover Points histogram for healthy trees

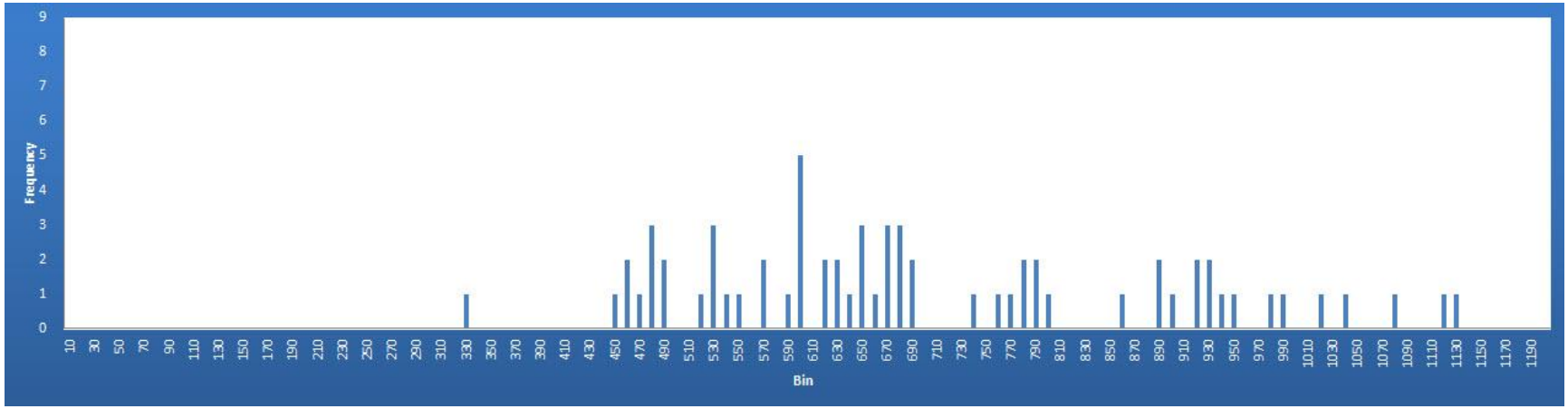

Figure 12 The SWIR/NIR Land Cover Points histogram for shrubs

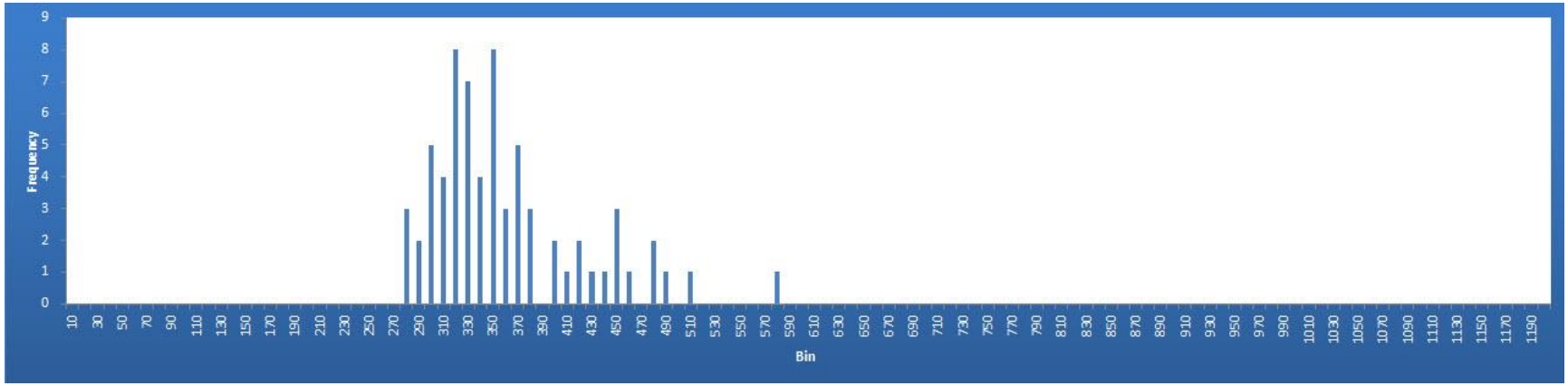

Figure 13 The SWIR/NIR Land Cover Points histogram for healthy trees

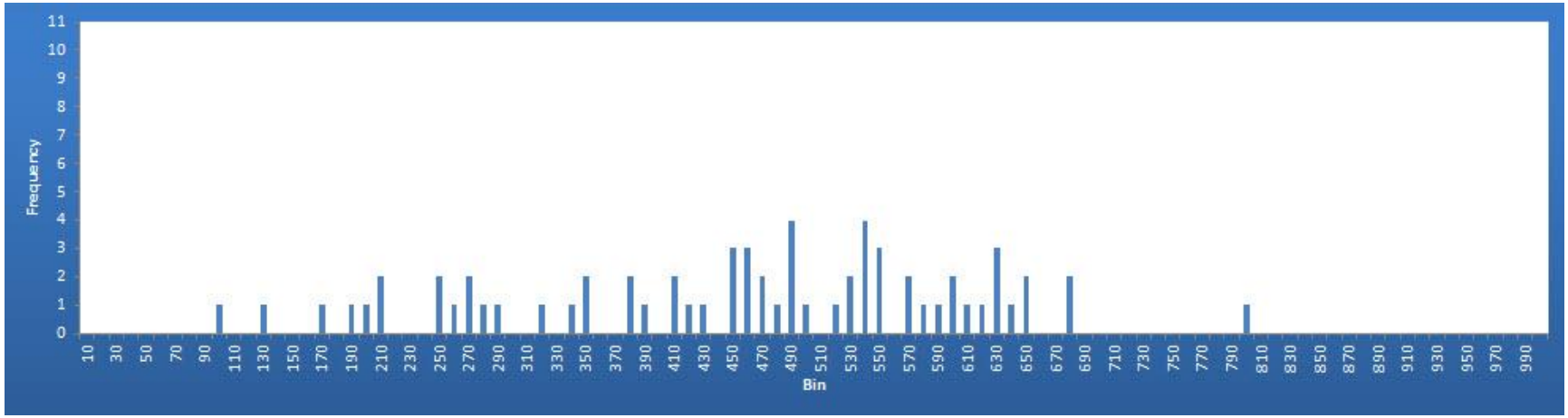

Figure 14 The NBR Land Cover Points histogram for shrubs

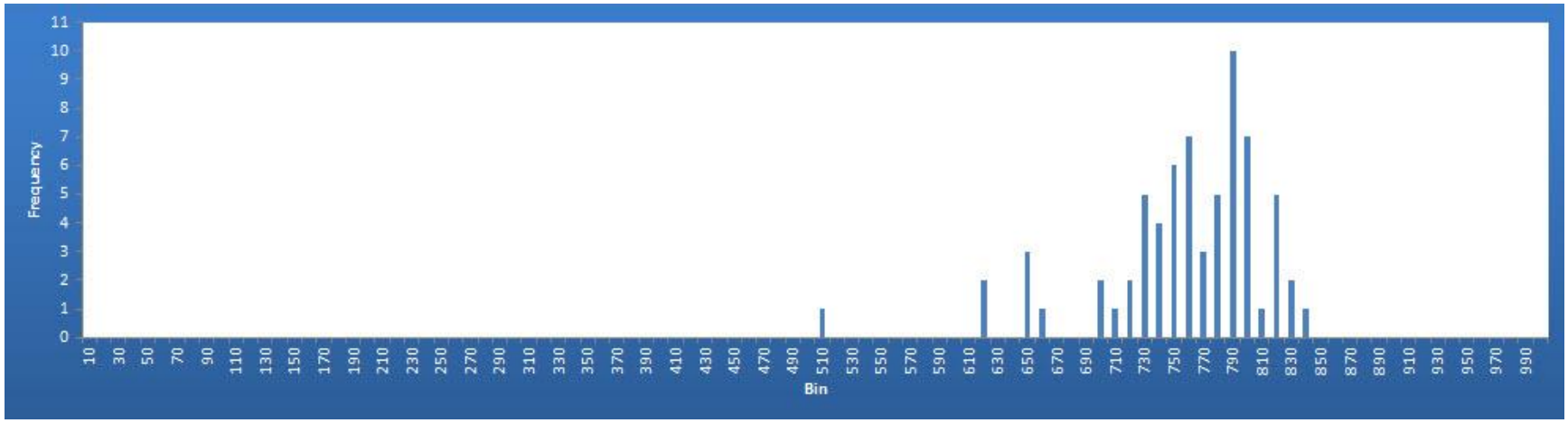

Figure 15 The NBR Land Cover Points histogram for healthy trees

Table 8 Indices and value ranges tested to determine which one best masked shrub without masking healthy trees. The ranges indicate the values used to map healthy trees.

	NBR =>640	SWIR/NIR =<510	SWIR/NIR =<460	TC WET =>-450	TC WET =>-560
Shrub masked	92%	85%	94%	97%	82%
HLH masked	4%	1%	7%	12%	3%

Using the ranges identified, the 1992 and 1993 CDR Landsat images, which had already been converted to NBR, were reclassified to identify all pixels with values lower than 640, and this area was converted to new polygons to be added to the mask. An example of this is shown in Figure 16. Although land cover categories representing dead trees fall between the ranges indicating healthy trees and shrub, and may be partially masked out by this method, these values were applied to Landsat images representing years before SOD is believed to have taken hold. If SOD was present in the forest before its discovery in 1994, it was in insignificant amounts. The layers created from this process were added to the mask to remove shrubbery and refine the study area.

Fire data and areas of other tree damage were also part of the mask. To remove recently burned areas from the study area, likely to contain dead trees which are not due to SOD, FRAP polygons were used. Two files were created: one containing all wild fires in the area which occurred in 1985 or later, and one containing all prescribed fires in the area, none of which occurred prior to 1985. To remove other causes of tree death from the study area, ADS 2005 to 2013 polygons with tree threat attributed to causes other than SOD were added.

The final study area was defined as the AOI less the areas masked out: non-forest NLCD data, the 1992 and 1993 Landsat shrub layers, FRAP fire polygons, and ADS disease polygons. By carefully shaping the study area, it was hoped that the final results would be more accurate.

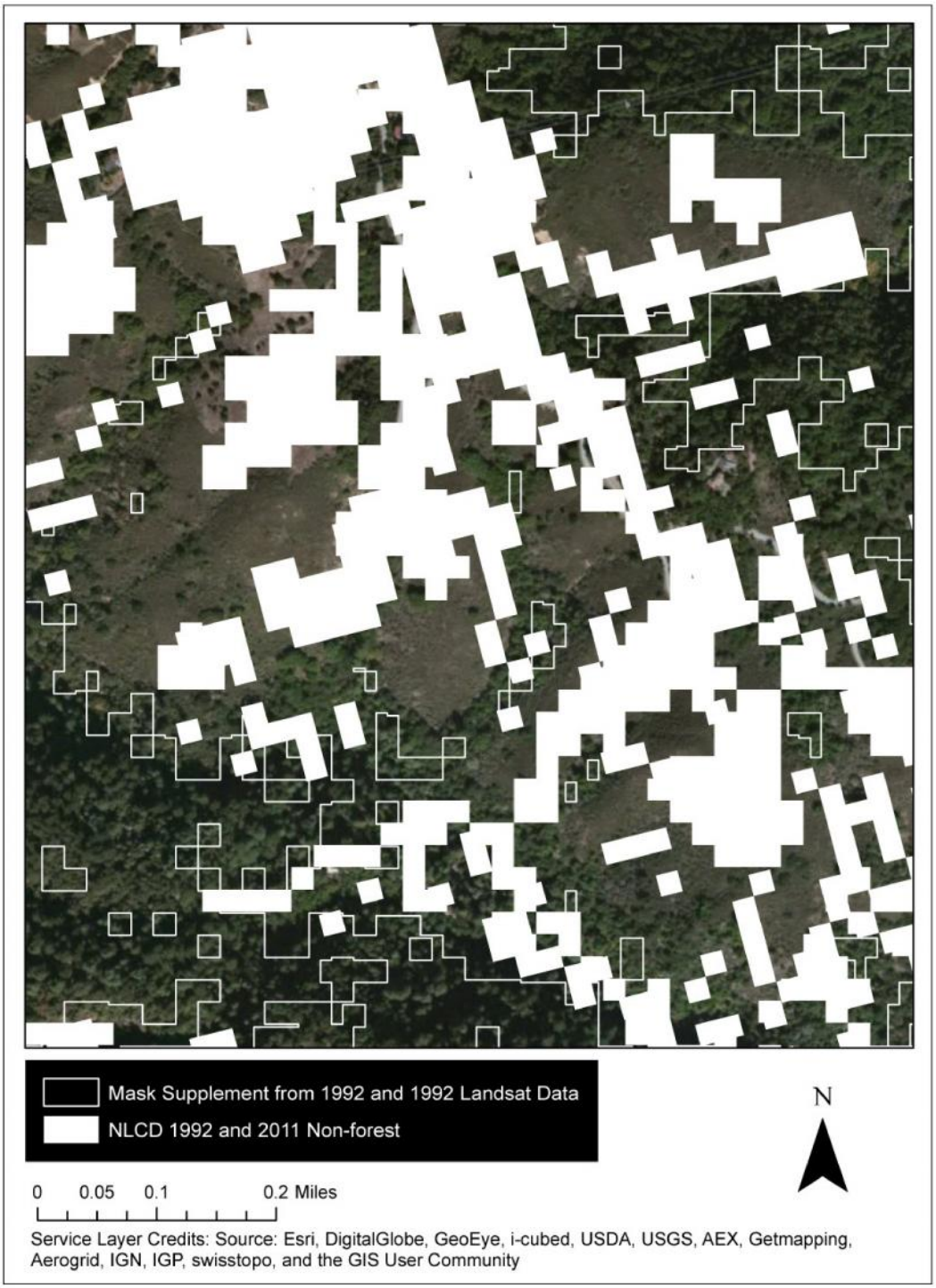

Figure 16 The NLCD non-forest layers, shown in solid white, were not sufficient to limit the mask to only forested areas. Landsat 1992 and 1993 data, used to supplement the mask, removed all white-outlined areas from the study area. Figure 9 shows the NLCD non-forest layers without the supplemental mask.

3.3.2 Identifying the Most Effective Index and Mapping 2011 Affected Areas

The premise of this project was that one could differentiate healthy tree canopy from areas of SD using Landsat data with an appropriate analysis index. Once the final study area was determined, it was necessary to select the formula and index to map tree death. The final step was to apply the chosen formula to the study area to map SOD infection.

The process of choosing an index to differentiate SD from HLH was similar to that used for shrubs. The mean and standard deviations showed too much overlap, so histograms were created to determine the index and ranges which captured the most points from each class while minimizing points from other classes. This project sought a formula that would accurately identify at least 60 percent of points in each class. Test value ranges were based on a comparison of histograms, shown in Appendix B, graphing spectral signatures of the full set of 33 SD points with a randomly-chosen subset of 33 HLH points. The SWIR/NIR, (Figures B1 and B2), NBR (Figures B3 and B4), NDMI (Figures B5 and B6), NDVI (Figures B7 and B8) and TC Wet (Figures B15 and B16) indices showed the best possibilities for differentiating these two classes with a minimum of overlap. Test ranges were compared to index raster values to identify the index and range which captured the maximum number of SD points and a minimum number of healthy points. Over 50 ranges, indices and combinations were tested and the three best results are shown in Table 9. Composite formulas which used two or more indices based on the OR function (if either index marks this point as SD, mark it as SD) increased false positives when compared to formulas using a single index, and composite formulas based on AND (mark this point as SD only if all other indices mark it as SD) increased false negatives. Formulas based on narrower ranges, even when combined with other formulas, created more false negatives because

the narrow ranges missed the same outliers. The best formulas were found by looking closely at the histograms and testing many ranges and indices against the index values.

Indices SWIR/NIR, NBR and a composite of the two had test ranges with errors less than 20 percent (Table 9), but the NBR index and range showed the most accurate SD classification with a low level of false positives, correctly categorizing 88% of points in both classes. These three indices and ranges were then compared to the Results Validation Points to measure accuracy and confirm that the same range was still the best choice when applied to the entire 2011 data set

Table 9 Three indices and value ranges compared to determine which one best differentiated SD from HLH

	SWIR/NIR 400-570	NBR 575-725	OR Combination
% SD Correct	85%	88%	91%
% HLH Correct	85%	88%	85%
SD Omission	15%	12%	9%
HLH Omission	15%	12%	15%
SD Map Accuracy	74%	78%	79%
HLH Map Accuracy	74%	78%	78%

3.3.3 Accuracy Assessment

The mapping results were assessed for accuracy by applying the formula to the Results Validation Points, and the most accurate index and range was applied to the time series to map SD change over time.

The Results Validation Points, described above, were used to extract the value of the containing pixel from the 2011 Landsat image with each index calculated. Tables 10, 11 and 12 show the error matrices for these three formulas upon application to the Results Validation Points. Although the NBR formula looked slightly more accurate when applied to the Land

Cover Points, it shows more false negatives and false positives when compared to the SWIR/NIR formula. The combination formula has more false positives than either of the other formulas. The SWIR/NIR formula is the best of the three, with 69% tree health mapping accuracy and 24% SD mapping accuracy. Based on these matrices, this project used the SWIR/NIR index with a range of 400-570 to map SD in the study area.

The SWIR/NIR index and range described above was used to classify the study area using the Landsat 2011 image. To facilitate comparison of non-aligned raster pixels, all pixels in the range were converted to centroid points, and all points that fell outside of the mask were considered to represent SD. The resulting 2011 SD layer, shown later in Figure 17 (as part of Chapter 4), is the map of SOD extent in 2011 produced using the methodology that was created and deployed for this project. The SWIR/NIR index was calculated for the 1994-2010 Landsat

Table 10 Error matrix for SWIR/NIR index applied to Results Validation Points with range of 400-570 classified as SD

	Observed Data				
Classification	**Tree Health**	**Serious Tree Death**	**Row Total**	**User Accuracy**	**Commission Error**
Tree Health	148	10	**158**	**94%**	**6%**
Serious Tree Death	56	21	**77**	**27%**	**73%**
Column Total	**204**	**31**	**235**		
Producer's Accuracy	**73%**	**68%**			
Omission Error	**27%**	**32%**			
Map Accuracy – Tree Health			**69%**		
Map Accuracy – Serious Tree Death			**24%**		

Table 11 Error matrix for NBR index applied to Results Validation Points with range of 575-725 classified as SD

Classification	Observed Data: Tree Health	Observed Data: Serious Tree Death	Row Total	User Accuracy	Commission Error
Tree Health	143	12	**155**	**92%**	**8%**
Serious Tree Death	61	19	**80**	**24%**	**76%**
Column Total	**204**	**31**	**235**		
Producer's Accuracy	**70%**	**61%**			
Omission Error	**30%**	**39%**			
Map Accuracy – Tree Health			**66%**		
Map Accuracy – Serious Tree Death			**21%**		

Table 12 Error matrix for OR Combination of NBR 575-725 and SWIR/NIR 400-570 indices applied to Results Validation Points

Classification	Observed Data: Tree Health	Observed Data: Serious Tree Death	Row Total	User Accuracy	Commission Error
Tree Health	135	7	**142**	**95%**	**5%**
Serious Tree Death	69	24	**93**	**26%**	**74%**
Column Total	**204**	**31**	**235**		
Producer's Accuracy	**66%**	**77%**			
Omission Error	**34%**	**23%**			
Map Accuracy – Tree Health			**64%**		
Map Accuracy – Serious Tree Death			**24%**		

CDR scenes, and the same 400-570 value range was applied to map the extent of SOD for each year. The final result was 18 maps, shown in Appendix C, one for each year 1994-2011.

3.4 Summary

This chapter presented the data and methodology used in this study, so other researchers can understand the preparation, processes followed, and methods of obtaining results. Crucial to the explanation of data sources was the discussion of sources of data error. No GIS data set is without errors, and understanding the limitations of each data set is important for interpretation of results. Construction of an accurate study area was complex, but was critical to clarifying the accuracy of the results and the accompanying interpretation of their significance for the problem at hand.

The next chapter will present the results of this process, including maps, an analysis of accuracy, and a discussion of trends and patterns.

CHAPTER FOUR: RESULTS

Chapter three described the methodology followed in this project, which created maps of canopy-level serious tree death for the Santa Cruz Mountains from 1994-2011. The project produced 18 maps, one for each year of the study, showing areas identified as canopy level tree death based on the SWIR/NIR index created from Landsat CDR scenes. The complete sequence of maps is provided in Appendix C. This chapter discusses the mapping highlights and evaluates accuracy of the final product.

4.1 Mapping Results

This project created maps for the first 18 years that SOD was known in the study area (Appendix C). These maps were used to identify areas of tree death as a means to discover areas infected with SOD, approximate the extent of contagion, and to compare areas of infection identified by the project results with known locations of SOD infection.

4.1.1 Map of Serious Tree Death in 2011

The 2011 map of serious tree death, in Figure 17, shows tree death is present throughout most of the study area, and especially dense on the more populated east side of the study area. Three areas – Areas A, B and C – contain notably fewer dead trees than other areas. These areas will be discussed in more detail below.

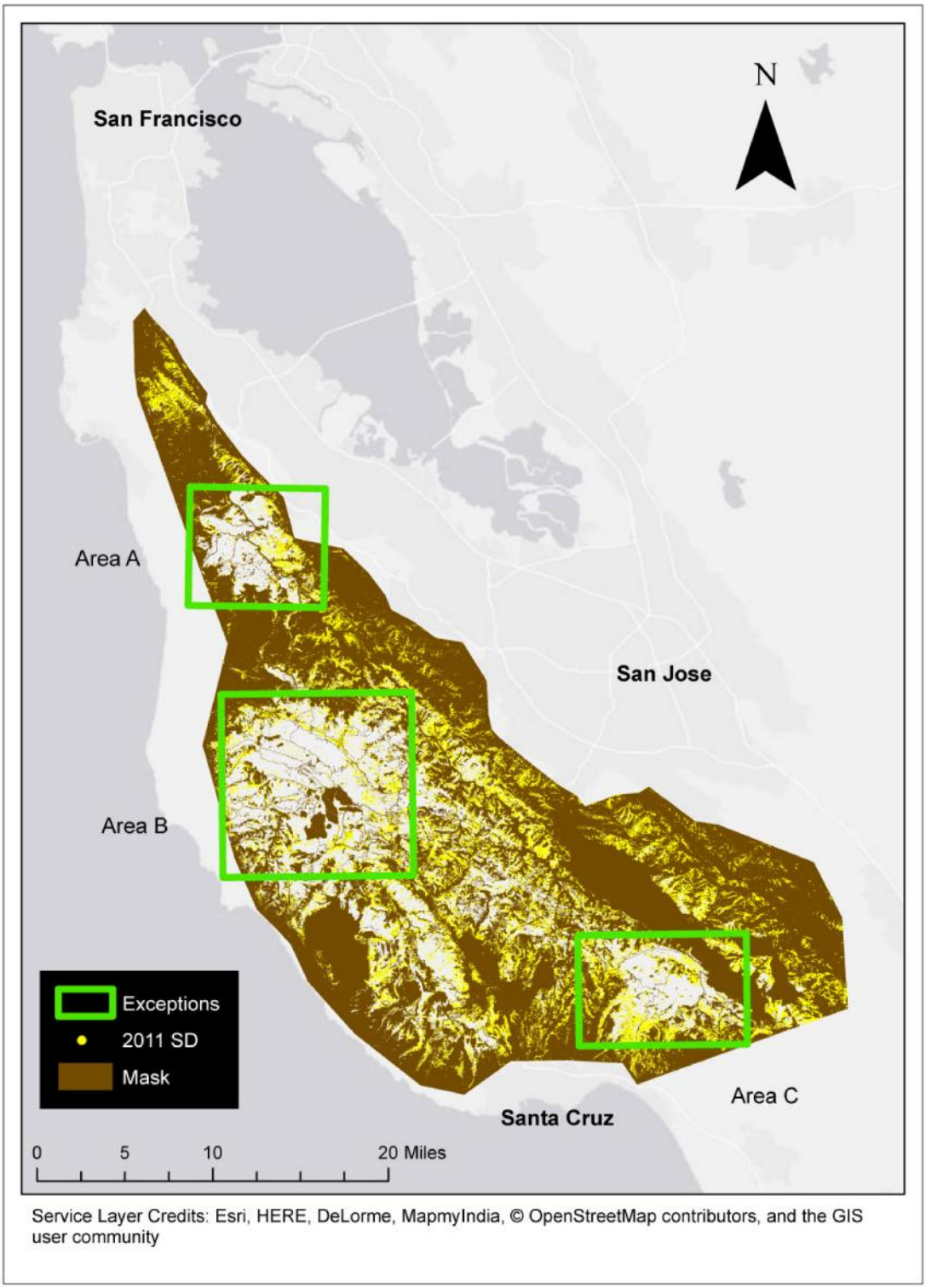

Figure 17 The 2011 SD extent in the study area. Areas with lower rates of tree death – Areas A, B and C – are marked in green.

This methodology classified 27 percent of pixels in the study area as containing dead trees in 2011, with the highest density on the east side of the study area. These slopes are generally east-facing, which may influence moisture or vegetation which makes the ecosystem more susceptible to SOD. These areas are also more densely populated than other parts of the study area. Consequently, they may be at increased risk of SOD due to more accessible, therefore heavier, recreational use, and proximity to homes in the interface zone which introduced the infection via nursery plants. A 27 percent infection rate is much higher than expected and may be a sign of inaccurate results.

Three areas stand out in this map for their relative lack of dead trees detected by this methodology. Area A, shown in Figure 17, straddles the ridge between Redwood City and the Pacific coast. This west-facing slope is parkland and preserved land, and this east-facing slope abutting Crystal Springs Reservoir is owned by the San Francisco Public Utilities Commission and closed to the public. Area B is on the coastal side of the mountain range, and is also parkland. Area C is Nisene Marks State Park, a park that is difficult to access except by a few trails which allow bicycles. With the exception of Highway 35 along the ridge in Area A, these areas are steep, largely inaccessible, and are among the most densely vegetated areas on the peninsula. Neither SODMAP nor ADS show any known SOD infestations in these three areas. These areas may have escaped SOD infestation due to forest monitoring and rapid removal of infected trees, because inaccessibility has prevented human transmission, or because the steep canyons have provided an inhospitable environment for the disease. It is also possible that these areas contain taller older-growth trees which obscure the view of dead trees lower in the canopy.

If this map is accurate, then tree death is widespread through the study area, and only a few areas have managed to escape. This would indicate that SOD's effects on the forest were extensive and rapid, with devastating consequences within twenty years of first detection.

4.1.2 Serious Tree Death Change From Previous Years

Although the 2011 map of serious tree death shows tree mortality throughout the study area, the result is not significantly different from 2010 or even 1994 (Appendix C). In every year, this methodology shows infestation throughout the study area, with no areas appearing to show more rapid spread of the disease than others. Overall, the number of pixels classified as SD varies from 11 percent in 1999 to 51 percent of the study area in 2009, detailed in Table 13.

The methodology classified 165,000 pixels as SD in 2010, and 208,000 pixels in 2011, a 26 percent increase. To facilitate comparison of multiple years of SD classification data, pixels were converted to centroid points. A comparison of new SD from 2010 to 2011, shown in Figure 18, shows 82,000 SD points in 2011 that were at least 31 m away from the nearest 2010 SD point. An inspection of these changes shows 2011 damage in the same areas as the 2010 damage, but covering a slightly greater areal extent.

A point density map of the new SD points, reproduced in Figure 19, shows the strongest increase in the southern portions of the study area. Figure 20 provides detail on one particular area which showed a significant number of pixels classified as new SD. Due to edge effects from the complex study area, larger continuous areas may show disproportionally strong results with the point density function.

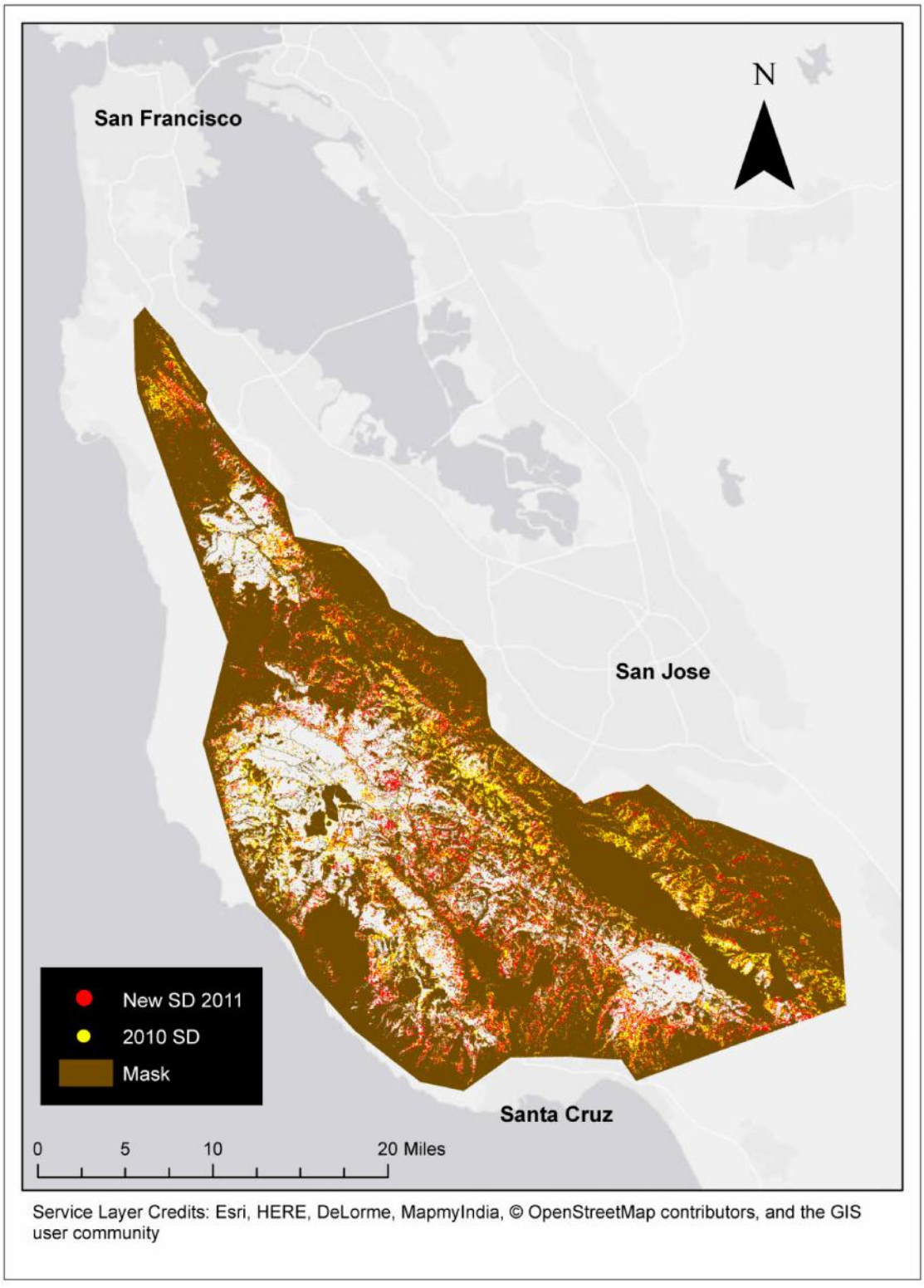

Figure 18 2010 SD and new 2011 SD points (at least 31 meters away from a 2011 point).

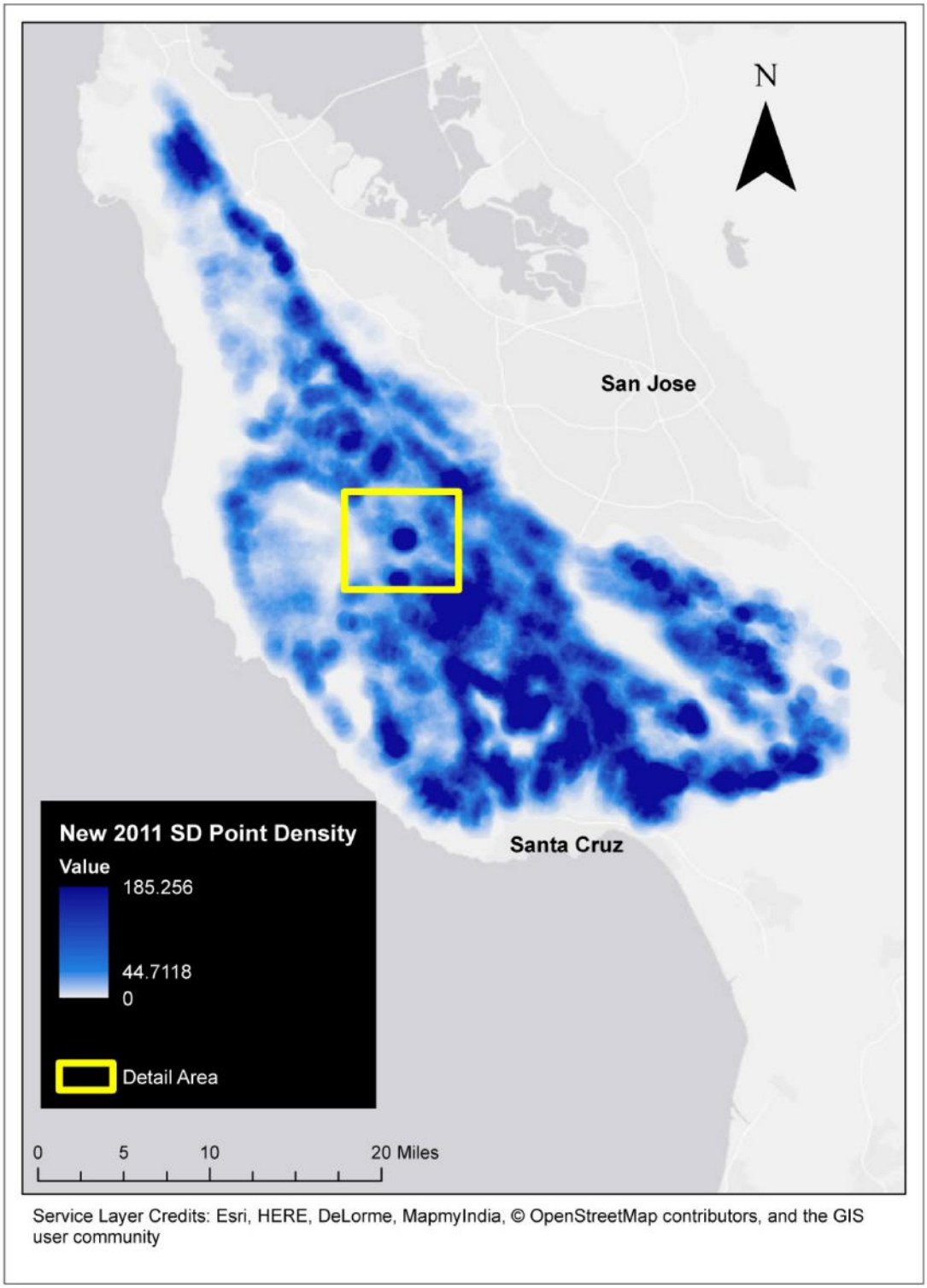

Figure 19 A point density map showing the areas with the most new SD in 2011 compared to 2010. Detail can be seen in Figure 20.

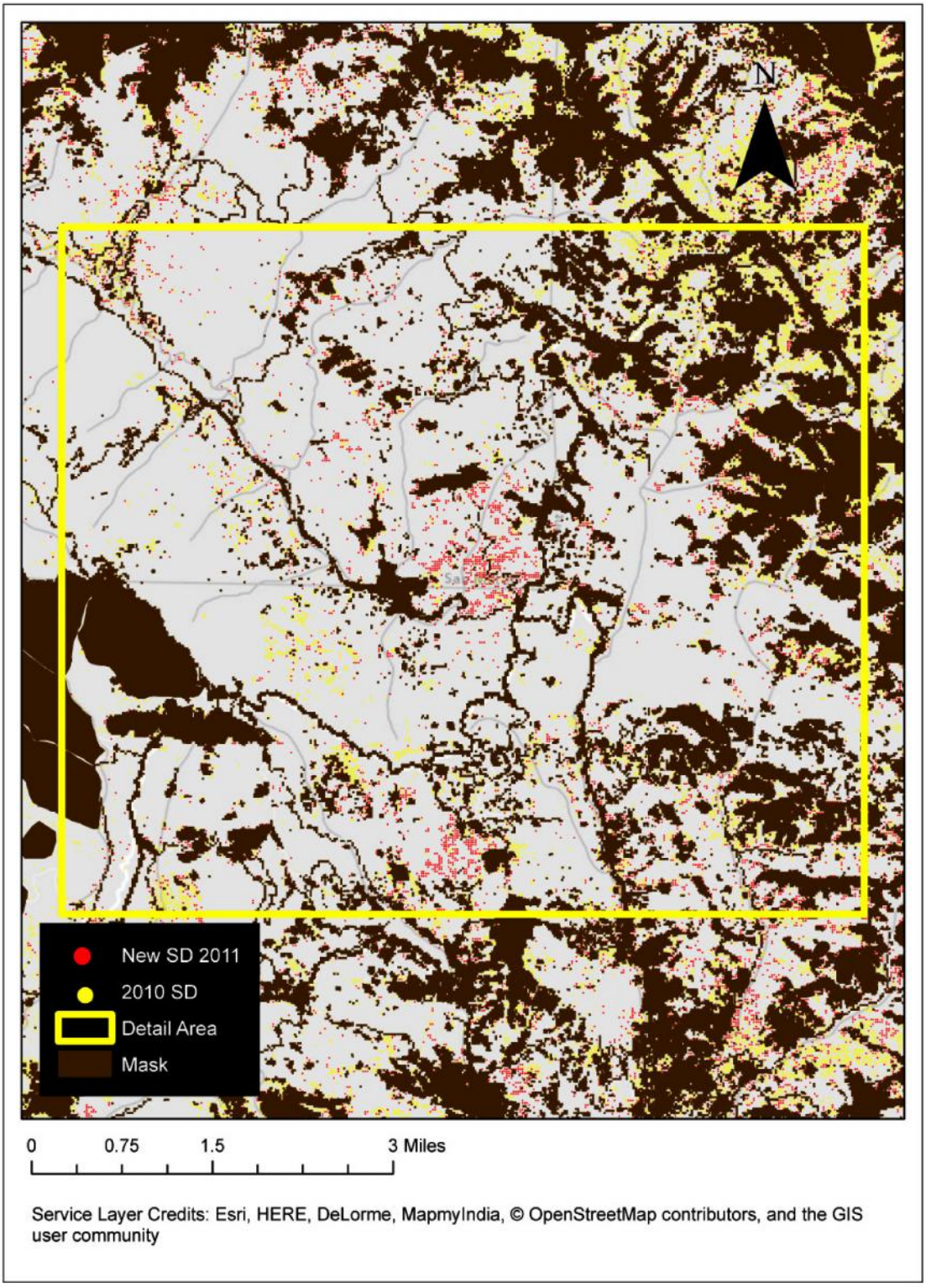

Figure 20 Detail of new SD points in 2011

Table 13 Number of pixels within study area identified as containing serious levels of tree mortality

Year	Day	SD Pixels	Percent of Total Area*	Increase from Previous Year	New SOD Pixels Since Previous Year	Percent of Total Area
1994	070	176,057	23%			
1995	089	265,448	34%	51%	75,552	10%
1996	124	120,302	15%	-55%	18,961	2%
1997	094	143,181	18%	19%	54,572	7%
1998	177	120,702	15%	-16%	41,773	5%
1999	180	89,280	11%	-26%	23,322	3%
2000	119	175,114	22%	96%	96,287	12%
2001	121	130,225	17%	-26%	36,047	5%
2002	156	194,596	25%	49%	69,067	9%
2003	095	230,463	29%	18%	89,315	11%
2004	114	204,170	26%	-11%	75,741	10%
2005	100	235,000	30%	15%	47,920	6%
2006	167	142,706	18%	-39%	21,616	3%
2007	106	200,631	26%	41%	69,928	9%
2008	157	159,868	20%	-20%	31,210	4%
2009	127	396,994	51%	148%	192,582	25%
2010	114	165,210	21%	-58%	7,537	1%
2011	117	208,452	27%	26%	82,067	11%

* Based on average of total pixels within study area for 1994, 1995, 2010 and 2011.

This project expected the 1994 SD map to show little tree death but, as can be seen in Appendix C Figure C1, it instead shows large areas of dead trees throughout the study area. Although SOD was not discovered until 1994, it may have been present in the forest before then, limited to a few small areas. In that case, the widespread tree mortality depicted would be due to causes other than SOD, but this is unlikely because anything causing tree death on this scale would have been noticed. More likely, it is an indication of unreliable results.

The widespread tree death shown in the map of each year's results was unexpected and brings the accuracy of the results into doubt. This issue is explored with some tabular data covering the period 1994-2011 in the next section.

4.1.3 Area of SOD infestation

One method to evaluate the change in SOD infestation over time is to look at the number of pixels classified as SD for each year. This value would be expected to be near 0 in 1994 and increase gradually, with some fluctuation for seasonality. Data captured early or later in the spring could show different total calculations due to different seasonal spectral responses. Values could also decrease if dead trees fall over and cease to be mapped.

Unfortunately, the pixel count shown in Table 13 does not conform to the logical expectation for a spreading infection. Initial pixel counts are much higher than expected, and show large annual variation. It may be notable that the lowest pixel count, 89,280, was for the image captured latest in the season, on day 180 of 1999, and the second highest pixel count, 265,448, was for an image captured early in the season.

This unexpected fluctuation in pixels classified as SD may be an indication that seasonal variation plays a much stronger role in the spectral signature than was anticipated in this project, and annual differences in rainfall and temperature may further confound the interpretation of the results. The results summarized in Table 13 are therefore a strong indicator that the results produced by this methodology are not reliable.

4.1.4 2011 Comparison to ADS and SODMAP

ADS and SODMAP are the most thorough SOD datasets publicly available. This study found SD throughout the study area, but current ADS and SODMAP data show SOD infection primarily in the central-east portion of the study area. If the methodology described in this project were reliable, then a comparison of this project's results with these datasets could highlight new areas of dead trees which might be SOD infection.

Figure 21 shows 2011 SD overlaid with the ADS polygons classified as SOD, and Figure 22 shows 2011 SD overlaid with the SODMAP confirmed SOD-positive infections. Both of these datasets show SOD primarily near the ridgeline in the central part of the study area. SODMAP collects data by field study, so most of their samples are near roads. ADS identifies areas of tree death by flying over them. Without field study, ADS is forced to identify a cause of tree death using other known information. If ADS is relying on SODMAP to tell them where SOD is present, then SOD tree death in other areas may be mistakenly assigned to other causes or may be undetected. A successful methodology to detect dead trees using satellite imagery could identify areas of concern that are not easily accessible by SODMAP field testers or that ADS hasn't prioritized for fly over.

The 2011 map of serious tree death produced by this project reveals one region that should be looked at more closely. In the southeast portion of the study area, between Los Gatos and Morgan Hill, is a large area of east-facing private land which was mapped by this methodology as containing large amounts of tree death, but has not been identified by either ADS or SODMAP as a known area of SOD infection. SODMAP collected eight samples in this area in 2013, in two locations, and all tested negative for SOD. The ADS flew this area in both 2012 and 2013 and found tree damage which they attributed to insects. Although analysis of this project's results shows that mapping results may be inaccurate, it appears that this area is already on the radar as a possible area for SOD, and will probably be watched closely for new infections.

An analysis of the maps produced by this project indicated that densely forested, steep, inaccessible areas are less susceptible to SOD, and identified an area in the southeast portion of the study area that should be looked at more closely as possibly infected by SOD. However,

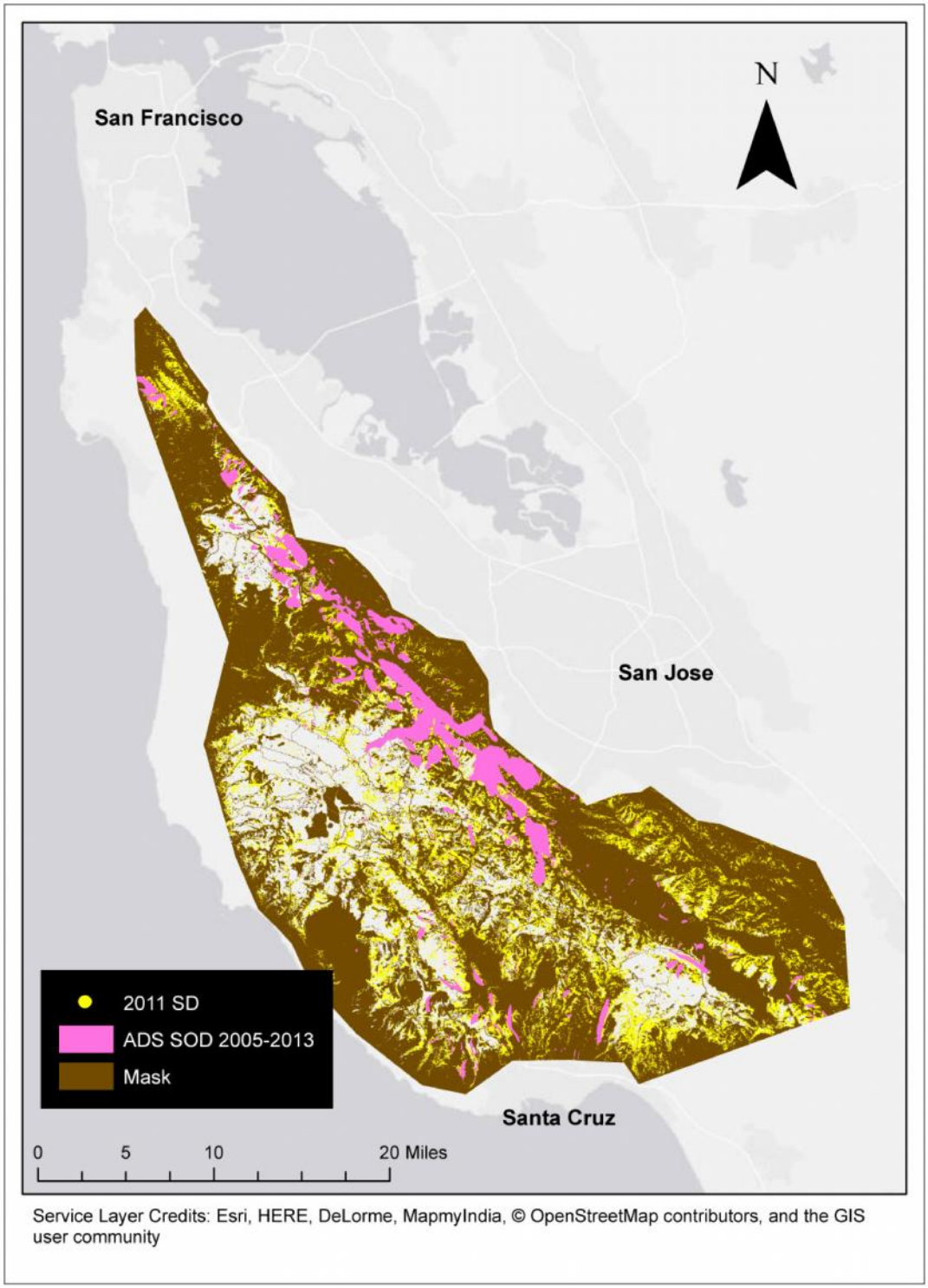

Figure 21 The 2011 SD pixels compared to ADS-identified SOD areas

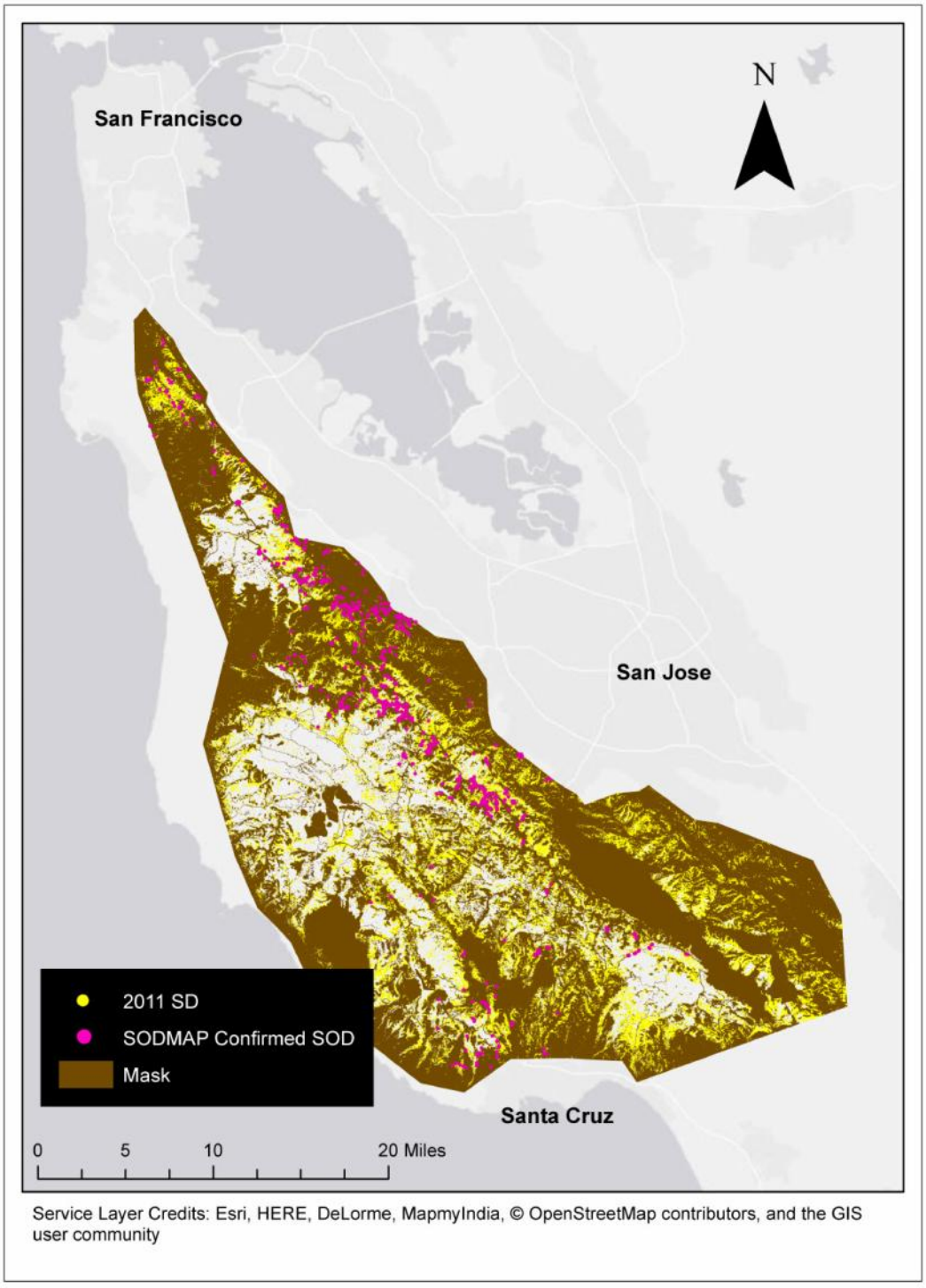

Figure 22 The 2011 SD pixels compared to SODMAP confirmed SOD infections

several factors indicate that these results may be unreliable, including the unexpectedly large numbers of pixels classified as dead trees, and the unforeseen seasonal variation. The reliability and accuracy of the results is taken up in the next section.

4.2 Accuracy Evaluation

From an analysis of the maps and tables showing this project's results, and the error matrices in the previous chapter, we have already seen indications that bring into doubt the reliability of the output – too many pixels are being classified as SD. The error matrix which evaluated the accuracy for the SWIR/NIR index and range 400-570 applied to the Results Validation Points measured that 68 percent of SD points were classified correctly and 73 percent of healthy trees were classified correctly. However, large numbers of pixels that appeared to contain only healthy trees were classified as SD, and the relatively larger number of healthy tree points within the sample strongly affected the overall mapping accuracy. Tree health was accurately mapped 69 percent of the time, but SD was only mapped correctly in 24 percent of the cases, as shown in the error matrix in Table 10 (Chapter 3). This means that approximately three quarters of pixels mapped as tree death are actually healthy trees. Unfortunately, this mapping method and results should therefore be considered unreliable.

A visual comparison of points marked falsely positive does not reveal any obvious reason for the misclassification. They do not contain small amounts of tree death, and they do not contain a particular type of tree. This indicates that the misclassification is due to spectral variation. Similar types of vegetation were observed producing values over a wide range, which caused an overlap in the index values produced by each land cover type. This is further confirmed by areas where SD-classified pixels appear and disappear over different years.

Although fluctuation over different years is partially due to seasonal changes, the variation in pixel values for the same land cover type created more variability than could be captured or excluded with a specific value range.

To rule out misclassification, both sets of points were verified to confirm accuracy. Both Land Cover Points and Results Validation Points SD points conform to the minimum standard of 10% canopy dead trees, but the non-random Land Cover points have an average of 21% dead tree cover, and the random Results Validation points have an average of 12%. This means that the index and range based on the Land Cover points is not optimized to pick up the low levels of SOD displayed in the Results Validation points.

A histogram analysis was applied to the Results Validation Points to determine which index and range would have mapped these points more accurately, and ranges were tested. To facilitate comparison, a randomly-chosen subset of the HLH points was used to equalize the numbers of HLH and SD points. The histograms of these points, shown in Appendix D, did not show differentiation as clearly as the Land Cover Points. There was only slight offset between the peaks of SD and HLH with the SWIR/NIR (Figures D1 and D2), NBR (Figures D3 and D4), NDMI (Figures D5 and D6) and the NDVI (Figures D7 and D8), and no offset for the other indices. No indices or ranges were found which produced better results than the SWIR/NIR formula used in this project.

To determine if an index and range could be more effective at identifying Results Validation Points with greater than 20% canopy SD, the four Results Validation Points meeting that threshold were tested, but no indices or ranges were found which could encompass all four SD points while excluding all HLH points. The best formula, when applied to the entire Results

Validation dataset, only picked up 20% (6 points) of the entire Results Validation SD point dataset. Even a classification based on 20% SD would still have captured HLH points.

Initial analysis of these project results seemed to indicate three areas which escaped SOD infestation, and one new area which should be looked at more closely. However, the number of pixels mapped as SD each year is not consistent with a spreading disease, and the analysis of the Results Classification Points found the mapping of SD to be only 24 percent accurate. Because of these reasons, these project results must be considered unreliable.

The next chapter discusses the broader implications of this interpretation, makes suggestions for further work, and draws conclusions about the project as a whole.

CHAPTER FIVE: DISCUSSION AND CONCLUSIONS

This project attempted to classify dead trees at the canopy level using 30 m raster imagery, as a proxy for mapping the spread of Sudden Oak Death since its discovery in 1994, and concluded that there is too much spectral variation to accomplish this reliably. The project sought a simple method to map SOD over a large area that could be adapted to other areas to form a complete picture of the state of SOD infestation on the west coast of North America. The motivation for this project was that these data could have been useful to quantify the disease impact, to evaluate success at disease management, and could have been adapted to map SOD in other susceptible areas. Unfortunately, the methodology described in this project identified too many false positives to be considered a dependable means to map SOD.

This study expected to find tree death spreading outwards from existing infected areas, with occasional instances of SOD popping up in new places. The possibility for a successful result seemed likely based on the promising Land Cover Points results. Unfortunately, the Results Validation points showed that many areas with healthy trees were misidentified as containing dead trees. Although the methodology was effective at mapping serious tree death at the canopy level, it is picking up too many false positives to produce reliable results to describe the phenomena at hand. The failure to accurately map tree death is due to a variety of spectral signatures produced by similar vegetation which led to overlap in each land cover type's value range. Unfortunately, within the confines of this project's goals – to find a simple method to map SOD over a large area – a more refined analysis was not possible. The remainder of this chapter discusses the implications of the project results, and makes suggestions for further research that might overcome some of the problems that this project experienced.

Preliminary analysis of results implied that dense forest was less susceptible to SOD, and that the southeast portion of the study area contained high levels of tree death not previously noted, but the poor results from the Results Validation Points showed that we could not substantiate these conclusions were accurate. Although this project failed to find a method to map SOD infestation, we can determine what caused the failure and what, if anything, could have been done to improve results.

The project identified pixels containing dead trees with a 24 percent accuracy rate. This low accuracy rate was due to large numbers of pixels containing healthy trees being falsely identified by the methodology as containing dead trees. This is due to a large variation in spectral signatures for the same land cover type. Even within small areas of healthy forest, SWIR/NIR index values ranged by up to 25 percent. While non-forest land cover areas were removed from the study area, there was still sufficient spectral signature variation within classes to cause confusion between pixels containing only healthy trees and those containing some dead trees. Although this project expected to address issues caused by sub-pixel sized features, and so approached this analysis by analyzing land cover at the canopy layer instead of at the tree-level, this wide range of pixel index values made it difficult to identify a value range which would exclude other land cover types. This project did not find a reliable method to map the locations of SOD based on 30 m raster data.

Similar projects analyzing tree health using Landsat imagery claim success, but they measured success differently than this project. Vogelmann, Tolk and Zhu (2009) used correlation with the ADS data as an indicator of success. Meddens et al. (2013) evaluated success based on correct classification of selected homogenous pixels. Meigs, Kennedy and Cohen (2011) and Mahon et al. (2002) performed field testing to evaluate results. It is likely that a pixel-based

validation such as that used by this project would have shown a comparable poor performance. This method of evaluation is objective, but is much more stringent than that applied to other studies of sub-pixel sized features. Despite the measured inaccuracies, the methodology described in this project may be useful at identifying hotspots of new infestation, but the large number of false positives makes it difficult to interpret the specific outcomes.

This project's methodology could have been improved with certain techniques. Specifically, a means could be found to address both the seasonal variability in pixel values across years, and the false positives. To remove or minimize annual variability, seasonal rainfall and temperature data would need to be incorporated into the analysis. This could be used to limit the analysis to data which represented land cover in roughly similar phenological conditions. This would necessarily require using fewer images to conduct the time series analysis because there would not be sufficient cloud-free images during the desired collection period. To remove false positives, two different methods could have been employed. Currently, the methodology identifies serious tree death as greater than 10 percent of pixel area containing dead trees. A higher percentage would have produced a more focused index value range and likely have decreased spectral overlap with pixels containing healthy trees. Another possibility would be to devise a custom index or identify an additional band which differentiated false positive tree death from actual tree death. Both of these were experimented with in this project without improvement to results, but a more intense focus on these two changes might reveal a solution. Although the aforeementioned methods might decrease the error rate found by this project, if the new methods proved complicated, it might make the methodology too difficult to be adapted and used by other users.

Some other methods which might have produced successful results include higher resolution images, additional Land Cover Points, a smaller study area or multi-date analysis. These options were considered but were discarded for reasons described below. Higher resolution data, used in place of or in conjunction with Landsat, would have improved feature resolution and project results. This was not considered because one project goal was to develop a method to map tree death over a large area, that could be adapted to other areas. Although many studies use data fusion methods to improve the feature differentiation of low-resolution satellite data, a methodology which required higher resolution data might make this methodology inadaptable to areas where such data was unavailable, or too costly to acquire, process, store and/or interpret. Another solution considered was to create additional Land Cover Points to more precisely identify each land cover type index value range. This was not pursued because a simple method which could be adapted by others could not rely on such a careful creation of sample points. The initial evaluation of the classification method showed satisfactory results using the Land Cover Points, so it was reasonable to proceed. Refining a SD mapping method using a smaller, more homogenous study area was considered. Decreased vegetation variation that would be typical of many smaller study areas might have made this methodology successful, even with low-resolution data. However, this project sought to develop methodology that could be adapted to map SOD throughout California, and only a large study area would capture the topographic variation necessary. A method which mapped SOD accurately in a homogenous area would likely fail if applied to large areas with more varied topography. Several successful studies of tree health used multi-date analysis to map subtle changes over multiple years. Based on the minor offsets visible in the Results Validation Points histograms shown in Appendix D, a method which detected slight changes in spectral signature might have been more effective.

However, this comparison would need to be performed between three or more sets of data, to eliminate outlier values, because of the pixel value variation observed. These methods discussed could have improved this project's results, but complex methodologies run the risk of discouraging others from adapting it. Although certain changes might lead to successful mapping of SOD on a small or large scale, in a way that this project did not, the root problem is large spectral variation for a single land cover type and overlap between land cover classes.

This project concludes that Landsat data was not able to accurately map tree death in this densely vegetated study area. In addition to unexpected seasonal variation, there was wide variation in pixel values for similar land cover types, which created overlap between classes which could not be contained or excluded with a specific value range.

This project had three original research questions:

1. Can canopy-level tree death indicating SOD infestation be accurately identified and mapped using Landsat remotely-sensed imagery?
2. Are vegetation indices alone sufficient to differentiate tree health and tree mortality from other types of land cover?
3. Will existing supplemental land cover data sets improve or simplify the classification process?

Although pixels containing dead trees could be identified using Landsat imagery, there was too much spectral signature overlap with other land cover types to produce an accurate result. Spectral signature overlap between dead trees and scrub meant that vegetation indices alone were not sufficient. Supplemental land cover data sets used to mask out non-forest and areas with other known causes of death were essential to ensure that the methodology was only applied to the target land cover type.

Although the research questions have been addressed, a successful methodology has not been found. A method is still needed to quantify SOD damage and assess forest health on a large scale. Until then, the ADS surveys are the best data available to assess SOD infestation. Ironically, the current drought in California which is killing trees from lack of water is likely to be the most effective treatment so far to slow the spread of SOD.

REFERENCES

Alexander, J. M. & S. V. Swain. 2010. Sudden Oak Death Integrated Pest Management in the Landscape. http://www.ipm.ucdavis.edu/PMG/PESTNOTES/pn74151.html (accessed Mar 13, 2014).

Barrett, T. M., D. Gatziolis, J. S. Fried & K. L. Waddell (2006) Sudden Oak Death in California: What Is the Potential? *Journal of Forestry,* 104**,** 61-64.

Beh, M. M., M. R. Metz, K. M. Frangioso & D. M. Rizzo (2012) The Key Host for an Invasive Forest Pathogen Also Facilitates the Pathogen's Survival of Wildfire in California Forests. *New Phytologist,* 196**,** 1145-1154.

Collins, B. R., J. L. Parke, B. Lachenbruch & E. M. Hansen (2009) The Effects of *Phytophthora Ramorum* Infection on Hydraulic Conductivity and Tylosis Formation in Tanoak Sapwood. *Canadian Journal of Forest Research,* 39**,** 1766-1776.

Cushman, J. H. & R. K. Meentemeyer (2008) Multi-scale Patterns of Human Activity and the Incidence of an Exotic Forest Pathogen. *Journal of Ecology,* 96**,** 766-776.

Davidson, J. M., A. C. Wickland, H. A. Patterson, K. R. Falk & D. M. Rizzo (2005) Transmission of *Phytophthora Ramorum* in Mixed-evergreen Forest in California. *Phytopathology,* 95**,** 587-596.

DOI-USGS. 1989-2011. "Landsat 4/5 TM Multispectral Imagery." Earth Explorer. http://earthexplorer.usgs.gov/ (accessed May 6, 2014).

---. *Product Guide Landsat Climate Data Record (CDR) Surface Reflectance*. US Geological Survey. US Geological Survey, December 2013.

---. 2014. Landsat Processing Details. http://landsat.usgs.gov/Landsat_Processing_Details.php (accessed May 14, 2014).

Filipe, J. A. N., R. C. Cobb, R. K. Meentemeyer, C. A. Lee, Y. S. Valachovic, A. R. Cook, D. M. Rizzo & C. A. Gilligan (2012) Landscape Epidemiology and Control of Pathogens with Cryptic and Long-distance Dispersal: Sudden Oak Death in Northern Californian Forests. *PLoS Computational Biology,* 8**,** e1002328.

Forestry Commission UK. 2014. *Phytophthora Ramorum* - Frequently Asked Questions. http://www.forestry.gov.uk/forestry/INFD-5UBESN (accessed Feb 9, 2014).

Garbelotto, M., P. Svihra & D. Rizzo (2001) New Pests and Diseases: Sudden Oak Death Syndrome Fells Three Oak Species. *California Agriculture,* 55**,** 9-19.

Geospatial Innovation Facility UC Berkeley and Center for Biodiversity and Conservation. 2003. Landsat Spectral Band Information. Berkeley, California. http://gif.berkeley.edu/documents/Landsat%20Band%20Information.pdf (accessed May 27, 2014).

Goodwin, N. R., N. C. Coops, M. A. Wulder, S. Gillanders, T. A. Schroeder & T. Nelson (2008) Estimation of Insect Infestation Dynamics Using a Temporal Sequence of Landsat Data. *Remote Sensing of Environment,* 112**,** 3680-3689.

Grünwald, N. J., M. Garbelotto, E. M. Goss, K. Heungens & S. Prospero (2012) Emergence of the Sudden Oak Death Pathogen *Phytophthora Ramorum*. *Trends in Microbiology,* 20**,** 131-138.

Guo, Q., M. Kelly & C. H. Graham (2005) Support Vector Machines for Predicting Distribution of Sudden Oak Death in California. *Ecological Modelling,* 182**,** 75-90.

Hansen, E., J. Parke & W. Sutton (2005) Susceptibility of Oregon Forest Trees and Shrubs to *Phytophthora Ramorum*: A Comparison of Artificial Inoculation and Natural Infection. *Plant Disease,* 89**,** 63-70.

Heath, Z., J. Moore, B. Oblinger & M. Woods. 2012. "2012 Aerial Survey Results: California." USDA-FS Pacific Southwest Region Forest Health Protection,. http://www.fs.usda.gov/Internet/FSE_DOCUMENTS/stelprdb5414677.pdf (accessed August 25, 2013).

Jin, S., L. Yang, P. Danielson, C. Homer, J. Fry & G. Xian (2013) A Comprehensive Change Detection Method for Updating the National Land Cover Database to Circa 2011. *Remote Sensing of Environment,* 132**,** 159-175.

Kelly, M. & K. Tuxen. 2001. Oakmapper. Berkeley, California. http://www.oakmapper.org/ (accessed 19 April 2013).

--- (2003) WebGIS for Monitoring "Sudden Oak Death" in Coastal California. *Computers, Environment and Urban Systems,* 27**,** 527-547.

Kelly, M., K. Tuxen & F. Kearns (2004) Geospatial Informatics for Management of a New Forest Disease: Sudden Oak Death. *Photogrammetric Engineering and Remote Sensing,* 70**,** 1001-1008.

Kluza, D. A., D. A. Vieglais, J. K. Andreasen & A. T. Peterson (2007) Sudden Oak Death: Geographic Risk Estimates and Predictions of Origins. *Plant Pathology,* 56**,** 580-587.

Liu, D., M. Kelly & P. Gong (2006) A Spatial–temporal Approach to Monitoring Forest Disease Spread Using Multi-temporal High Spatial Resolution Imagery. *Remote Sensing of Environment,* 101**,** 167-180.

Mahon, L., C. Fischer, L. Levien & J. Mai. *The Use of Remotely Sensed Data for the Detection, Mapping and Monitoring of Sudden Oak Death*. United States Department of Agriculture United States Forest Service. USDA-FS, 2002.

Maloney, P. E., S. C. Lynch, S. F. Kane, C. E. Jensen & D. M. Rizzo (2005) Establishment of an Emerging Generalist Pathogen in Redwood Forest Communities. *Journal of Ecology,* 93**,** 899-905.

Mascheretti, S., P. J. P. Croucher, A. Vettraino, S. Prospero & M. Garbelotto (2008) Reconstruction of the Sudden Oak Death Epidemic in California Through Microsatellite Analysis of the Pathogen *Phytophthora Ramorum*. *Molecular Ecology,* 17**,** 2755-2768.

McGinnis, L. (2008) Tree Heartwood Extracts Halt Sudden Oak Death. *Agricultural Research,* 56**,** 10-11.

Meddens, A. J. H., J. A. Hicke, L. A. Vierling & A. T. Hudak (2013) Evaluating Methods to Detect Bark Beetle-caused Tree Mortality Using Single-date and Multi-date Landsat Imagery. *Remote Sensing of Environment,* 132**,** 49-58.

Meentemeyer, R., D. Rizzo, W. Mark & E. Lotz (2004) Mapping the Risk of Establishment and Spread of Sudden Oak Death in California. *Forest Ecology and Management,* 200**,** 195-214.

Meentemeyer, R. K., N. E. Rank, D. A. Shoemaker, C. B. Oneal, A. C. Wickland, K. M. Frangioso & D. M. Rizzo (2008) Impact of Sudden Oak Death on Tree Mortality in the Big Sur Ecoregion of California. *Biological Invasions,* 2008**,** 1243-1255.

Meigs, G. W., R. E. Kennedy & W. B. Cohen (2011) A Landsat Time Series Approach to Characterize Bark Beetle and Defoliator Impacts on Tree Mortality and Surface Fuels in Conifer Forests. *Remote Sensing of Environment,* 115**,** 3707-3718.

Parke, J., E. Oh, S. Voelker, E. Hansen, G. Buckles & B. Lachenbruch (2007) *Phytophthora Ramorum* Colonizes Tanoak Xylem and is Associated with Reduced Stem Water Transport. *Phytopathology,* 97**,** 1558-1567.

Quinn, J. W. 2001. Band Combinations. Portland State University. http://web.pdx.edu/~emch/ip1/bandcombinations.html (accessed September 25, 2013).

Ramage, B. S. & K. L. O'Hara (2010) Sudden Oak Death-Induced Tanoak Mortality in Coast Redwood Forests: Current and Predicted Impacts to Stand Structure. *Forests,* 1**,** 114-130.

Ramage, B. S., K. L. O'Hara & A. B. Forrestel (2011) Forest Transformation Resulting from an Exotic Pathogen: Regeneration and Tanoak Mortality in Coast Redwood Stands Affected by Sudden Oak Death. *Canadian Journal of Forest Research,* 41**,** 763-772.

Rizzo, D. M., M. Garbelotto & E. M. Hansen (2005) *Phytophthora Ramorum*: Integrative Research and Management of an Emerging Pathogen in California and Oregon Forests. *Annual Review of Phytopathology,* 43**,** 309-335.

Sutton, W., E. Hansen, P. Reeser & A. Kanaskie (2009) Stream Monitoring for Detection of *Phytophthora Ramorum* in Oregon Tanoak Forests. *Plant Disease,* 93**,** 1182-1186.

USDA-FS Forest Health Monitoring Program. 1978-2013. "Aerial Detection Monitoring." United States Department of Agriculture, United States Forest Service. http://www.fs.usda.gov/detail/r5/forest-grasslandhealth/?cid=fsbdev3_046696 (accessed May 6, 2014).

USDA-FS Pacific Southwest Region. 2014. Aerial Detection Survey: Methodology. Vallejo, CA. http://www.fs.usda.gov/detail/r5/forest-grasslandhealth/?cid=stelprdb5429568 (accessed August 25, 2013).

USDA Animal and Plant Health Inspection Service. 2012. APHIS List of Regulated Hosts and Plants Proven or Associated with *Phytophthora Ramorum*. http://www.aphis.usda.gov/plant_health/plant_pest_info/pram/downloads/pdf_files/usdaprlist.pdf (accessed August 8, 2013).

Vogelmann, J. E., B. Tolk & Z. Zhu (2009) Monitoring Forest Changes in the Southwestern United States Using Multitemporal Landsat Data. *Remote Sensing of Environment,* 113**,** 1739-1748.

APPENDIX A: HOSTS REGULATED FOR *PHYTOPHTHORA RAMORUM*

Table A1: Proven host plants regulated for *Phytophthora Ramorum*

Scientific Name	Common Name(s)
Acer macrophyllum	Bigleaf maple
Acer pseudoplatanus	Planetree maple
Adiantum aleuticum	Western maidenhair fern
Adiantum jordanii	California maidenhair fern
Aesculus californica	California buckeye
Aesculus hippocastanum	Horse chestnut
Arbutus menziesii	Madrone
Arctostaphylos manzanita	Manzanita
Calluna vulgaris	Scotch heather
Camellia spp.	Camellia - all species, hybrids and cultivars
Castanea sativa	Sweet chestnut
Cinnamomum camphora	Camphor tree
Fagus sylvatica	European beech
Frangula californica (Rhamnus californica)	California coffeeberry
Frangula purshiana (*Rhamnus purshiana*)	Cascara
Fraxinus excelsior	European ash
Griselinia littoralis	Griselinia
Hamamelis virginiana	Witch hazel
Heteromeles arbutifolia	Toyon
Kalmia spp.	Mountain laurel - all species, hybrids and cultivars
Lithocarpus densiflorus	Tanoak
Lonicera hispidula	California honeysuckle
Laurus nobilis	Bay laurel
Magnolia doltsopa (Michelia doltsopa)	Michelia
Maianthemum racemosum (Smilacina racemosa)	False Solomon's seal
Parrotia persica	Persian ironwood
Photinia fraseri	Red tip photinia
Pieris spp.	Andromeda, Pieris - all species, hybrids and cultivars
Pseudotsuga menziesii var. *menziesii*	Douglas fir

Table A1 (continued)

Scientific Name	Common Name(s)
Quercus agrifolia	Coast live oak
Quercus cerris	European turkey oak
Quercus chrysolepis	Canyon live oak
Quercus falcata	Southern red oak
Quercus ilex	Holm oak
Quercus kelloggii	California black oak
Quercus parvula var. *shrevei*	Shreve's oak
Rhododendron spp.	Rhododendron (including azalea) – all species, hybrids and cultivars
Rosa gymnocarpa	Wood rose
Salix caprea	Goat willow
Sequoia sempervirens	Coast redwood
Syringa vulgaris	Lilac
Taxus baccata	European yew
Trientalis latifolia	Western starflower
Umbellularia californica	California bay laurel, pepperwood, Oregon myrtle
Vaccinium ovatum	Evergreen huckleberry
Viburnum spp.	Viburnum – all species, hybrids and cultivars

Source: USDA Animal and Plant Health Inspection Service (2012)

APPENDIX B: INDEX ANALYSIS HISTOGRAMS FOR LAND COVER POINTS

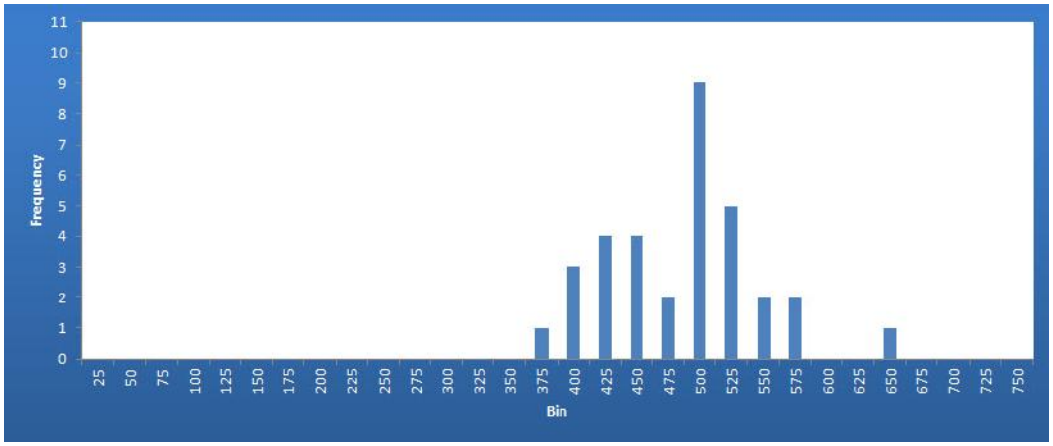

Figure B1 The SWIR/NIR Land Cover Points histogram for serious tree death.

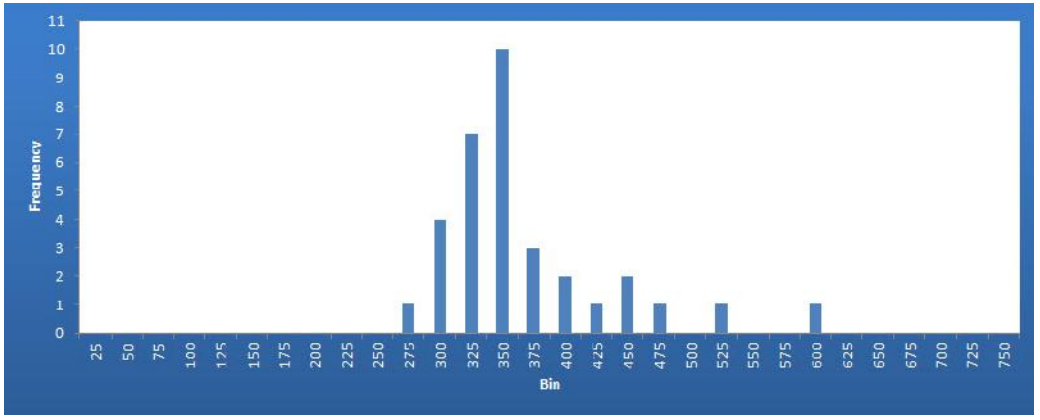

Figure B2 The SWIR/NIR Land Cover Points histogram for healthy trees. This index is a good option because the peaks of the two histograms are separated and don't overlap with large quantities in the other graph. This index was one of three considered to differentiate healthy from SD points, and the range of 400-570 was ultimately used.

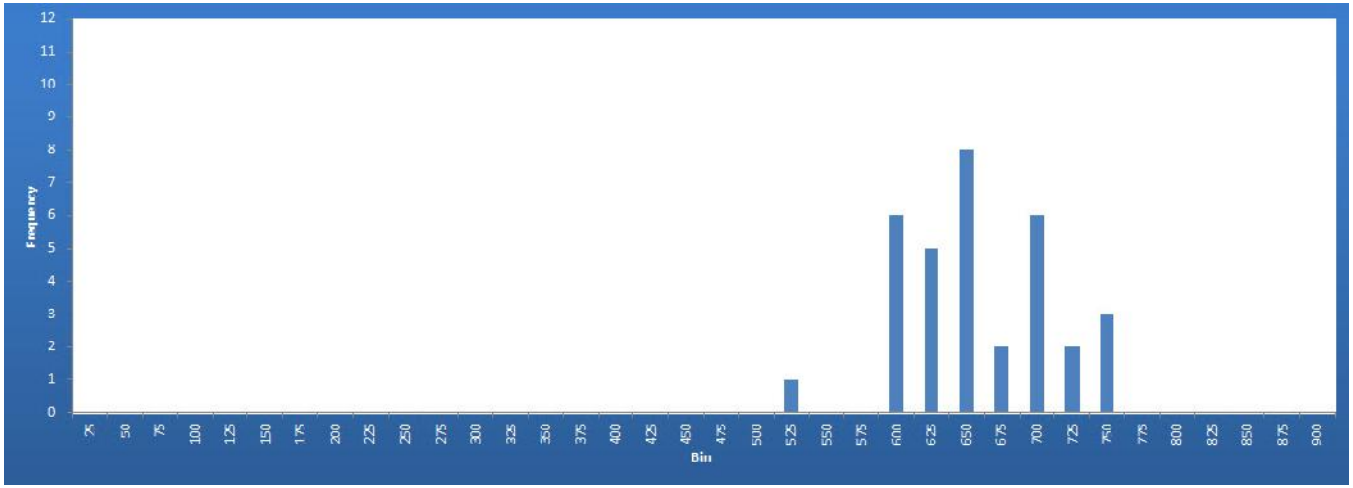

Figure B3 The NBR Land Cover Points histogram for serious tree death.

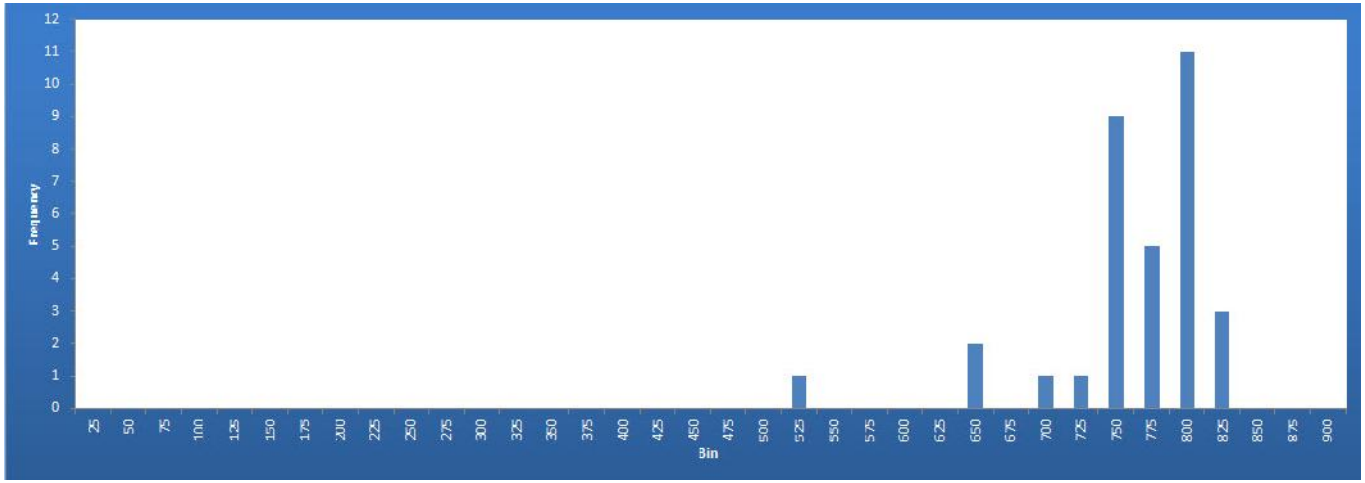

Figure B4 The NBR Land Cover Points histogram for healthy trees. This index was not chosen because the left HLH peak overlaps with three of the SD points.

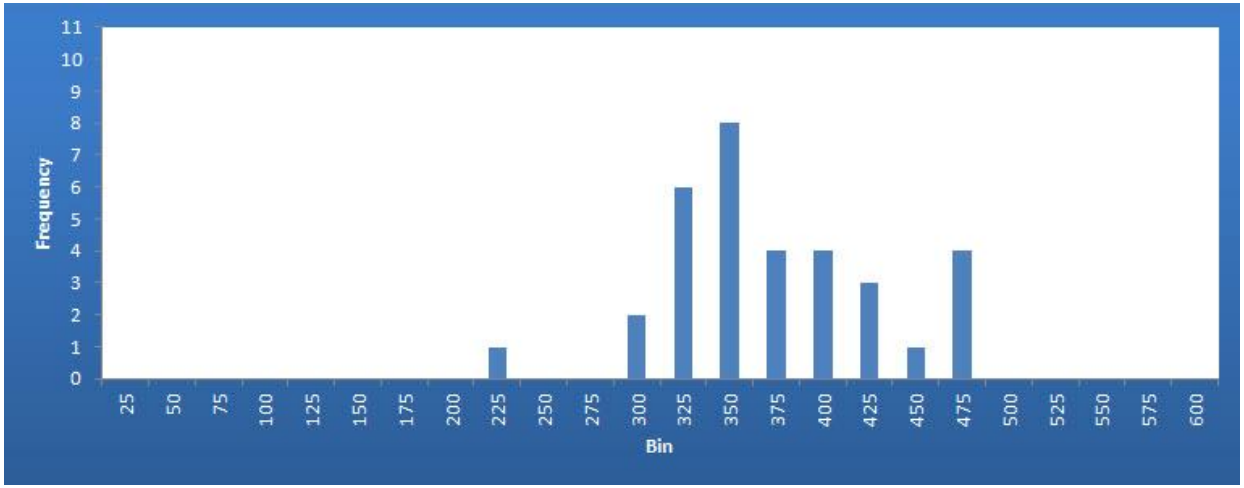

Figure B5 The NDMI Land Cover Points histogram for serious tree death.

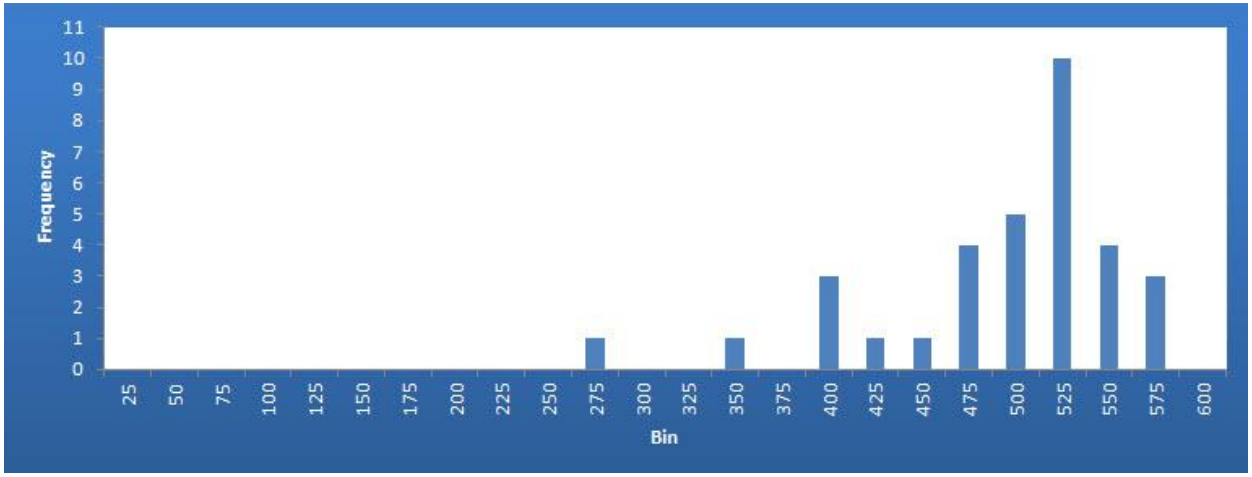

Figure B6 The NDMI Land Cover Points histogram for healthy trees. This index was considered for use to differentiate the healthy and SD points. Although many of the points are in overlapping ranges, the peaks of the histograms are separated and do not overlap with points in the other class

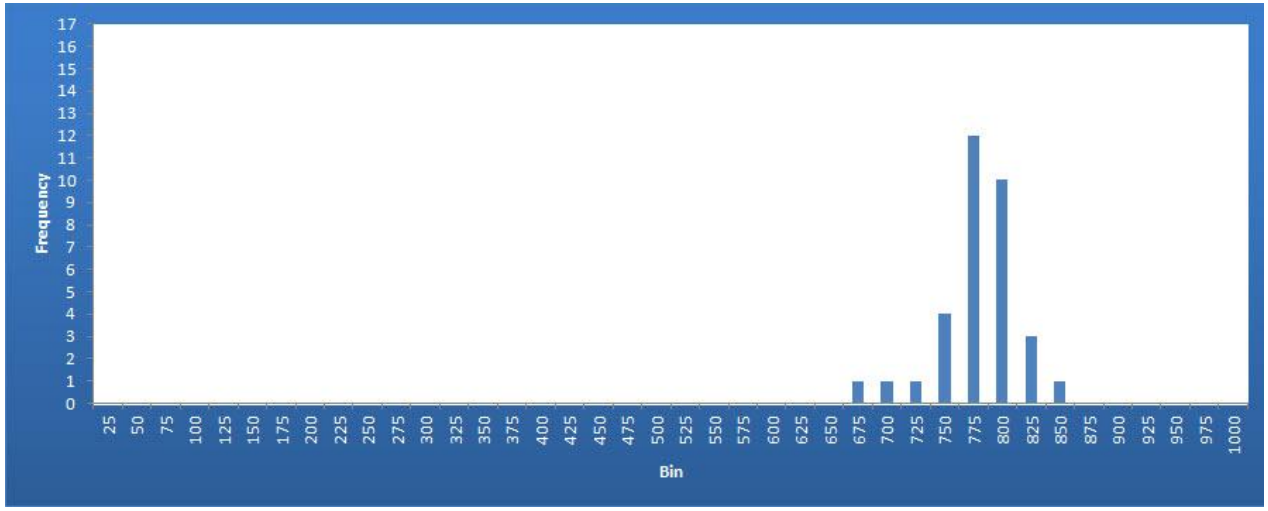

Figure B7 The NDVI Land Cover Points histogram for serious tree death.

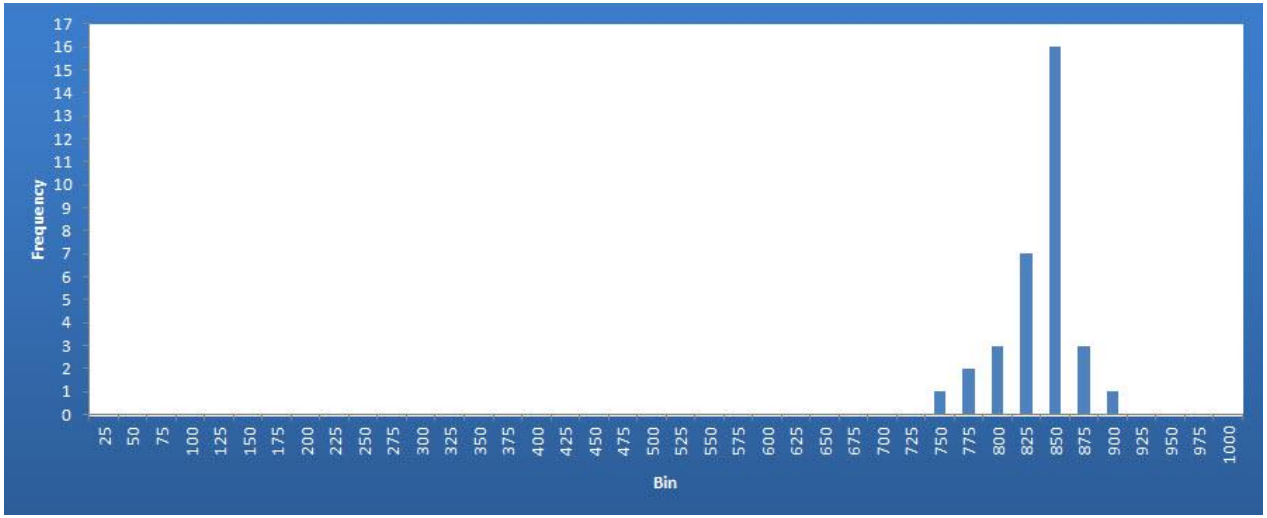

Figure B8 The NDVI Land Cover Points histogram for healthy trees. This index is not ideal because the main curve of each histogram is so close to the other, and most of the points are in overlapping ranges.

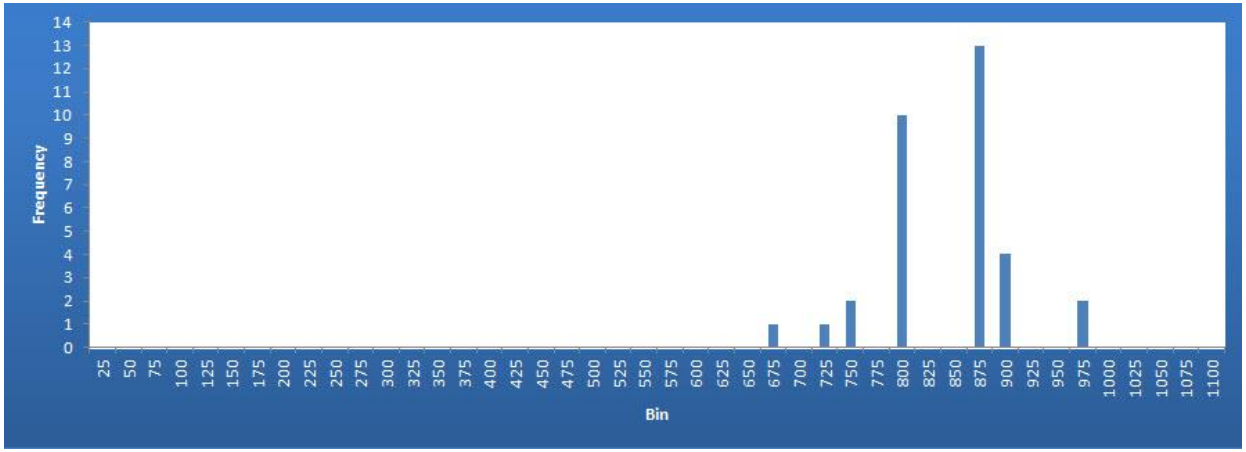

Figure B9 The RGI Land Cover Points histogram for serious tree death.

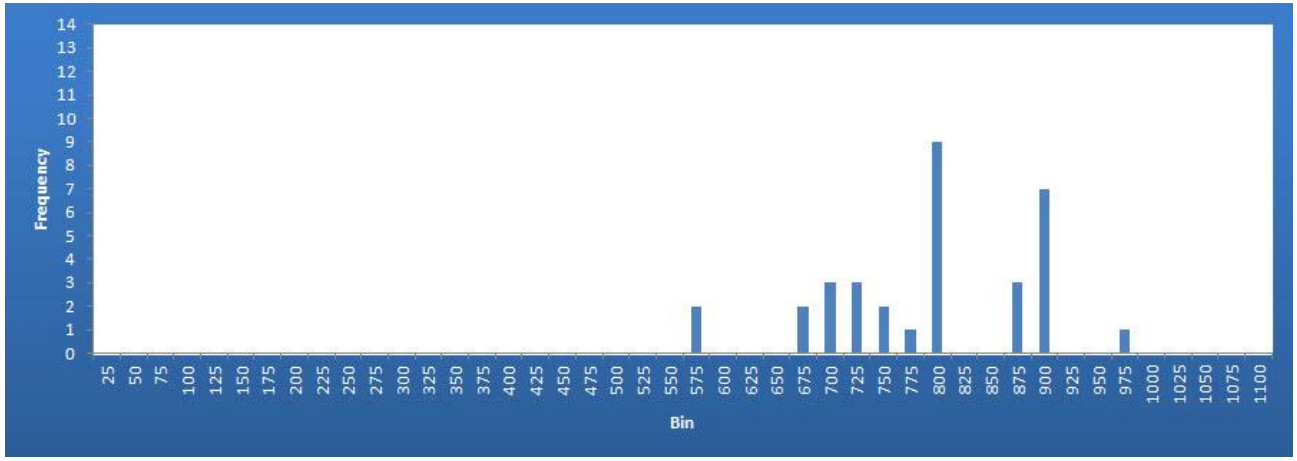

Figure B10 The RGI Land Cover Points histogram for healthy trees. This index was not used because here is too much overlap between the ranges and the peaks.

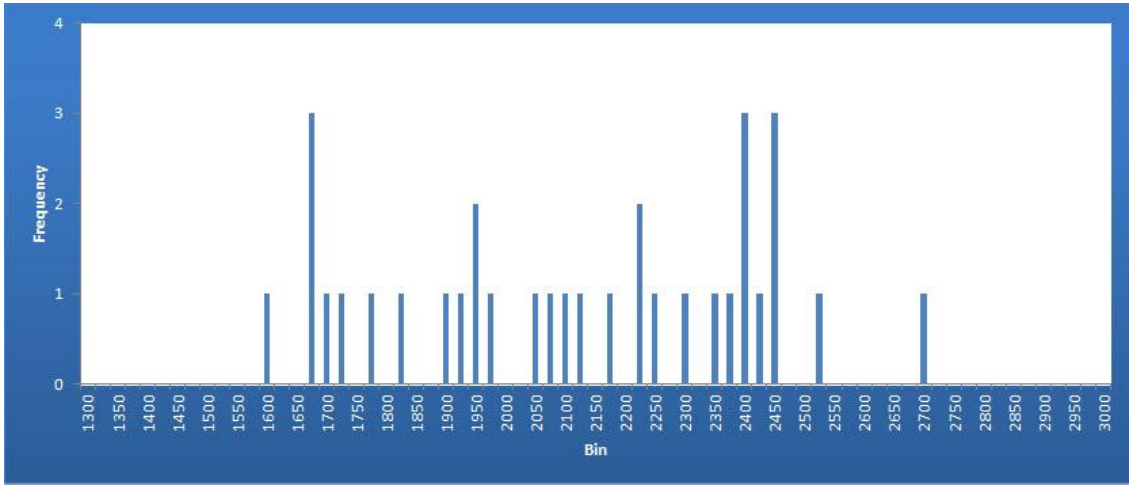

Figure B11 The Tasseled Cap Bright Land Cover Points histogram for serious tree death.

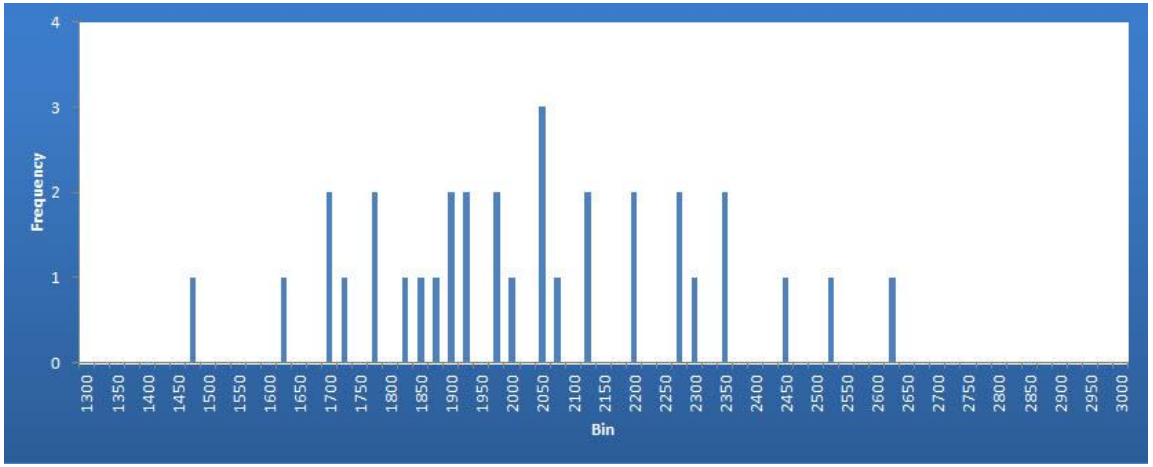

Figure B12 The Tasseled Cap Bright Land Cover Points histogram for healthy trees. This index was not used because there was no large a range of values in each chart, no clear histogram peak, and too much overlap.

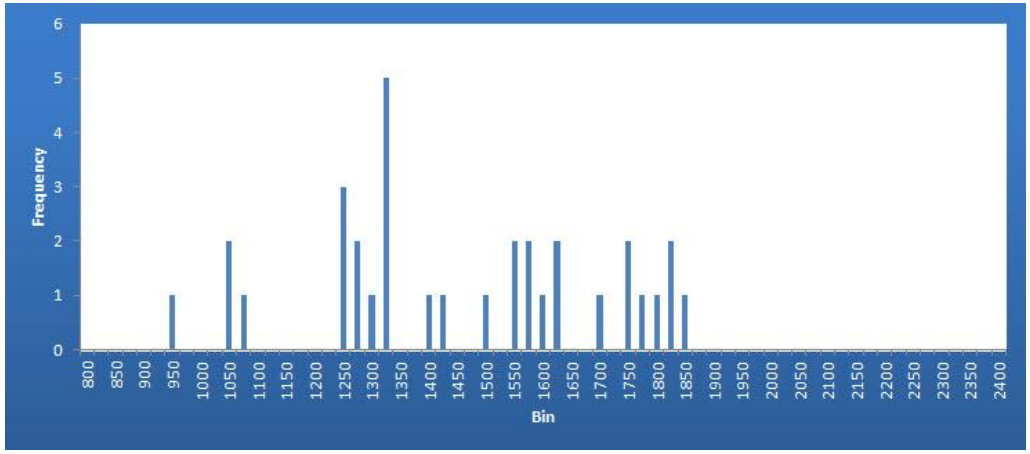

Figure B13 The Tasseled Cap Green Land Cover Points histogram for serious tree death.

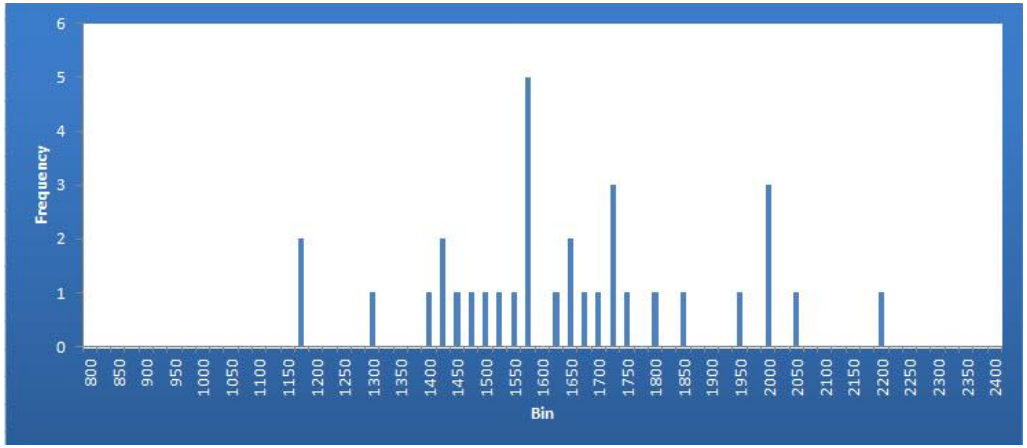

Figure B14 The Tasseled Cap Green Land Cover Points histogram for healthy trees. This index was not used because the values are spread over too great a range with too much overlap between the two classes.

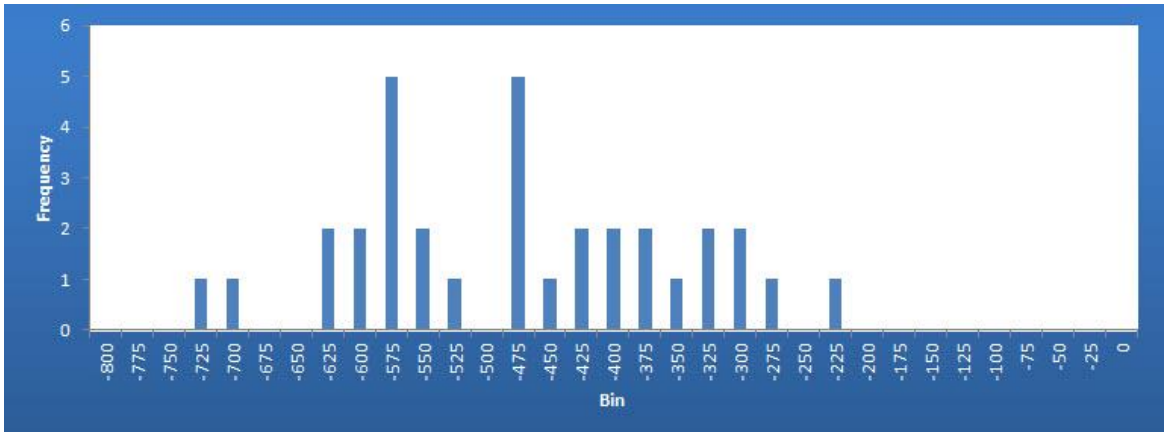

Figure B15 The Tasseled Cap Wet Land Cover Points histogram for serious tree death.

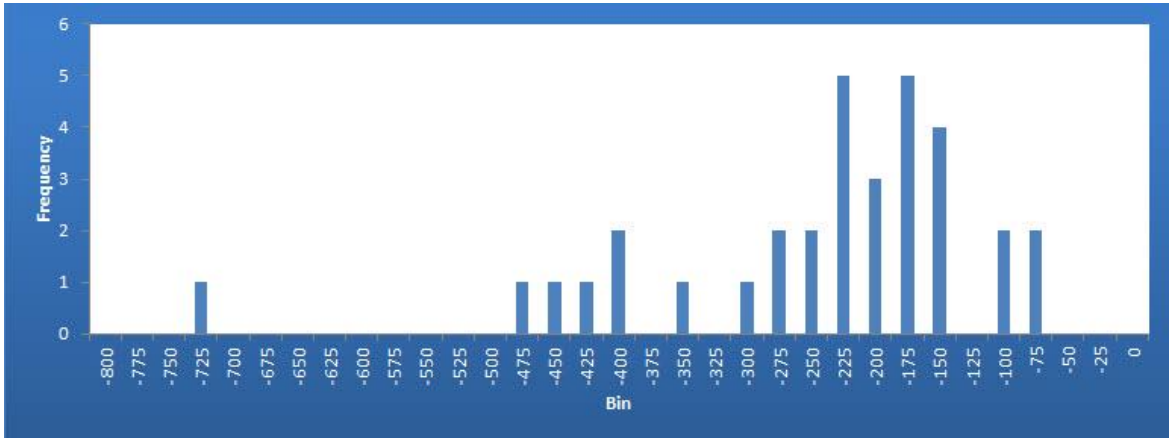

Figure B16 The Tasseled Cap Wet Land Cover Points histogram for healthy trees. This index was considered for use to differentiate the healthy and SD points. Although there is undesireable overlap between the ranges, the histogram peaks are separated and there are few overlapping points at the peak ranges.

APPENDIX C: PREDICTED MAPS OF SUDDEN OAK DEATH

Figure C1 The extent of serious tree death in 1994. Each pixel classified as SD is displayed as a single yellow point. Non-forested areas, masked out, are shown in brown.

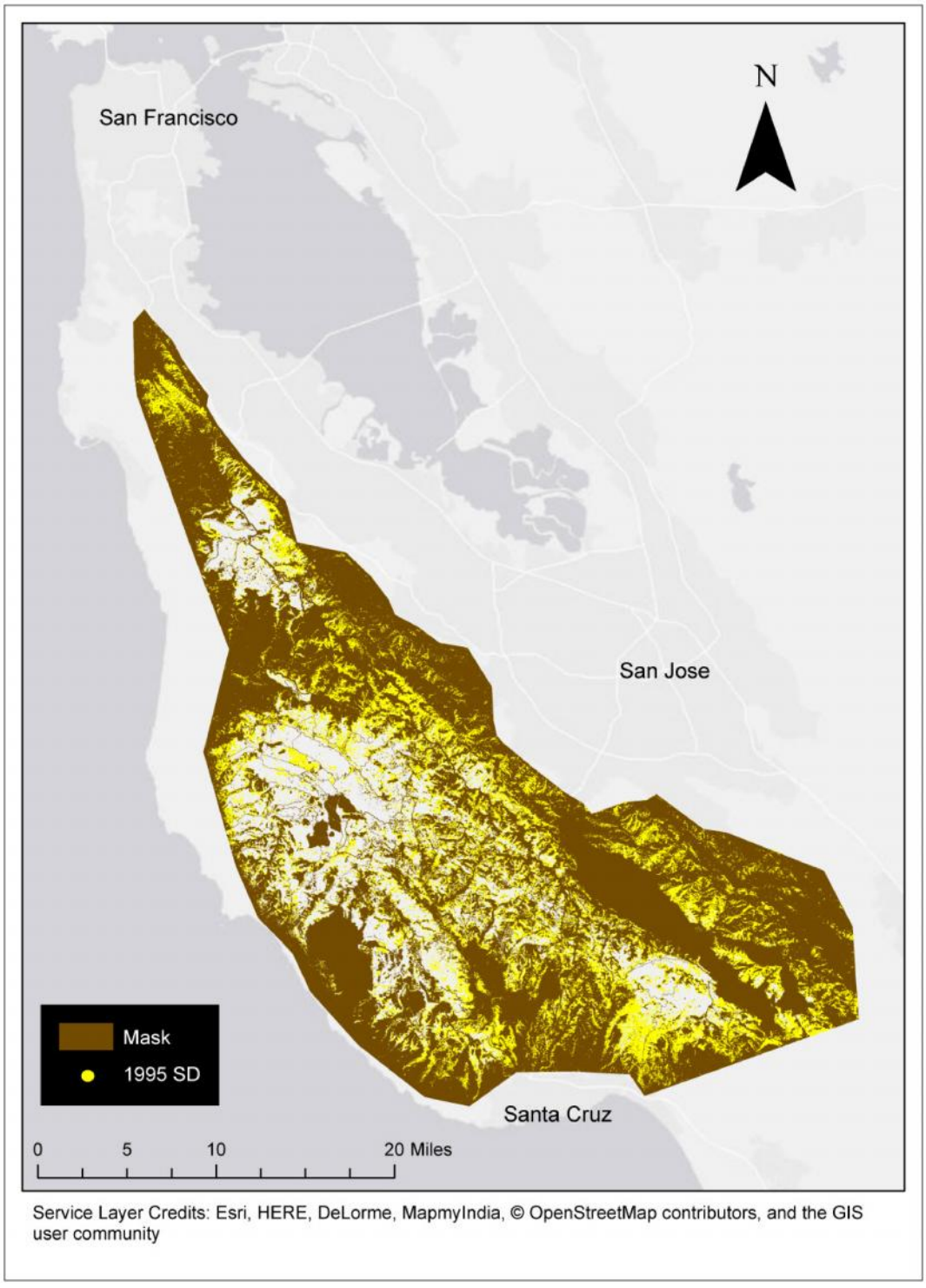

Figure C2 The extent of serious tree death in 1995. Each pixel classified as SD is displayed as a single yellow point. Non-forested areas, masked out, are shown in brown.

Figure C3 The extent of serious tree death in 1996. Each pixel classified as SD is displayed as a single yellow point. Non-forested areas, masked out, are shown in brown.

Figure C4 The extent of serious tree death in 1997. Each pixel classified as SD is displayed as a single yellow point. Non-forested areas, masked out, are shown in brown.

Figure C5 The extent of serious tree death in 1998. Each pixel classified as SD is displayed as a single yellow point. Non-forested areas, masked out, are shown in brown.

Figure C6 The extent of serious tree death in 1999. This year's data showed the fewest pixels classified as SD. Each pixel classified as SD is displayed as a single yellow point. Non-forested areas, masked out, are shown in brown.

Figure C7 The extent of serious tree death in 2000. Each pixel classified as SD is displayed as a single yellow point. Non-forested areas, masked out, are shown in brown.

Figure C8 The extent of serious tree death in 2001. Each pixel classified as SD is displayed as a single yellow point. Non-forested areas, masked out, are shown in brown.

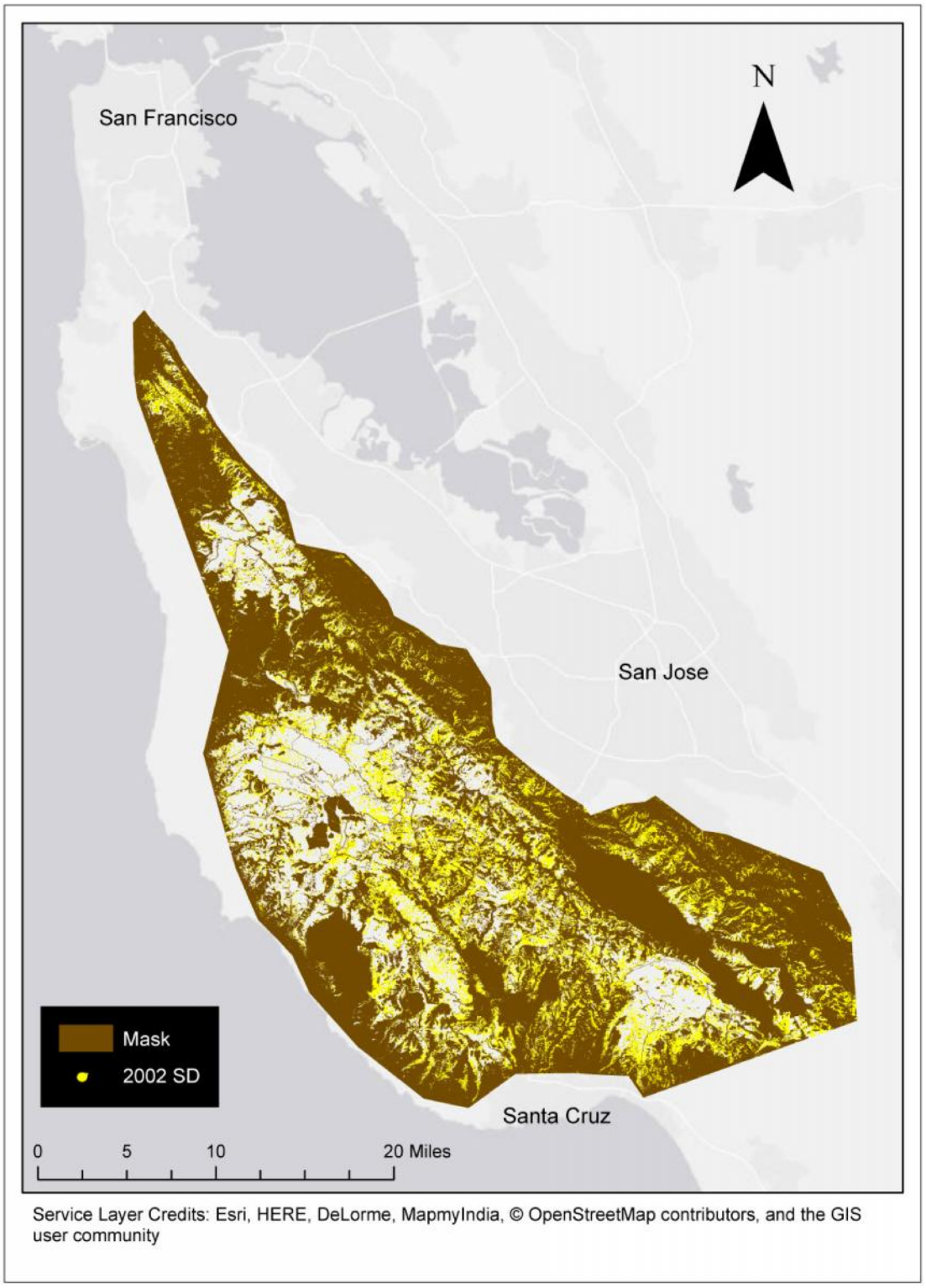

Figure C9 The extent of serious tree death in 2002. Each pixel classified as SD is displayed as a single yellow point. Non-forested areas, masked out, are shown in brown.

Figure C10 The extent of serious tree death in 2003. Each pixel classified as SD is displayed as a single yellow point. Non-forested areas, masked out, are shown in brown.

Figure C11 The extent of serious tree death in 2004. Each pixel classified as SD is displayed as a single yellow point. Non-forested areas, masked out, are shown in brown.

Figure C12 The extent of serious tree death in 2005. Each pixel classified as SD is displayed as a single yellow point. Non-forested areas, masked out, are shown in brown.

Figure C13 The extent of serious tree death in 2006. Each pixel classified as SD is displayed as a single yellow point. Non-forested areas, masked out, are shown in brown.

Figure C14 The extent of serious tree death in 2007. Each pixel classified as SD is displayed as a single yellow point. Non-forested areas, masked out, are shown in brown.

Figure C15 The extent of serious tree death in 2008. Each pixel classified as SD is displayed as a single yellow point. Non-forested areas, masked out, are shown in brown.

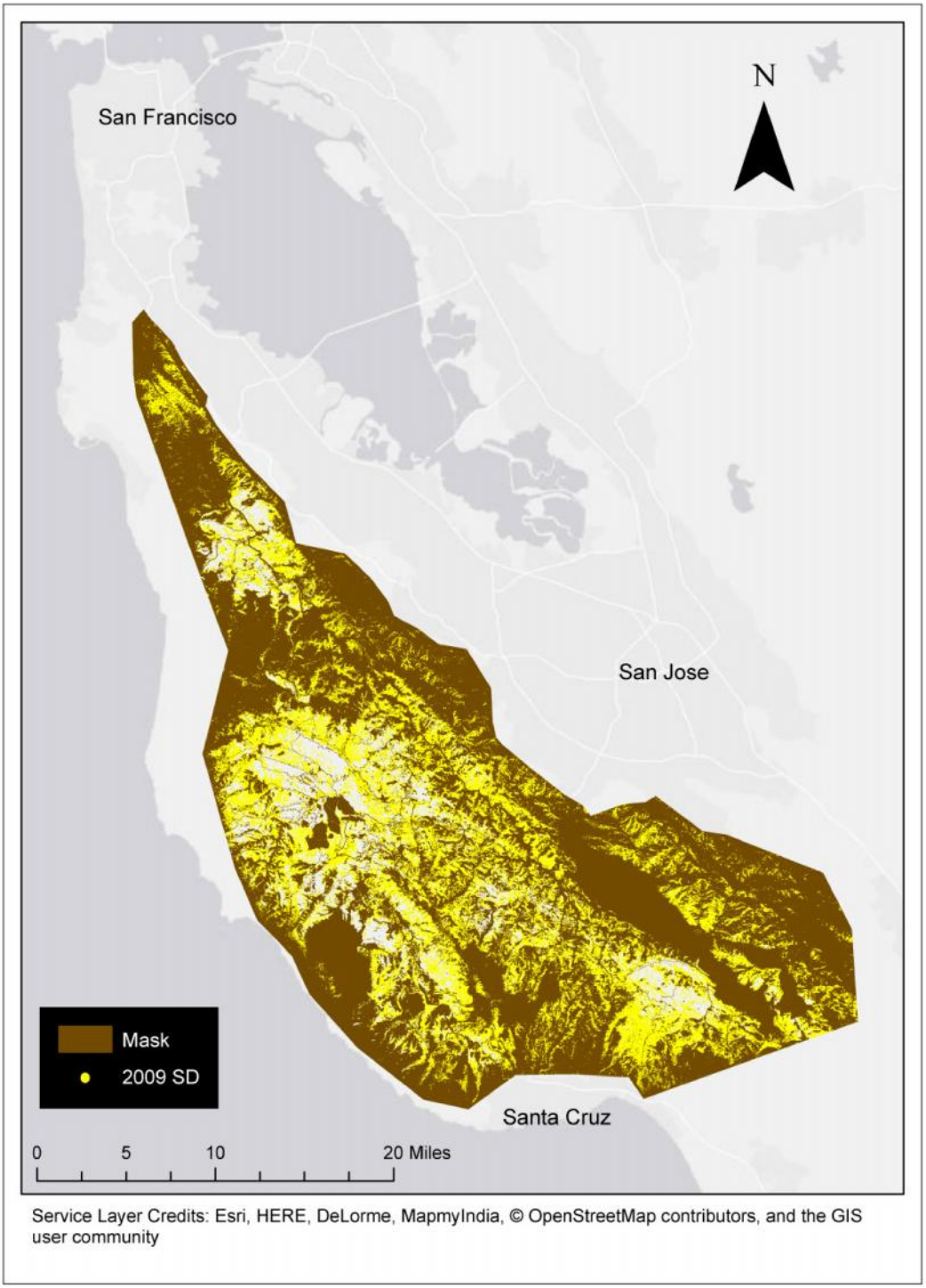

Figure C16 The extent of serious tree death in 2009. This year's data showed the most pixels classified as SD. Each pixel classified as SD is displayed as a single yellow point. Non-forested areas, masked out, are shown in brown.

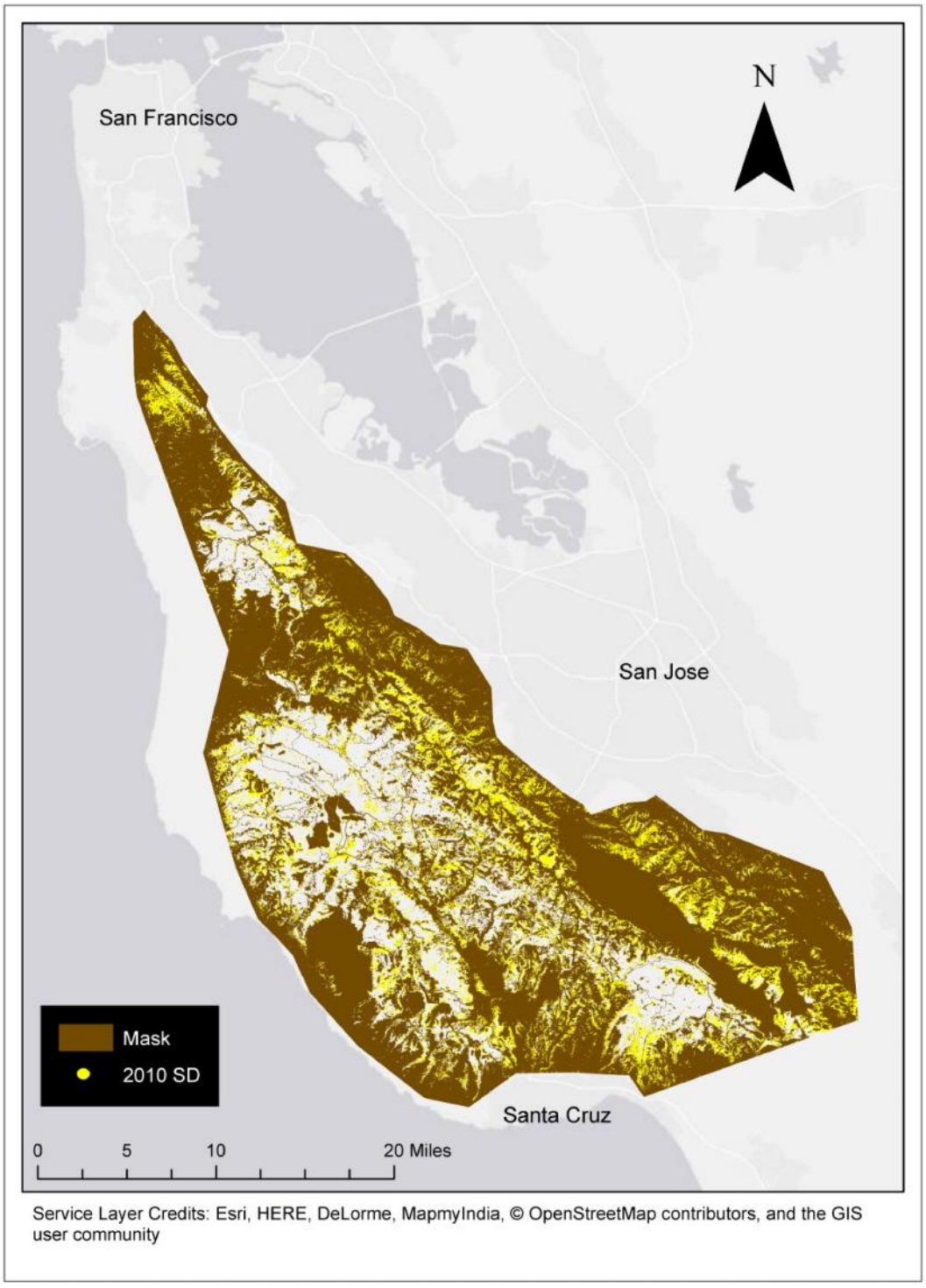

Figure C17 The extent of serious tree death in 2010. Each pixel classified as SD is displayed as a single yellow point. Non-forested areas, masked out, are shown in brown.

Figure C18 The extent of serious tree death in 2011. Each pixel classified as SD is displayed as a single yellow point. Non-forested areas, masked out, are shown in brown.

APPENDIX D: HISTOGRAMS FOR RESULTS VALIDATION POINTS

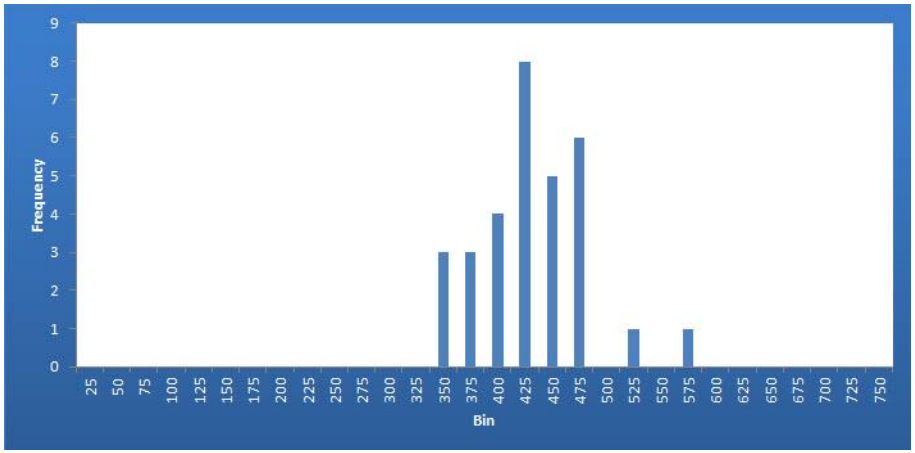

Figure D1 The SWIR/NIR Results Validation Points histogram for serious tree death.

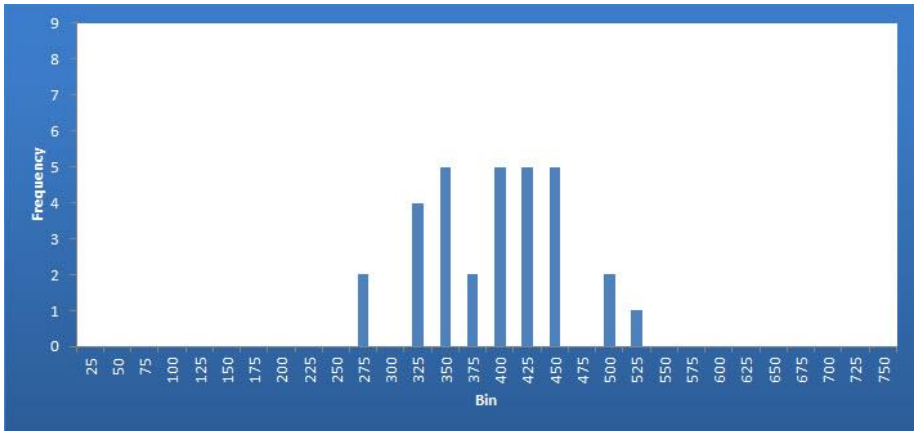

Figure D2 The SWIR/NIR Results Validation Points histogram for healthy trees. The main range for the SD points in Figure D1 is shifted slightly to the right in comparison to the HLH points.

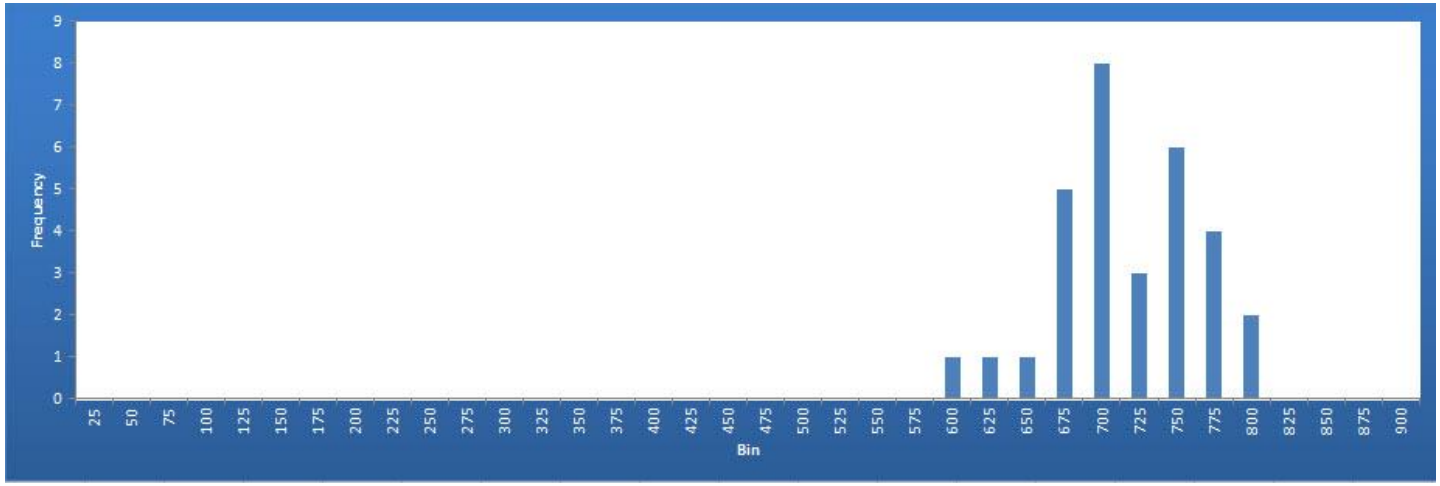

Figure D3 The NBR Results Validation Points histogram for serious tree death.

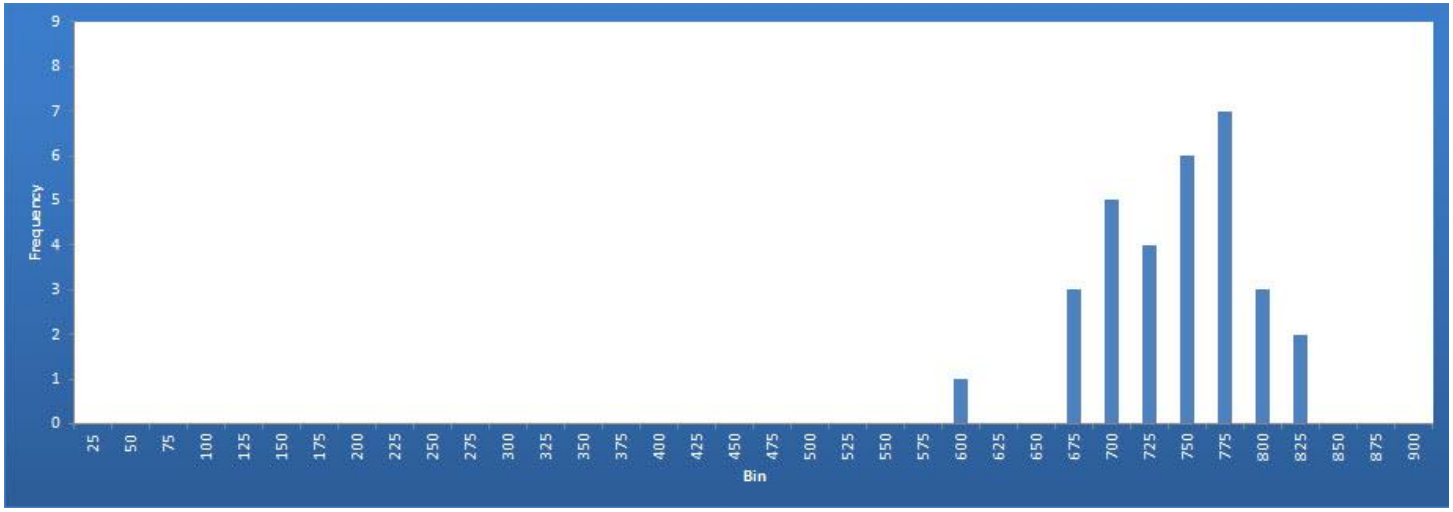

Figure D4 The NBR Results Validation Points histogram for healthy trees. The main curve for SD points, in Figure D3, is shifted slightly to the left in comparison to the HLH points.

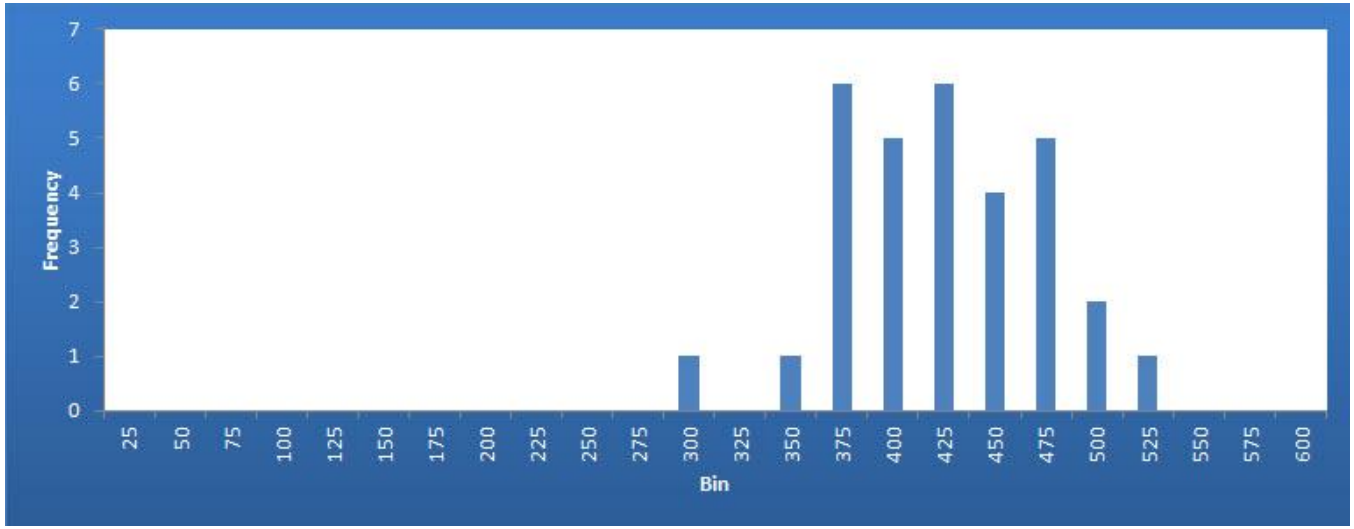

Figure D5 The NDMI Results Validation Points histogram for serious tree death.

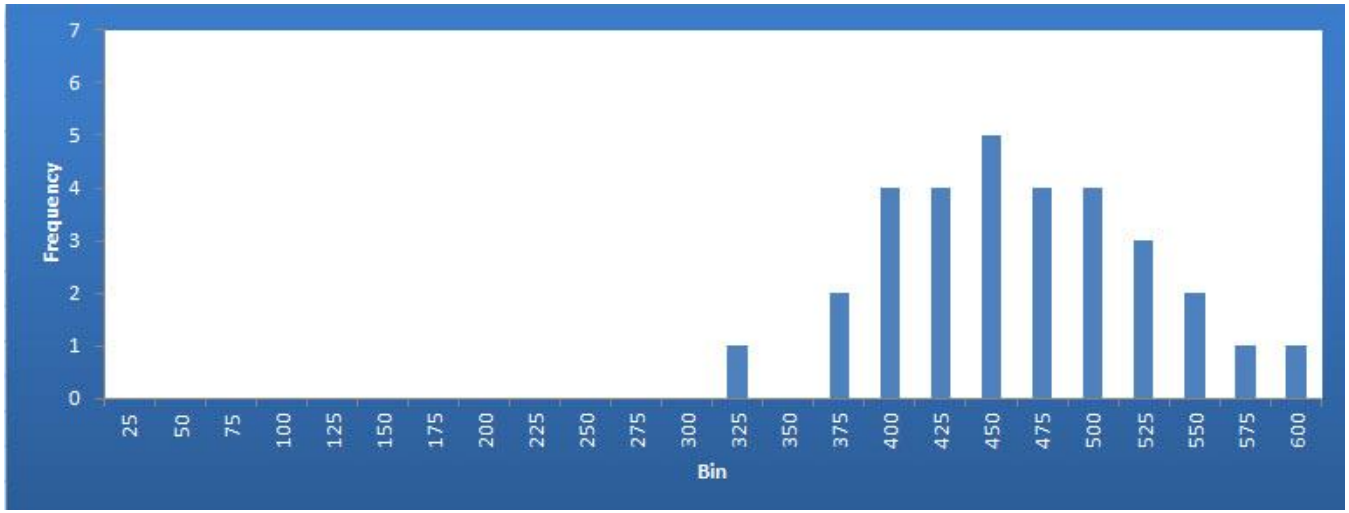

Figure D6 The NDMI Results Validation Points histogram for healthy trees. The main range of the SD points in Figure D5 is shifted slightly to the left in comparison to the HLH graph.

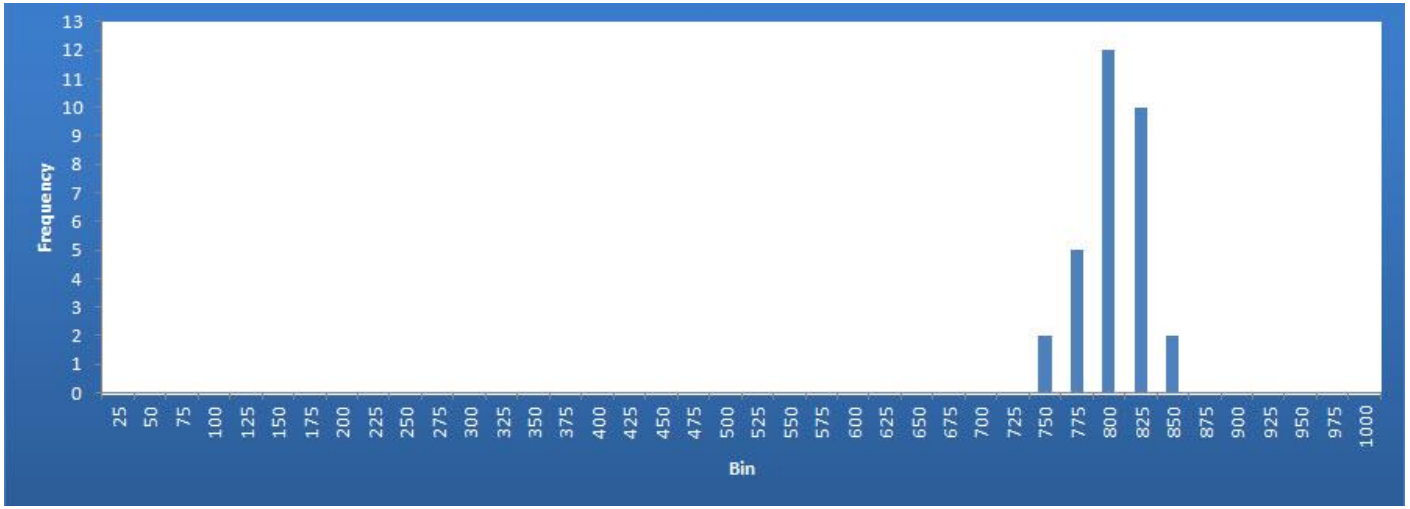

Figure D7 The NDVI Results Validation Points histogram for serious tree death.

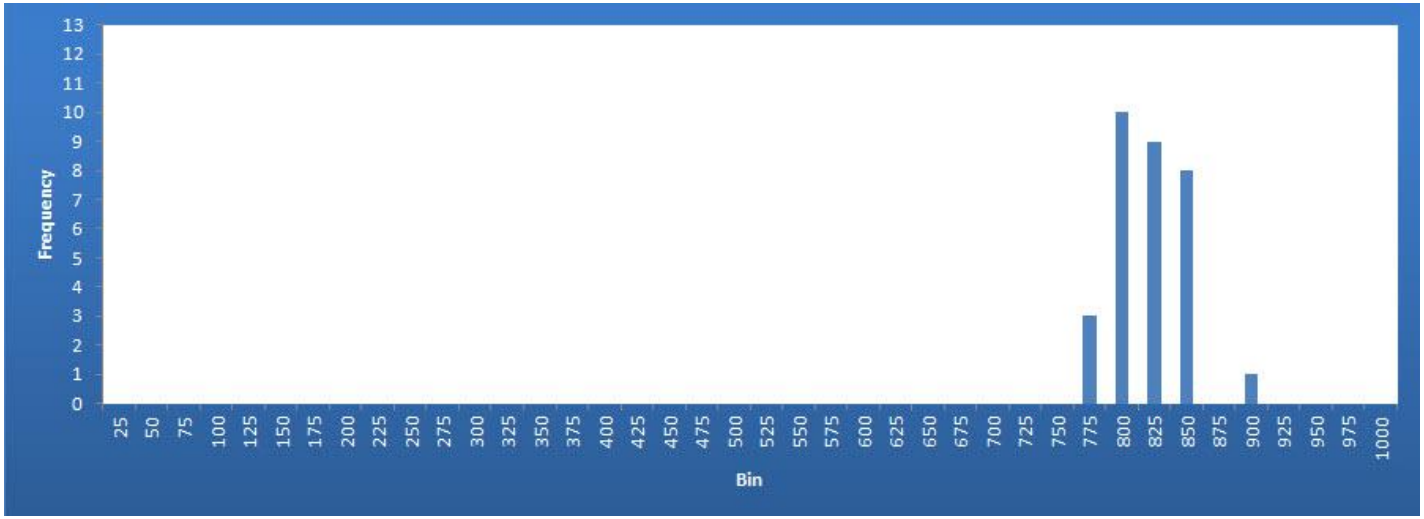

Figure D8 The NDVI Results Validation Points histogram for healthy trees. The main body of SD points in Figure D7 is shifted slightly to the right in comparison to HLH.

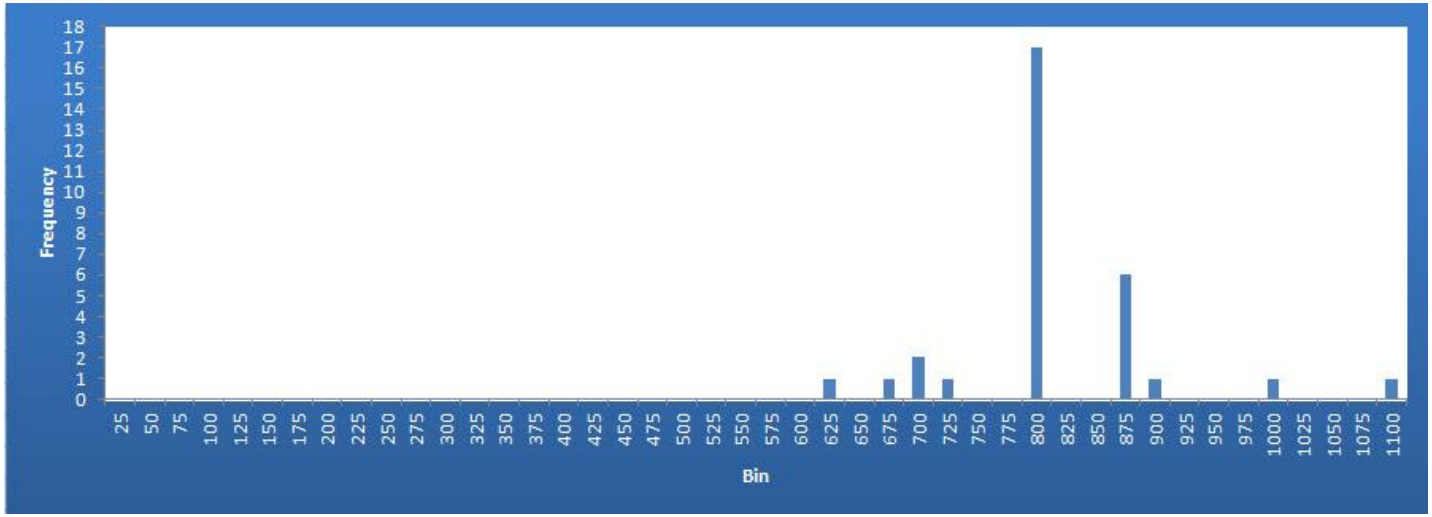

Figure D9 The RGI Results Validation Points histogram for serious tree death.

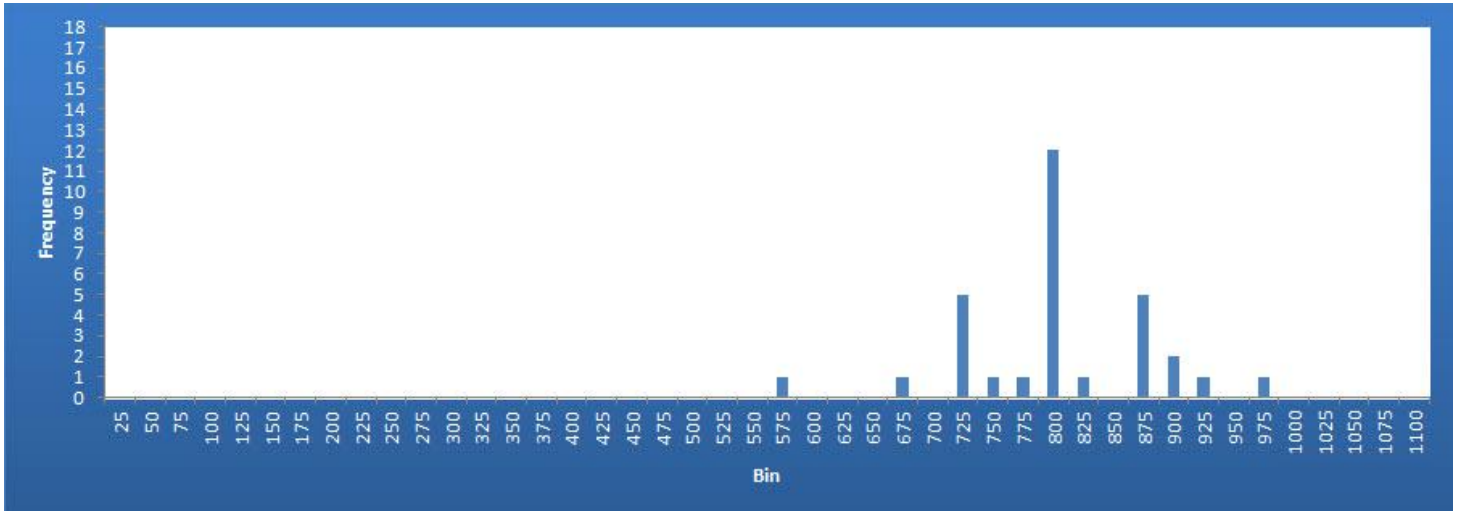

Figure D10 The RGI Results Validation Points histogram for healthy trees. There is correlation between the main sets of points in these ranges so this index is not useful for differentiating the classes.

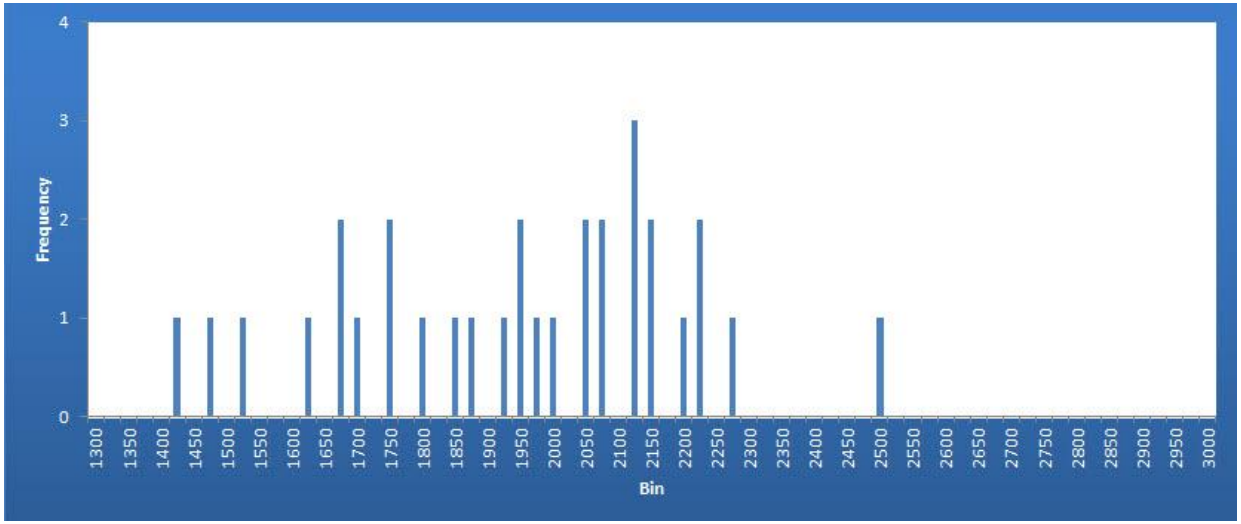

Figure D11 The Tasseled Cap Bright Results Validation Points histogram for serious tree death.

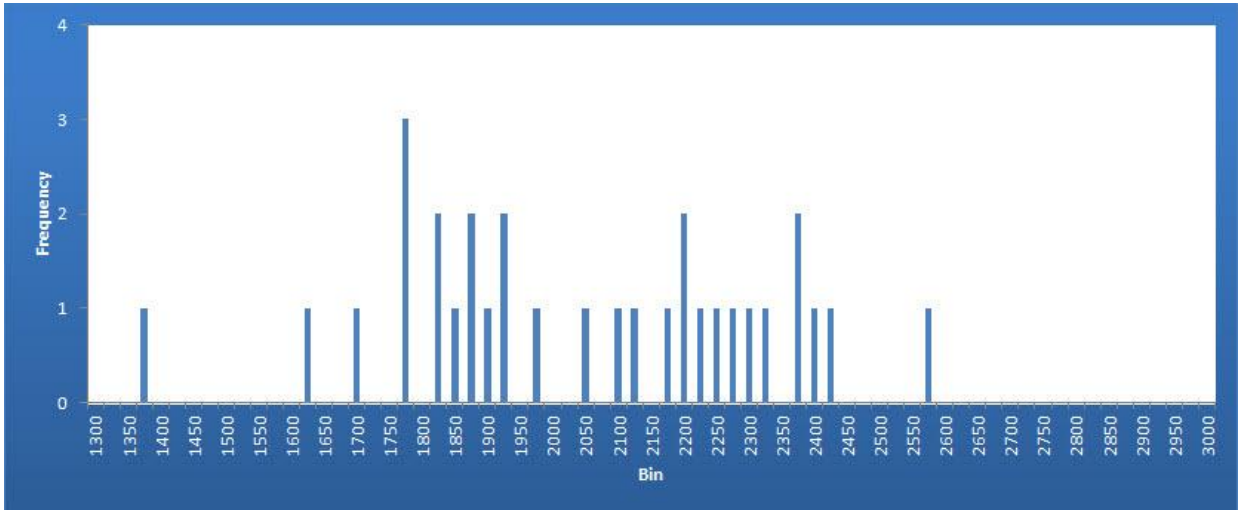

Figure D12 The Tasseled Cap Bright Results Validation Points histogram for healthy trees. The values are spread over too wide a range to be able to use this index to identify a change in spectral signature.

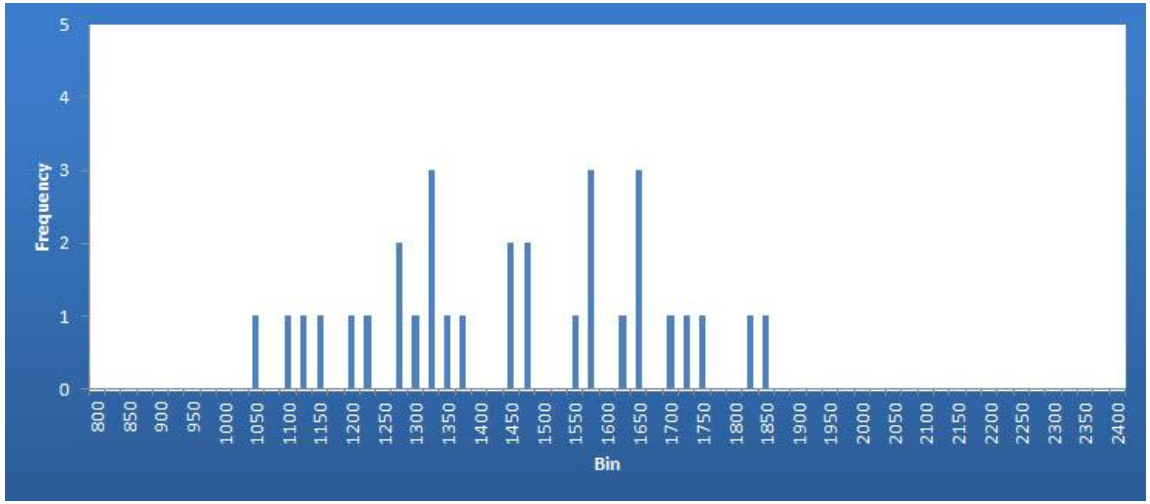

Figure D13 The Tasseled Cap Green Results Validation Points histogram for serious tree death.

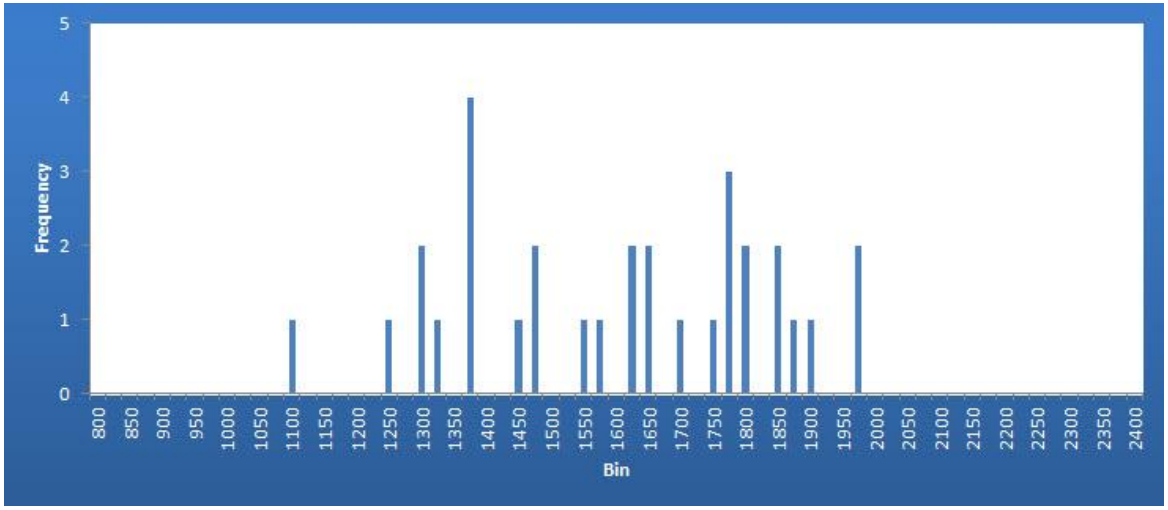

Figure D14 The Tasseled Cap Green Results Validation Points histogram for healthy trees. The values are spread over too wide a range to be able to use this index to identify a change in spectral signature.

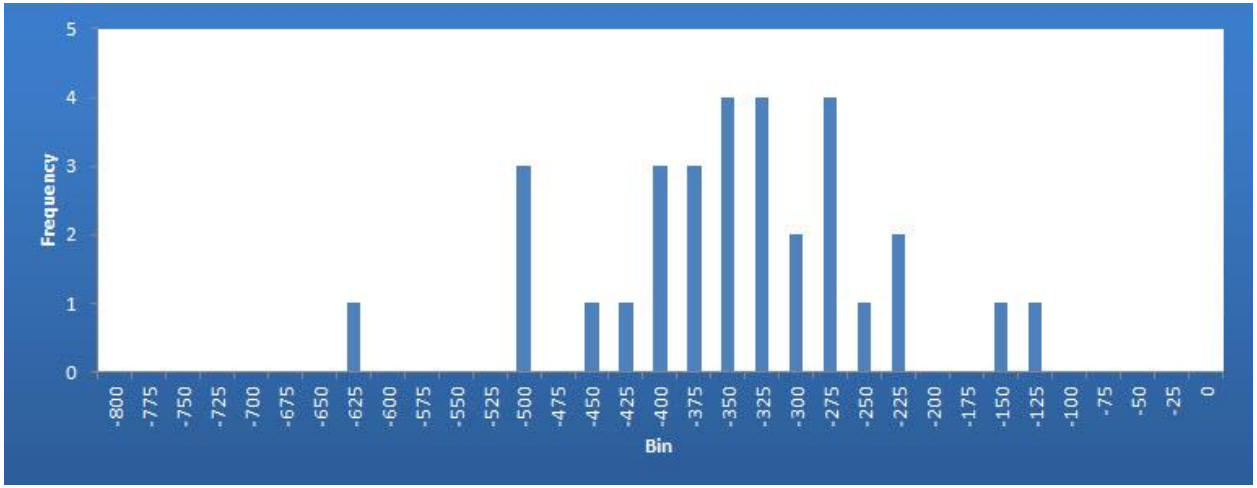

Figure D15 The Tasseled Cap Wet Results Validation Points histogram for serious tree death.

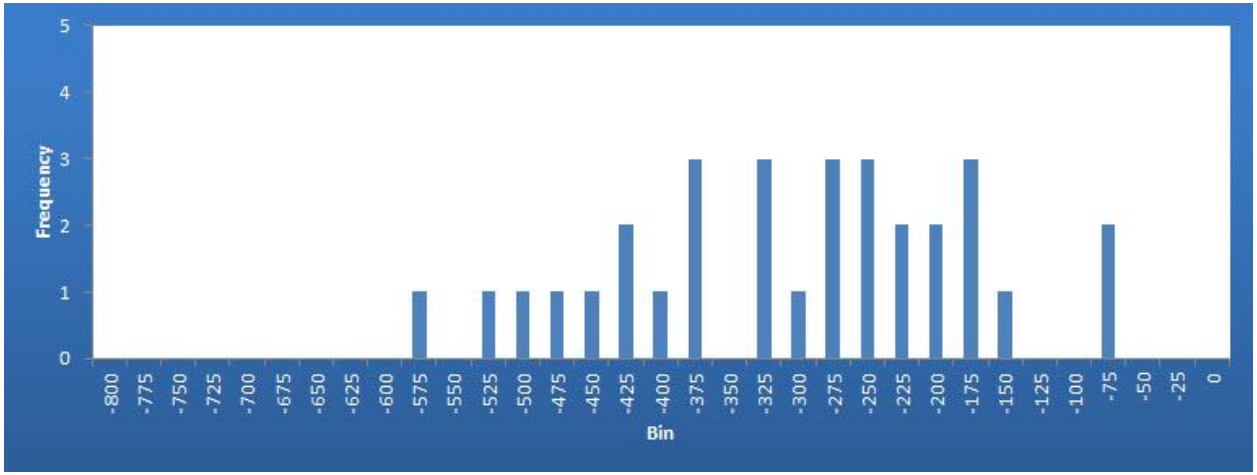

Figure D16 The Tasseled Cap Wet Results Validation Points histogram for healthy trees. The values are spread over too wide a range to be able to use this index to identify a change in spectral signature.